UNIVERSITÀ DEL SALENTO

FACOLTÀ DI SCIENZE MATEMATICHE FISICHE E NATURALI

DOTTORATO DI RICERCA IN FISICA
XX CICLO

TESI DI DOTTORATO

PULSED LASER DEPOSITION OF MULTICOMPONENT GLASSES FOR ERBIUM-DOPED WAVEGUIDE AMPLIFIERS

Tutore:

Ch.mo Prof. MAURIZIO MARTINO

Dottorando:

FRANCESCO ROMANO

Lecce, 2008

Contents

Introduction 1

Thesis overview 5

Chapter 1 7

1.1 WDM Systems 8
1.2 Properties of Erbium Ions 10
1.3 Operation principle and fundamental properties of EDWA 11
1.4 Materials for EDWA development 17
1.4.1 Lithium Niobate 17
1.4.2 Al_2O_3 18
1.4.3 Polymers 18
1.4.4 Glasses 19
1.4.4a Oxyfluoride Silicate Glasses 21
1.4.4b Tellurite Glasses 22
1.5 The state of the art in glass-based EDWAs 24

Chapter 2 29

2.1 Optical Planar Waveguides: Theory 30
2.2 Methods for Planar Waveguide fabrication 33
2.2.1 Magnetron Sputtering 34
2.2.2 Chemical Vapor Deposition 34
2.2.3 Sol-Gel Processing 35
2.2.4 Ion exchange technique 35
2.3 Pulsed Laser Deposition Technique 36
2.3.1 PLD: Operation principle 36
2.3.2 Advantages of PLD technique 38

2.3.3 PLD of glass oxide planar waveguides......39
2.4 PLD: experimental apparatus......40
2.5 Pulsed laser deposition of tellurite planar waveguides......42
2.5.1 Experimental......42
2.5.2 Results......44
2.5.3 Discussion......52
2.6 Pulsed laser deposition of oxyfluoride silicate planar waveguides......54
2.6.1 Experimental......54
2.6.2 Results......56
2.6.3 Discussion......61

Chapter 3 64

3.1 Rectangular Waveguides......65
3.2 2D waveguide fabrication......66
3.2.2 Reactive Ion Etching: operation principle and apparatus......67
3.2.2 Reactive Ion Etching of glasses......69
3.3 2D waveguide fabrication by "Standard Method"......70
3.3.1 Experimental......70
3.3.2 Results......71
3.3.3 Discussion......75
3.4 2D waveguide fabrication by "Inverse Method"......76
3.4.1 Experimental......76
3.4.2 Results......79
3.4.3 Discussion......82

Chapter 4 85

4.1 Methods for Optical Waveguide Analysis......86
4.1.1 Finite-Difference Time-Domain method (FDTD)......87
4.1.2 Beam Propagation method (BPM)......88
4.2 Design of a Y-junction......89
4.2.1 Y-junction geometry......89
4.2.2 Numerical Results......91
4.2.3 Discussion......95

Future Works and Conclusion **96**

References **98**

Publications **107**

Acknowledgements **109**

Introduction

In the past two decades, optical communications has totally changed the way we communicate. It is a revolution that has fundamentally transformed the core of telecommunications, its basic science, its technology, and its industry.
The explosive growth of internet has generated an increasing request of higher bandwidth and speed in telecom systems. Internet traffic in fact, is continuously growing, and even by reasonably conservative estimates, it doubles every year, due to the ever increasing bandwidth requirements of voice, video, and data traffics.
The market demand for higher-capacity transmission was supported by the fact that computers continued to become more powerful and needed to be interconnected. Therefore optical networks started to developed and nowadays they are gradually penetrating into the metropolitan areas, and finally to the customer premises.
Even if optical telecommunication developed very rapidly, it took more than 25 years from the early pioneering ideas of signal transmission by optical way to the first large-scale commercial deployments of optical communications: the Northeast Corridor system linking Washington with New York in 1983 and New York with Boston in 1984. The first transatlantic fiber system, TAT8, was deployed four years later, in 1988.
Different discoveries and new technologies have permitted to reach this goal.
The transmission and processing of signals carried by optical beams rather than by electrical currents has been a topic of great interest since the early 1960s, when the invention and the development of lasers provided a stable source for such applications. In the 1970s the development of low-loss optical fibers lead up to the birth of *integrated optics* and "optical integrated circuits" started to replace conventional electrical integrated circuits in signal processing. In fact, optical fibers and waveguides exhibited many advantages over the standard electrical interconnection methods (i.e. metallic wires and radio link through the air), namely immunity from electromagnetic interference, freedom from electrical short circuits, safety in combustible environment, small size and above all low costs.

Another milestone in the optical communication revolution is represented by the invention of the Erbium Doped Fiber Amplifier (EDFA) in 1987: R.J. Mears and co-worker [1] at the University of Southampton and E. Desurvire et al. [2] from AT&T Bell Laboratories, published simultaneously their results on the optical amplification obtained in optical fiber doped with trivalent ions of erbium. The first EDFA, marketed in 1989, revolutionized the telecom systems. The signal amplification, in fact, has a key role in the long-distance transmission systems and the possibility to regenerate the signal by an optical scheme and not by the conventional electrical method (i.e. converting the optical signal in electrical signal, amplifying it and then re-converting it) allowed to reduce the costs integrating in a single fiber both the transmission and the amplification of the signal.

The most recent technology innovation in optical fiber communications is the Wavelength Division Multiplexing (WDM). The WDM innovation represents a revolution inside the optical communications revolution, allowing the latter to continue its exponential growth.

Vigorous R&D in WDM technologies led to the first large-scale deployment of a commercial WDM system in 1995: the deployment of the NGLN system in the long-distance network of AT&T. In the years that followed, WDM gave rise to the explosive growth of optical communications. In early 1996, three research laboratories reported prototype transmission systems breaking through the terabit/second barrier for the information capacity carried by a single fiber [3,4,5]. This breakthrough launched lightwave transmission technology into the “tera era.” All three approaches used WDM techniques. Five years later, in 2001, a WDM research transmission experiment demonstrated a capacity of 10 Tb/s per fiber [6].

EDFA and WDM technology are undoubtedly the two engines of the ongoing growth of optical telecommunication.

The optical amplifiers play a vital role in today’s dense WDM metro networks. The generic requirements for the optical amplifiers used in metro space include high optical performance, small size and low cost. Although EDFA continues to have a great success, it presents some difficulties especially concerning the signal distribution on Metro Area Network (MAN) and Local Area Network (LAN). In fact there are two profound

differences between metropolitan optical networks and long haul ones. Firstly, the traffic in metro networks is extremely dynamic due to the frequent optical add/drop activities; secondly the exceptionally cost-sensitive nature of metro/access networks usually requires an order of magnitude improvement or further on network's total cost/performance ratio compared to their long-haul counterparts.

The metro networks are dynamic and simultaneously transport data with bit rates ranging from kilobits per second to multiple gigabits per second with different types of signal protocols and formats. Therefore flexibility, simplicity, scalability, performance, size, cost, and the power consumption are the goals of the metro network design.

Actually R&D efforts are devoted to study new solutions to achieve all these requirements in a single device. Moreover the need to integrate is very important for WDM systems and unfortunately fiber technology can't fulfill all their requirements. A fiber-based wavelength division multiplexing system with 40 channels (i.e. 40 different wavelengths) need at least of 120 different components and each one must be connected manually to the other ones [7]. Moreover, concerning the fiber amplifiers, several meters of fiber (~ 10 m) are necessary to obtain the amplification due to the low erbium concentration feasible in fibers.

These two aspects, namely integration and the need of high erbium concentration, can be achieved by the planar waveguide configuration, in which it is possible to integrate on a single substrate all the components of a WDM system as the source, the amplifier and the multiplexer.

As a consequence the research in the last decade concentrated on the development of planar waveguide based devices and in particular on waveguide optical amplifier.

There are three kinds of optical amplifiers used in the metro networks to meet the evolving networking demands: broadband optical amplifiers, banded optical amplifiers, and single-channel optical amplifiers. Among these broadband optical amplifiers are undoubtedly the most attractive, since they allow to amplify all the signals of a WDM system in a single step. It is noticeable that such amplifiers should exhibit the broader transmission band as possible and a flat gain in this band. In this way it possible to increase the number of transmitted channels and to amplify all the signals equally.

Therefore the research of new classes of materials that allow to fulfill these two aspects is a very interesting and fruitful field and a particular attention is devoted to materials suitable for erbium (or most in general rare-earth) doping [8]. In particular multicomponent glasses have very unique features (depending on their composition), such as high erbium solubility and high transmission at the telecom wavelengths, therefore they are vey appealing for the development of optical amplifier.

At the same time the study of new techniques to realize planar waveguide, starting from these materials, has became a very significant research field. A very promising technique for the deposition of erbium-doped materials is the Pulsed Laser Deposition (PLD) technique. PLD has, in fact, a high potential to produce complex glassy films for integrated optical applications with improved optical performances. The main advantage of PLD, when compared to other deposition methods, is its capability to allow the stoichiometric transfer of the starting material to the deposited layer.

To obtain integrated optical amplifiers, a further aspect must be considered: the optical signal must be “guided” through the optical circuit. To fulfil this requirement it is necessary to realize optical waveguides supporting lateral confinement of the signals (2D waveguides). Therefore new strategies to obtain signal confinement must be studied, and new fabrication processes must be exploited with particular attention to the final requirement of integration.

In this work, all this aspects will be developed, in particular great attention will be devoted to the properties of erbium doped glasses and the work will be focused in particular to tellurite and silicate glasses for their promising characteristics. Further the deposition process will be studied, since in PLD, several parameters must be controlled and optimised in order to achieve the desired film quality and structure. The goal to reach is the control of the stoichiometry of the films and of their optical properties.

Two different approach to realize 2D waveguide, named Standard and Inverse methods will be proposed. Finally the design of an optical coupler for the development of an integrated optical amplifier is presented.

Thesis overview

The thesis is outlined as follows:

Chapter 1: The properties of the rare-earth ions and in particular of the Er^{3+} ions will be presented, and the mechanism of optical amplification by Er doping will be discussed. The properties of erbium host materials, suitable for the realization of amplifiers for WDM systems will be described and a particular attention will be devoted to the properties of tellurite and silicate glasses. Finally the state of art in Erbium Doped Waveguide Amplifiers will be presented

Chapter 2: The planar waveguide configuration and the light propagation in planar waveguides will be described. The methods for the realization of planar waveguides will be presented, and the advantages of pulsed laser deposition technique respect to the other methods will be highlighted. The deposition apparatus and the experimental conditions to deposit tellurite and silicate planar waveguides will be described. The results concerning the compositional, morphological and propagation properties of the optical waveguide will be presented and discussed.

Chapter 3: While planar (or slab) waveguides restrict light propagation in one dimension (1D waveguide), channel or ridge waveguides confine the light in two dimensions (2D waveguide): 2D waveguides will be depicted.
Two different approaches to realize 2D waveguides will be presented, namely "Standard" and "Inverse" methods. The two different methods will be discussed and applied, and the experimental procedures will be depicted.

The propagation and structural properties of the 2D waveguides will be reported and discussed.

Chapter 4: The design of a Y-junction coupler will be illustrated. Particular attention will be devoted to the description of the employed simulation method, the Finite Difference Beam Propagation Method (FD-BPM). The results regarding the optimization of the Y-junction structure, will be presented and discussed.

Chapter 1

Erbium-Doped Waveguide Amplifiers

Contents

1.1 WDM Systems 8
1.2 Properties of Erbium Ions 10
1.3 Operation principle and fundamental properties of EDWA 11
1.4 Materials for EDWA development 17
1.4.1 Lithium Niobate 17
1.4.2 Al_2O_3 18
1.4.3 Polymers 18
1.4.4 Glasses 19
1.4.4a Oxyfluoride Silicate Glasses 21
1.4.4b Tellurite Glasses 22
1.5 The state of the art in glass-based EDWAs 24

One of the crucial steps that mainly contributed to the development of optical communication systems was the advent, during the 80s, of the Erbium-Doped Fiber Amplifier (EDFA) [9,10]. In fact an EDFA is able to optically regenerate a signal around 1.55 μm and by the use of this all-optical process avoids the double opto-electronic conversion that represented the bottleneck for the performance of the network. The success of the EDFA combined with the continuous improvement of glass integrated optics technologies [11] gave a strong impulse towards the development of planar Erbium-Doped Waveguide Amplifiers (EDWAs) [9].

In this chapter, the operation principles of EDWA will be described: in the first section a brief introduction to Wavelength Division Multiplexing (WDM) system will be provided, in the second section the properties of trivalent erbium ions will be presented. The third section is devoted to the operation principle and properties of EDWA, then the

properties of suitable materials for supporting erbium doping will be described and finally in the last section the state of the art in EDWAs will be outlined.

1.1 WDM Systems

Wavelength division multiplexing (WDM) is a method that allows to overcome the mismatch between the high transmission capacitance of the optical fiber and the limitation of the electrical components which produce and manage the signals. In WDM systems, the optical transmission spectrum (see Fig. 1.1) is divided into a number of non-overlapping wavelength (or frequency) bands, with each wavelength supporting a single communication channel. Thus, by allowing multiple WDM channels to coexist on a single fiber, one can employ the huge fiber bandwidth, on condition that one can design and develop appropriate network architectures, protocols, and algorithms to handle the signals.

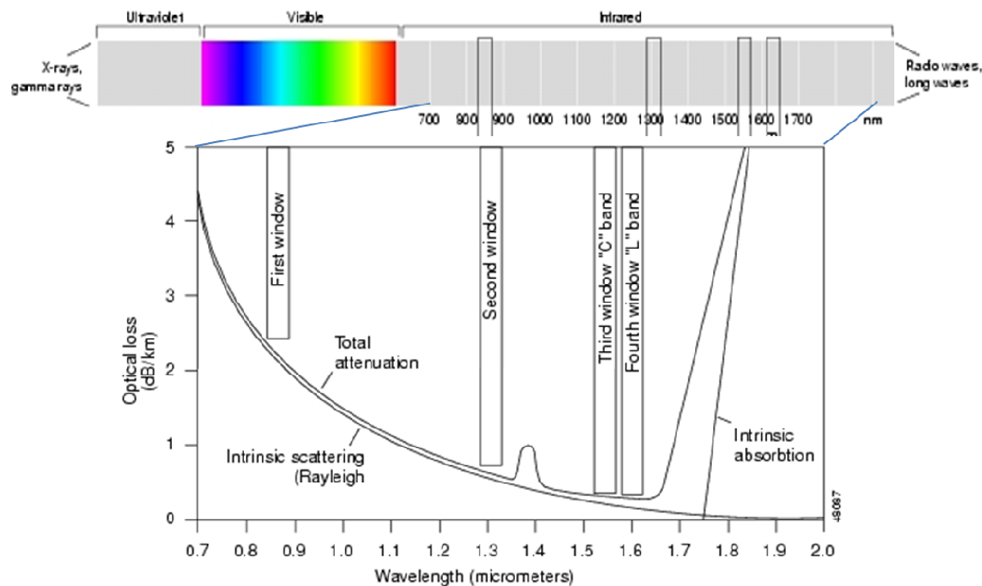

Fig. 1.1. Diagram of the electro-magnetic spectrum: the transmission windows employed in optical telecommunication are evidenced along with the total attenuation curve of silica fibers.

Multiple functions must be exploited by a WDM system (fig 1.2) , therefore complex and high-specification opto-electronic integrated circuits are required and must be implemented. Actually several devices have to be developed and then integrated onto a single substrate: each channel requires a separate laser source, then it is necessary to

combine (multiplex), transmit and split (de-multiplex) the channels, then the signals must be detected and processed.

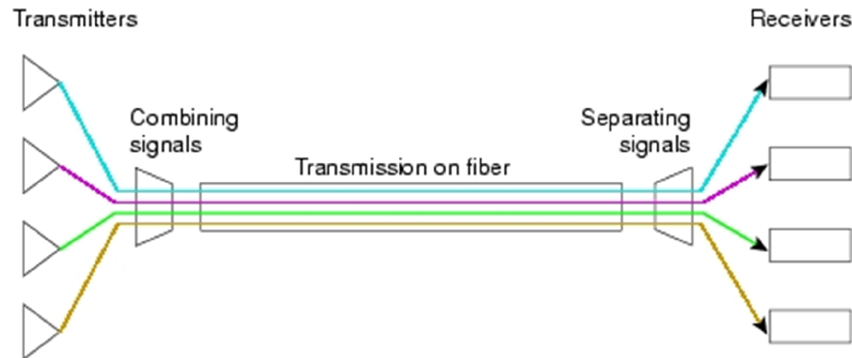

Fig. 1.2: Functions required by a WDM system.

Generally, for mass production, optical integrated circuits for WDM systems need to be compact, reliable, and easy to assemble, moreover optical circuits can be made from a range of materials, each with their own strengths and weaknesses, and each material defines the method by which the different components are integrated on the optical circuit, namely Monolithic or Hybrid Integration [12]

In monolithic integration, all the active and passive components are etched into a single substrate. Obviously monolithic integration can only be achieved using active materials, e.g. III-V semiconductors based on InP, GaAs and Si. In a monolithic scenario, the whole device is made from the same material, which may not be the optimal material for each individual component, therefore reduced performances can be obtained. However the assembly of the optical circuit is much easier, resulting in more reliable and robust devices.

In hybrid integration, active and passive components are fabricated from glass or other materials incapable of light generation (as Lithium Niobate), therefore some active components, such as lasers, have to be coupled onto the substrate of the device. Tolerances are critical, and misaligned components can result in failure of the device. Hybrid integration, however, allows each component to be fabricated from the most suitable material for its operation, with accompanying performance benefits. In this thesis an hybrid approach will be considered, focusing on two main aspects: the study of

suitable materials and techniques to realize low loss transmission planar waveguides and amplifiers, and the analysis of the most suitable methods from a technological point of view, to achieve lateral confinement and to allow integration.

While the technology for the fabrication of passive planar devices such as splitters, and (de)multiplexers is now quite well developed and devices based on this technology are now commercially available [13], to further improve WDM technology is necessary to develop optical amplifiers which can be integrated with these devices. Such amplifiers can be used to compensate the losses in splitters or other components, or can also be used as preamplifiers for active devices such as detectors.

The development of erbium doped waveguide amplifiers (EDWA) is the subject of this thesis and a detailed discussion about operation principle and the state of the art of EDWA will be provide in the next sections.

1.2 Properties of Erbium Ions

Erbium is a rare earth element belonging to the group of the Lanthanides. When embedded in a solid, erbium generally assumes the trivalent Er^{3+} state, which has the electronic configuration [Xe]-$4f^{11}$. The Er^{3+} ion has an incompletely filled 4f-shell, allowing for different electronic configurations with different energies due to spin-spin and spin-orbit interactions [14]. Radiative transitions between most of these energy levels are parity forbidden for free Er^{3+} ions. However, when Er is incorporated in a solid, the surrounding material perturbs the 4f wave functions. This has two important consequences. First, the host material can introduce odd-parity character in the Er 4f wave functions, making radiative transitions weakly allowed. Secondly, the host material causes Stark-splitting of the different energy levels, which results in a broadening of the optical transitions. Figure 1.3a shows a schematic energy level diagram of the Er^{3+} ion, labeled using Russell-Saunders notation. Since radiative transitions in Er^{3+} are only weakly allowed, the cross sections for optical excitation and stimulated emission are quite small, typically of the order of 10^{-21} cm^2, and the radiative lifetimes of the excited states are long, up to several milliseconds [15]. When Er is excited in one of its high lying levels, it rapidly relaxes to lower energy levels via multi-

phonon emission. This results in typical excited state lifetimes ranging from 1 ns to 100 ms. The transition from the first excited state ($^4I_{13/2}$) to the ground state ($^4I_{15/2}$) is an exception to this rule. Due to the large transition energy (0.8 eV) multi-phonon emission is unlikely, resulting in high lifetime, depending on host material, e.g up to ~14.5 ms and ~13.5 ms for silicate and soda-lime silicate glasses respectively [15, 16], and efficient emission at 1.54 µm. However, the emission wavelength is relatively insensitive to the host material, because the 4f shell is shielded from its surroundings by the filled 5s and 5p shells [15].

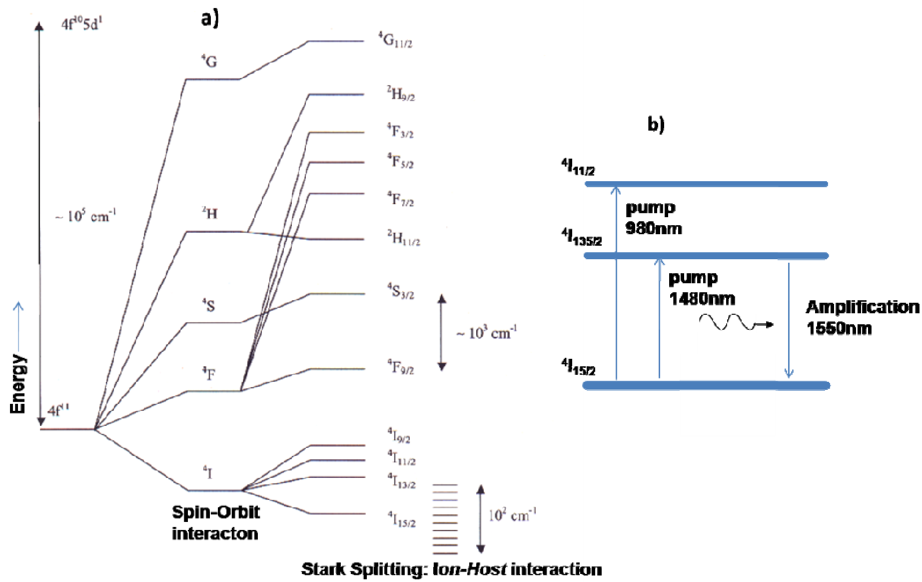

Fig. 1.3: **a)** Energy level of Er^{3+} labeled using Russell-Saunders coupling. **b)** Pumping scheme for Erbium amplification.

1.3 Operation principle and fundamental properties of EDWA

Optical amplification can be achieved in fibers and waveguides, by means of trivalent erbium ions. Erbium-doped materials are of great interest in optical communications technology, as they can serve as the gain medium in optical amplifiers operating at the standard telecommunications wavelength of 1.5 µm.

Er^{3+} ions, when incorporated in a solid host, show the well-defined energy levels of the 4f-shell electronic configurations, described previously (see Fig. 1.3a). In particular, for amplifier operation, the $^4I_{15/2}$, $^4I_{13/2}$, and $^4I_{11/2}$ levels are fundamental. In fact, erbium acts as the active medium of a three level laser, as schematically shown in the three level diagram represented in figure 1.3b, where $^4I_{15/2}$, $^4I_{13/2}$, and $^4I_{11/2}$ represent the ground state, the metastable state and the excited state, respectively. The transition from the first excited state to the ground state ($^4I_{13/2} \rightarrow {}^4I_{15/2}$) occurs at ~1.53 μm and actually it is employed to provide the gain in optical fiber amplifiers in long-distance telecommunication links worldwide. Erbium ions are pumped to the excited energy levels by the absorption of light from the pump source, usually at 980 nm or 1480 nm. The transition from the metastable state to the ground state has a very long lifetime compared to other downward transitions, thus allowing to achieve the population inversion condition. To regain the equilibrium distribution, the electrons, which are pumped to the metastable state, can either revert to the ground state spontaneously (spontaneous emission), or they can be stimulated by some incident photons (signal) of exactly the energy corresponding to the drop to the fundamental state (stimulated emission). While spontaneous emission increase the noise in the amplifier, the stimulated emission lead to the signal amplification.

Absorption and emission cross-sections

Erbium doped amplifiers are characterized by two quantity, namely the absorption, σ_a, and emission, σ_e, cross-sections defined as [17]:

$$P_{abs} = \sigma_a I \qquad (1.1)$$

$$P_{em} = \sigma_e I \qquad (1.2)$$

where P_{abs} and P_{em} represent the absorbed and emitted power respectively and I is the intensity of the incident light per unit area.

The link between the emission and absorption cross section is given by the McCumber relationship [18]:

$$\sigma_e(v) = \sigma_a(v) \exp\left[(\varepsilon - hv)/kT\right] \qquad (1.3)$$

where ν is the frequency of the interacting photon, ε is the mean transition energy needed to excited an Er^{3+} ion from the ground state to the first excited state, h is the Planck's constant, k is Boltzmann's constant and T is the absolute temperature.

The McCumber theory was successfully applied in several applications and for the description of solid state lasers, fibers, and waveguide amplifiers [19,20,21]. Moreover the McCumber theory is very attractive since it is based on general assumptions: first of all the population of Stark levels (of the same degenerate level) is assumed to have a thermal distribution, further the broadening of each Stark level is considered small with respect to kT.

Lifetime

A fundamental parameter to characterize the performances of an erbium-doped waveguide amplifiers is the metastable level lifetime. In general the lifetime of a level is inversely proportional to the probability per unit time that the ion will decay from the excited level: the population of an excited level varies exponentially with time with a constant equal to the lifetime. When there are several pathways for the population to decay, the total probability is the sum of the individual probabilities for each pathway. The two main pathways are the radiative and nonradiative ones, and hence the lifetime is given by [22]:

$$1/\tau = 1/\tau_r + 1/\tau_{nr} \qquad (1.4)$$

where τ is the total lifetime, τ_r is the radiative lifetime, and τ_{nr} is the non-radiative lifetime.

In erbium doped amplifiers the radiative lifetime arises from the fluorescence from the metastable level to the ground level. Non-radiative lifetime depends on the coupling between the vibrations of the host lattice ions and the states of the rare earth ions, consequently τ_{nr} depends largely on the host nature and composition [23]. Lifetime is a very important parameter since long lifetimes lead to low noise and high power conversion efficiency amplifiers.

Linewidth broadening

Although the electronic transitions of an isolated ion are very well defined, broadening of the energy levels occurs when the ions are incorporated into a matrix (as the glass of the optical fiber or waveguide) and thus the amplification window is also broadened. This broadening can be both homogeneous (all ions exhibit the same broadened spectrum) and inhomogeneous (different ions in different host locations exhibit different spectra).

In glasses, both the homogeneous and inhomogeneous broadening can be quite large, as compared to crystals [16]. Homogeneous broadening arises from the interactions with phonons of the glass, while inhomogenous broadening is caused by differences in the glass sites where the different ions are hosted [24]. In fact different sites expose ions to different local electric fields, which shifts the energy levels via the Stark effect. In addition, the Stark effect also removes the degeneracy of energy states having the same total angular momentum. Thus, for example, the trivalent Erbium ion (Er^{+3}) has a ground state with $J = 15/2$, and in the presence of an electric field it splits into $J + 1/2 = 8$ sublevels with slightly different energies. The first excited state is characterized by $J = 13/2$ which gave rise to 7 Stark manifold. Transitions from the $J = 13/2$ excited state to the $J= 15/2$ ground state are responsible for the gain at 1.5 μm wavelength.

Gain in erbium doped amplifiers

The gain is the most important parameter to evaluate the performance of an erbium doped amplifier.

The gain spectrum of the EDWAs has several peaks which are smeared by the broadening mechanisms described above. The net result is a broad spectrum. It is evident that the broad gain-bandwidth of EDWAs make them particularly useful in wavelength-division multiplexed communications systems as a single amplifier can be utilized to amplify all signals being carried on a fiber and whose wavelengths fall within the gain window.

The gain is defined as $G = 10\log(P_{out}/P_{in})$, where P_{out} and P_{in} represent the power at the output of the amplifier and the power injected in the amplifier, respectively.

Three definitions of gain are generally used from a practical point of view to characterize the optical amplifier [22]:

1. The net gain is the change in signal power as a result of propagation through the amplifying device, i.e., the useful gain.
2. The internal gain is the net gain minus the insertion losses outside the absorption band, i.e. how much the signal is amplified if the background losses were zero.
3. Relative gain is the change in signal power out of the device as a result of pumping the device.

The two main specifications that should be considered for commercial applications, are the net gain per length unit GL (dB/cm) and the net gain per pump power unit GP (dB/mW).

Noise in erbium doped amplifiers

The principal source of noise in erbium doped amplifiers is Amplified Spontaneous Emission (ASE).

ASE has a spectrum very similar to the gain spectrum of the amplifier. In fact, Er^{3+} ions in excited states can decay to the fundamental state by stimulated and spontaneous emission. Spontaneous emission occurs randomly, depending upon the host structure and inversion level. Photons are emitted spontaneously in all directions, but a fraction of the emitted photons can be captured and guided by the waveguide. The photons captured may then interact with other rare earth ions, and thus be amplified by stimulated emission. Therefore the initial spontaneous emission is amplified in the same manner as the signals, hence the term Amplified Spontaneous Emission (ASE).

The noise figure (NF) of the amplifiers is commonly used as a measure of the degradation of the signal-to-noise ratio for signal passing through the amplifier ($NF=SNR_{in}/SNR_{out}$). The expression to calculate the optical noise figure is given by [22]

$$NF(dB) = 10log_{10}\left(\frac{P_{ASE}}{h\nu B_0} + \frac{1}{G}\right) \qquad (1.5)$$

where ν is the signal frequency, P_{ASE} is the noise power (due to ASE) at the same frequency, h is the Planck's constant, B_o is the bandwidth of the optical spectrum analyzer at the signal frequency ν.

Equation 1.5 assumes that no noise is injected at the input of the amplifier (i.e., a shotnoise-limited input signal). It must be underlined that only few papers give such a value, which seems to be in the range 3- 4 dB [25].

Ion-Ion Interactions

In erbium doped amplifiers an important limiting factor is due to the interaction between rare earth ions. This process is relevant in the case of clustered materials [14]. The most important process between two ions of the same species is co-operative upconversion.
This process involves two neighboring ions excited to the metastable level. Energy is transferred nonradiatively from one atom (the donor) to the other atom (the acceptor) and the latter is promoted to a level with higher energy respect to the metastable one. In the case of Er ions the levels involved are the $^4I_{13/2}$ and the $^4I_{9/2}$ (fig. 1.4). Once in this state, the acceptor ion may then decay rapidly and non-radiatively, or alternatively return to the metastable state and subsequently emit light. In the case of oxide glasses, the relaxation is rapid and nonradiative, and hence the result of co-operative upconversion is to reduce the performance of the amplifier. In co-operative upconversion both the two interacting ions must be in the metastable state so, it becomes important only at high excitation levels. Moreover, co-operative upconversion reduces the metastable state lifetime and causes a non-exponential luminescence decay.

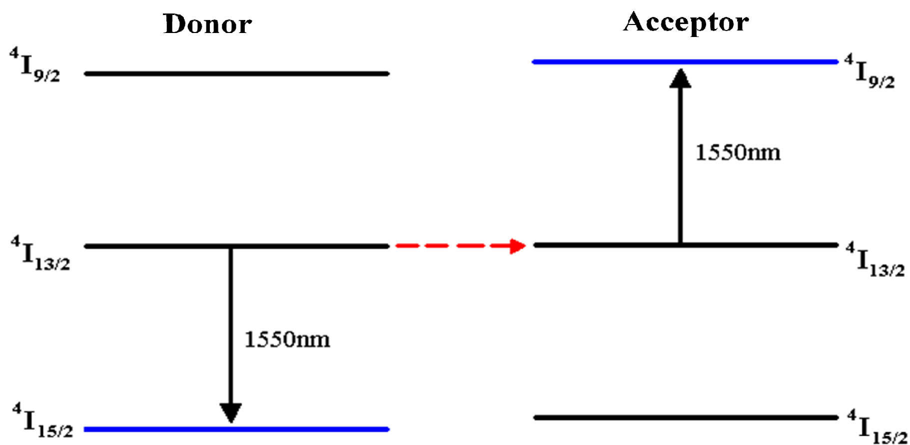

Fig. 1.4: Schematic diagram of the co-operative upconversion process.

It must be underlined that the ion-ion interaction can also represent an useful process as in the case of co-doping with different ions. In fact it can be employed in novel pumping schemes whereby excitation is provided to one species and transferred to the other, allowing different pump sources to be used. Examples of such mechanisms are the Er/Yb codoping schemes adopted in EDWAs to increase the luminescence efficiency of the Er^{3+} ion by coupling to the absorption bands of the Yb codopant.

1.4 Materials for EDWA development

As evidenced by the previous sections the performances of an EDWA strongly depend by the nature of the host materials for the erbium doping, since the interaction between the rare earth ions and the host influence the characteristics of the amplifiers, namely the emission and absorption cross-sections, the lifetime of the metastable level and the gain of the amplifier. Silica was the first rare earth host to be studied, since optical telecommunications were based on silica fibers, therefore the properties of all the other host materials are habitually compared with those of silica. The following sections do not represent a complete and exhaustive description of all the materials employed for EDWAs development, for example semiconductor hosts are not mentioned even if a lot of research efforts have been spent in the last years in this field. Semiconductor in fact are very attractive for technological reasons because of the possibility of integrating intense narrow-band light sources directly on the integrated optical circuits, using well established microelectronics processing techniques.

1.4.1 Lithium Niobate

Lithium niobate has received attention as a host for rare-earth ions because of the possibility of exploiting its electro-optic, acousto-optic and nonlinear properties to produce a range of rare-earth doped integrated optoelectronic devices from modulators to switches and filters [26,27]. Doping can be achieved readily by thermal diffusion, ion exchange [28], or by ion implantation [29]. Most work on this material has been concentrated on erbium doping to produce devices for the 1.5 μm telecommunication window. Different erbium-doped $LiNbO_3$ waveguide devices, including lasers and

planar waveguides, have been produced [30,31]. Such devices have been produced by thermal diffusion of erbium into lithium niobate, however, being an equilibrium process, rare-earth clustering limits the maximum concentration of optically active erbium which can be incorporated into the host.

A great advantage in rare-earth doped lithium niobate is that the co-operative upcoversion is less problematic than in the case of Er-doped silica, since absorption and emission spectra of erbium in lithium niobate are narrower and as a consequence the probability of energy transfer processes between rare earth ions is reduced [32].

1.4.2 Al_2O_3

Recently, pure aluminium oxide (Al_2O_3) has been studied both as host for rare-earth ions, in particular erbium, and as a material for waveguide fabrication [33]. This is principally due to the high solubility of erbium in alumina and its high refractive index (n = 1,64) which make it possible to produce silica-clad fibers and waveguides which exhibit high optical mode confinement and are capable of small bend radii. The increased solubility of Er in Al_2O_3 respect to SiO_2 results from the valence match between the rare-earth dopant and the substituted cation (Al^{3+}). The optically active Er^{3+} ions readily substitute for aluminium ions occupying octahedral sites in alumina. Moreover, in the Al_2O_3 lattice one-third of Al^{3+} octahedral sites are unoccupied, and hence a large number of Er^{3+} ions can be incorporated without suffering from up-conversion [34]. In addition, the Er^{3+} emission linewidth can extend up to 55 nm in alumina [35], compared to around 10 nm in pure silica, making erbium-doped alumina waveguides promising candidates for WDM applications [32].

1.4.3 Polymers

Polymers can be considered excellent hosts for rare earth ions, as they can incorporate erbium ion complexes containing multifunctional organic ligands at higher concentrations than in EDFA's. Moreover, Er in these materials exhibit broader luminescence spectra as compared to those of Er in pure silica [36,37] or some other inorganic hosts. In addition, polymers have lower cost with respect to crystalline

materials as lithium niobate and offer more flexible fabrication methods to elaborate optical waveguides [38]. moreover polymers display high transparency, low dispersion, and easy engineering for the control of various optical parameters such as refractive index and birefringence [39].

Several authors have reported spectroscopic investigations on erbium-containing polymers and their applications in infrared active optical devices. Recently, a FWHM of 70 nm has been demonstrated for Er-doped polymer luminescence spectra around 1550 nm [40]. Moreover, an optical gain coefficient up to 0.9 cm^{-1} at 1540 nm has been demonstrated in erbium complex doped polymethylmethacrylat (PMMA) [41].

1.4.4 Glasses

Glass hosts are very attractive for the development of integrated optics devices for two main reasons: first of all they are amorphous materials so they can be easily deposited (i.e. without lattice constant constraints) onto crystalline substrates, secondly glass materials can be suitable modified in order to fulfill the requirements of different integrated optics devices, consequently they facilitate the integration of more function onto a single substrate. Concerning the development of EDWAs, glass hosts must satisfy two important requisites, from one hand they must allow the higher erbium concentration as possible, in order to improve the performance of the amplifier, from the other hand they have to provide the broader and flatter gain as possible. In fact for an efficient WDM operation, the Er^{3+}-doped amplifiers with broadband and flat gain characteristics are required to compensate and maintain the gain at each channel, so that the gain excursion over the whole spectral width can be minimized.

Two main approaches can be followed to satisfy these two requirements. The first approach is based on modifying the structure of silica-based glasses, since they present many advantages in terms of system compatibility with the standard silica fibers. In the second approach, non-silica glass hosts, intrinsically capable of broader gain than silica EDWA, have been studied and developed.

The first method to modify the structure of silica glasses is based on Al_2O_3 and P_2O_5 codoping of the glass (these glasses are known as Al/P silica) [42] which disperse Er^{3+}

ions in the silica glass matrix and thereby increase the Er sites in the glass network. The modification of the glass structure, with Al_2O_3-P_2O_5 addition, leads to an increase in the value of the full width at half maximum (FWHM) of the Er^{3+} emission from ~10 nm in pure silica to 44 nm in Al/P silica [14].

A material which has been recently attracted attention as host for luminescent rare-earth ions is silicon-rich silica. This material consists of silica doped with an excess of silicon in the form of nanometer-sized clusters or crystallites. It can be thought of as a three-dimensionally confined silicon system in which the confinement is produced by the silicon–silica boundary. The embedded silicon clusters may be either amorphous or crystalline, and because of quantum confinement effects, emit light in the visible and near-infrared region. Such material has been studied for some time as a promising candidate for light emission from silicon [43,44], but photoluminescence efficiencies were low [45] as, even for nanoclusters as small as 2 nm in diameter, the silicon remains predominantly an indirect gap semiconductor. However, when co-doped with rare-earth ions the situation is dramatically improved: intense rare-earth emission can be obtained, and doping with erbium allows access to the 1.5 µm spectral region. Indirect excitation of erbium photoluminescence via coupling between the absorption bands of the silicon nanoclusters and erbium excited states has been demonstrated [46] and recently optical gain at 1.5 µm was demonstrated in silicon-rich silica, by using a low-cost commercial LED [47].

To increase the value of the FWHM new classes of glasses have been studied and the most relevant family is represented undoubtedly by the fluorozirconate glasses. In these hosts the FWHM for the 1500 nm Er^{3+} transition is 65 nm [14, 48]. Consequently Er^{3+}-doped fluorozirconate glass amplifiers have been considered as an alternative to Al/P silica-based devices. Although the emission and the gain curves are much broader (respect to silica-based glasses) in Er-doped zirconium-barium-lanthanum-aluminum-sodium fluoride (ZrF_4–BaF_2–LaF_3–AlF_3–NaF: ZBLAN) glass, it suffers from three main disadvantages. The first disadvantage is related with the low phonon energy of ZBLAN (~580 cm^{-1}), which makes the device unsuitable for pumping at 980 nm due to an enhanced “excited state absorption” at the pump wavelength [49]. As a result, the device is only pumped at 1480 nm. The second major problem is that the glass cannot be

heavily doped with Er^{3+}, as the concentration at which the quenching starts to dominate is above 1000 ppm [50]. The third problem is the comparatively poor stability and durability of ZBLAN glasses. It is much weaker than Al/P silica. The unsuitability of Er^{3+}-doped ZBLAN and limitation of Al/P silica led to a search for other glass hosts which can dissolve higher concentrations of Er^{3+} ions without causing the concentration quenching and, at the same time, can exhibit a broader FWHM than Al/P silica and ZBLAN.

Good candidates to achieve these two characteristics are phosphate glasses. Phosphate glasses in fact show higher emission cross section than silicate and Al/P silica. Moreover, in phosphate glasses, unlike in silica-based glass, the co-operative upconversion and the ion clustering effects are prevented because of a weak interaction among the rare earth ions so it is possible to achieve a high rare earth concentration and consequently a high amplifier gain [51,52].

In this thesis both these two approaches, namely the use of silica based and no-silica based glass hosts will be investigated. In particular, two different glass hosts will be studied, namely oxyfluoride silicate glasses and tellurite glasses.

1.4.4a Oxyfluoride Silicate Glasses

Silica-based glasses are very interesting for the development of integrated optics devices, since they can be easily coupled with standard silica fibers.

Oxyfluoride silicate glasses, therefore, are of particular interest as hosts for Er^{3+} ions, since they retain the structural features of both silicate and fluoride glasses.

An important advantage of oxyfluoride silicate glasses is that these glasses can be doped to relatively high concentrations of rare-earth ions without inducing ion-ion clustering and the consequent reduction of fluorescence lifetime and quantum efficiency. The incorporation of fluorine, which creates non-bridging oxygen and F^- sites, potentially become responsible for F^- ion like local environment for rare earth ions.

As silicate glasses, oxyfluoride hosts are chemically and mechanically much more stable than fluoride glasses, further they present good characteristics (very similar to pure silica glass) for fibers and waveguides development as the enhanced devitrification resistance.

Therefore, the oxyfluoride silicate glass hosts can potentially offer the best features of both fluorides and silicates by combining the spectroscopic properties of fluoride hosts and the durability and mechanical properties of the silica glass.

At the beginning the research activity about oxyfluoride silicate hosts, concentrated on the feature of glass ceramics, since they presents a strong erbium up-conversion luminescence ($^4S_{3/2}\rightarrow{}^4I_{15/2}$) due to the very low phonon energy of the ceramic phase [53,54]. Er^{3+}-doped glass ceramic devices with higher Er^{3+}-ions concentration (50 times), with higher fluorescence quantum efficiency at 1.55 μm and with flatter gain bandwidth than Al/P silica based devices have been demonstrated [55,56,57].

Unfortunately glass ceramics present very high scattering losses, due to the high concentration of ultra-fine crystals. Therefore oxyfluoride glasses were preferred to their ceramic counterpart.

The glass composition considered in this thesis work is: $65SiO_2$ - $11Na_2O$ - $3Al_2O_3$ - $10LaF_3$ - $10PbF_2$ - $1ErF_3$ (wt%). A detailed discussion on the properties of the bulk glass is presented in [58]. It is worth noting that the most important parameter in oxyfluoride materials is the F/O ratio since it determines the glass structure and properties. In particular the composition presented in this work exhibit an F/O ratio of 0.353 which leads to a high refractive index (~ 1.65) and an UV absorption edge of 3.9 eV. Concerning the Er^{3+} spectroscopic properties, which are fundamental for the performances of the erbium-doped amplifiers, the oxyfluoride glass exhibit an absorption cross-section of ~ 3.5×10^{-21} cm^2, larger than Al/P silica [14], a correspondent emission cross-section of ~7.5×10^{-21} cm^2 and a large bandwidth at 1.55 μm, with a FWHM up to 35 nm. Moreover the lifetime of the $^4I_{13/2}$ level, results in a value of 9.5 ms.

1.4.4b Tellurite Glasses

A limiting process for the performances of an EDWA is the multiphonon relaxation which can rapidly depopulate the high excited states and therefore quench the luminescence [14]. Such processes occur only when a small number of phonons are required to bridge the energy gap between the upper and lower electronic states of the rare-earth ion. In the case of erbium, the energy gap of the $^4I_{13/2}$ to $^4I_{15/2}$ transition is

approximately 6500 cm^{-1}. The phonon cut-off energy of silica is 1100 cm^{-1}, and therefore the rare-earth luminescence at 1535 nm is weakly quenched at room temperature in silica. Glass hosts with a lower phonon energy than in silica, such as fluoride glasses, can reduce the contribution of multiphonon relaxation and improve the quantum efficiency. The disadvantages of fluoride glasses, as the low chemical stability and the low erbium doping level, lead to the study of new low phonon hosts. Tellurite glasses have the lowest phonon energy among oxide glass formers (~ 780 cm^{-1}), moreover they present a good chemical stability and high rare earth solubility, more than 5000 ppm [59]. In 1997 Mori et al. [60] and Yamada et al.[61] showed the possibility to use TeO_2 for erbium-doped amplifiers and demonstrated a flat gain over 70 nm in an Er-doper TeO_2 fiber.

Tellurite glasses present two other important characteristics for the development of planar amplifier, namely an high transmission range (0.35-5 μm), and an high refractive index which increases the emission cross section [62,63].

Unfortunately tellurite glasses present some drawbacks. First of all the pumping scheme at 980 nm is not enough efficient. In fact, due to the low phonon energy, the non-radiative decay of the $^4I_{11/2}$ level is too slow, therefore the population of this level become relevant and the efficiency of the amplifiers is reduced. Moreover tellurite glasses present a low softening point and as a consequence these glasses can suffer from thermal damage.

To overcome these problems it is possible to add in the matrix host actuator ions as tungsten or boron, in order to increase the phonon energy and consequently to reduce the lifetime of the $^4I_{11/2}$ level [64,65].

In this thesis a tungsten-tellurite glass will be considered with nominal composition 45%TeO_2–39%WO_3–15%Na_2O–1%ErO_3. A detailed discussion about the glass preparation and characterization can be found in [66]. In particular the studied glass presented a high refractive index ($n > 2$) and a high absorption and emission cross section (~7.6×10^{-21} cm^2). The experimental lifetime of the 1.5 μm emission resulted in a value of ~ 2 ms, this very low value was attributed to the high OH content (up to 8.2×10^{19} ions/cm^3).

1.5 The state of the art in glass-based EDWA

The development of an EDWA requires the fabrication of a waveguide structure, i.e. a structure that allows to propagate both the signal and the pump through the optical amplifier. It is evident that such waveguide must support propagation modes: the description of the fundamental conditions to realize propagation modes in a waveguide will be provided in the next chapters, in particular planar waveguides (1D waveguide) and channel waveguide (2D waveguide) will be described. From a technological point of view, 2D waveguides are more useful than planar waveguides, and the methods for their fabrication can be roughly divided in two major groups:

- ✓ multi-step methods;
- ✓ direct writing methods.

Both methods can require in a first step the realization of planar waveguides, then thin film deposition methods are necessary (such as Pulsed Laser deposition, Radio-Frequency Magnetron Sputtering (rf-MS), Sol-Gel, Chemical Vapour Deposition (CVD), Flame Hydrolysis Deposition (FHD)).

In multi-step method, the pattern of the waveguides is at first realized on a mask (by conventional photolithographic methods) and finally in the last phase the 2D structures are “written” on the film (duplicating the mask) by Reactive Ion Etching (RIE), Ion Exchange technique, and UV or ion beam imprinting.

In direct writing methods the waveguides are directly written on the glass (both bulk or thin film) by a focused laser beam (UV laser or femtosecond laser) or by an ion beam.

It is straightforward that there are several possible combinations of materials and methods to realize 2D waveguides, moreover even limiting the discussion to glass-based devices it is quite difficult to compare the performances of different EDWAs realized starting from different materials and employing different methods.

A further difficulty must be highlighted in this context: the authors do not agree regarding the parameters to be used for describing the performances of the amplifiers. For example some authors refer to the increase of the transmitted signal without consider the absorption and propagation losses (signal enhancement), while others refer to the net gain of the amplifier. Moreover a discrepancy can be found concerning the definition of

the input power since some authors refer to the real power injected into the waveguide, while in some papers only the power at the end of the input fiber is reported without consider the insertion losses.

For the previous motivations the discussion in next section will be restricted to those papers presenting well defined and non-ambiguous parameters. Moreover the state of the art in EDWAs will be described limiting the discussion to phosphate, silicate and tellurite glasses since they are the most attractive and promising glass hosts for EDWA development.

Phosphate glasses

The first high performance EDWA based on phosphate glasses was demonstrated by Yan et al. in 1997 [67]. A thin film of phosphate glass with a high erbium concentration (5.3×10^{20} ions/cm^3) was deposited by rf-magnetron sputtering. A 2D waveguide was then obtained depositing a SiO_2 layer onto a 1-µm-thick Er-doped glass layer, and then etching the waveguide pattern into this SiO_2 layer using standard photolithography technique. A net optical gain at 1.535 nm of 4.1 dB was measured in a 10-mm-long Er-doped phosphate glass waveguide amplifier pumped at 980 nm with a pump power of 21 mW. This high gain at relatively low pump power was attributed to the very low co-operative upconversion coefficient in this glass, caused by the homogeneous distribution of Er in the glass, as well as by the high mode confinement due to the high refractive index.

In 2002 Wong and co-workers realized a 10-mm-long amplifier in a phosphate glass using Ion Exchange technique [68]. Er-Yb codoping was used (2%Er_2O_3-2%Yb_2O_3 (%wt)). In this case the 2D structure was obtained by realizing an aluminum mask onto the glass by photolithography and liftoff techniques before the ion exchange process. A net gain of 3.3 dB/cm was obtained at a pump power of 120 mW..

In 2004 a high gain and compact amplifier (3mm-long waveguide) was obtain by Patel et al. [69], by using electric field assisted Ag^+ diffusion in a highly doped (8%Er_2O_3-12%Yb_2O_3 (%wt))) phosphate glass. As in the previous case the 2D waveguide was obtained by realizing a metal pattern onto the glass surface before the diffusion process.

4.1 dB/cm net gain was demonstrated at 150 mW (980 nm) pump power, this is the highest gain obtain for phosphate glass amplifiers.

It is worth mentioning two recent works on phosphate glass amplifiers, realized by direct writing method. Liu et al. realized Er-Yb codoped waveguide amplifiers by means of a focused proton beam [70], while Della Valle and co-workers obtained a 3.7 cm-long Er-Yb codoped amplifier by femtosecond laser writing [71]. Even if the net gain was not very high (1.72 dB/cm and ~2 dB/cm respectively), these techniques appeared very attractive for their versatility.

Silica based glasses

In 1997 Lin and co-workers demonstrated an EDWA based on a soda-lime silicate glass, by using a "collimated sputtering" method [72]: a thick (3μm) polymide layer was used to defined the waveguide pattern (onto the substrate) by photolithography and dry etching processes, then Er doped films were deposited by sputtering onto the pattern and finally the polymide mask acted as a sacrificial layer for a liftoff process that produced a ridge waveguide array onto the substrate. Very low loss waveguides, 1.7 cm-long, were obtained (propagation losses as low as 0.4 dB/cm) by this method. Using an erbium doping level of 3.3% wt, a signal enhancement of 15.4 dB was obtained (at a 40 mW pump power), that compensated for both the Er absorption (7.5 dB) and propagation losses (0.7 dB) and resulted in a net gain of 4.2 dB/cm. This value still remains the highest value reported in literature for glass based EDWA.

Al/P silica buried-channel waveguides were obtain in 2003 by Huang et al. by sol-gel method followed by reactive ion etching technique [73]. 5 cm-long Er-Yb codoped waveguides were obtained (Er 0.25% mol- Yb 0.25% mol). A 1.1 dB/cm net gain was obtained at 175 mW pump power. Even if this value is not very high it is the highest for Al_2O_3:P_2O_5:SiO_2 hosts.

Pelli et al. in 2004 succeeded in realizing low loss planar (propagation losses < 0.6 dB/cm) and channel waveguides in soda-lime silicate glasses by ion exchange [74]. The silicate glass presented an Er-Yb codoping (Er 2.3×10^{20} ions/cm^3- Yb 3.8×10^{20} ions/cm^3).The channel waveguides were realized by conventional photolithography of a

metal mask on the glass surface, followed by the ion exchange process. A 1.5 dB/cm net gain was obtained using a pump power of 250 mW.

Very recently Psaila et al. [75] employed femtosecond laser writing method to obtain a waveguide amplifier in an Er-Yb codoped oxyfluoride glass (1%Er_2O_3-2%Yb_2O_3 (%wt)). The glass composition was very similar to that presented in this thesis since both glass precursors were prepared by IMR group in Leeds. A net gain of 0.72 was obtained and propagation losses as low as 0.34 dB/cm were demonstrated.

Tellurite glasses

Tellurite glass slab optical waveguides were demonstrated in the last years, but the realization of 2D waveguides, which are the building block of any integrated devices, still appears a challenge mainly because of the low chemical durability of these glasses.

Tellurite planar waveguides were obtained by different deposition techniques.

In 2003 Caricato and co-workers, at the University of Lecce, obtained very good quality tellurite waveguides by means of pulsed laser deposition technique [76]. The propagation losses were as low as 0.8 dB/cm, this value is the lowest value reported for tellurite planar waveguides.

More recently Intyushin et al. demonstrated the possibility to employ rf-magnetron sputtering technique to obtain tellurite thin films in which the rare earth ions remain active [77].

In 2006 Sakida and co-workers obtained tellurite waveguides by ion exchange technique. The propagation losses for such waveguides were 3.10 dB/cm at 632 nm [78].

The group of Prof. Righini, tried different methods to obtained 2D waveguides, namely ion exchange and femtosecond laser writing but they did not succeed, in the first case the photolithographic process damaged the waveguide surface, while femtosecond laser caused a decrease of the refractive index, making the process useless for waveguide fabrication [79]. Recently they succeeded in channel waveguide fabrication by means of ion beam irradiation method: tellurite glasses were irradiated through a silicon mask with a 1.5 MeV N^+ collimated beam. Because of the short lengh (7 mm) and the

multimode features of the waveguides the propagation properties and the optical gain of the amplifiers were not characterized [80].

Chapter 2

Pulsed Laser Deposition of Tellurite and Oxyfluoride Planar Waveguides

Contents

2.1 Optical Planar Waveguides: Theory 30
2.2 Methods for Planar Waveguide fabrication 33
2.2.1 Magnetron Sputtering 34
2.2.2 Chemical Vapor Deposition 34
2.2.3 Sol-Gel Processing 35
2.2.4 Ion exchange technique 35
2.3 Pulsed Laser Deposition Technique 36
2.3.1 PLD: Operation principle 36
2.3.2 Advantages of PLD technique 38
2.3.3 PLD of glass oxide planar waveguides 39
2.4 PLD: experimental apparatus 40
2.5 Pulsed laser deposition of tellurite planar waveguides 42
2.5.1 Experimental 42
2.5.2 Results 44
2.5.3 Discussion 52
2.6 Pulsed laser deposition of oxyfluoride silicate planar waveguides 54
2.6.1 Experimental 54
2.6.2 Results 56
2.6.3 Discussion 61

Optical waveguides are fundamental components in Wavelength Division Multiplexing (WDM) systems, since they can have both passive or active functions in an optical integrated circuit. First of all an optical waveguide operates as interconnection between the different devices of an optical circuit, so it simply transmits the signals; moreover, it

can have an active task as in the case of optical amplifiers. In this chapter the propagation in optical planar waveguides will be outlined, followed by a brief description of the standard techniques employed to realize planar waveguides. Afterward the Pulsed Laser Deposition technique will be described, highlighting its advantages with respect to the other techniques. The experimental setup for Pulsed Laser Deposition of planar waveguides realized in this thesis will be illustrated. Finally the main results obtained for both tellurite and silicate planar waveguides will be presented and discussed.

2.1 Optical Planar Waveguides: Theory

A planar waveguide is characterized by parallel planar boundaries with respect to one direction while it is infinite in the lateral direction. Of course, because it is infinite in two dimensions, it can not be a practical waveguide for optical integrated circuits, nevertheless the study of propagation in planar waveguides represents the basis for the analysis of most technologically relevant waveguides, e.g. waveguides with rectangular cross section.

In the three layer structure sketched in figure 2.1, all the layers are assumed to be infinite in extent in the y and z directions and both the bottom and the top layers are assumed semi-infinite in the x direction while the middle layer has a thickness t. In the figure n_s, n_f, n_c, represent the indices of refraction of the different layers. In an effective waveguide, n_s represents the refractive index of the substrate, n_f the refractive index of the film (i.e. the guiding layer), and n_c the index of the cladding (typically the top layer is the air, hence $n_c = 1$).

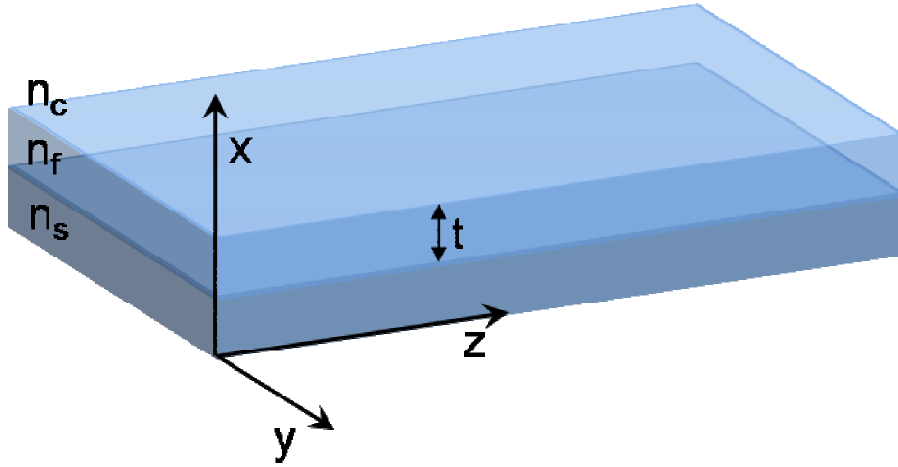

Fig. 2.1: Diagram of a three layer planer waveguide.

A complete and exhaustive treatment of light propagation in planar waveguides was tackled by numerous authors [81,82]. The most interesting aspect of propagation in optical waveguides is represented by the existence of propagation modes, i.e. spatial distributions of "optical energy" in one or more dimensions. The definition of an optical mode can be obtain mathematically by solving the Maxwell's wave equation:

$$\nabla^2 \boldsymbol{E}(\boldsymbol{r}, t) = \left[\frac{n^2(\boldsymbol{r})}{c^2}\right] \partial^2 \boldsymbol{E}(\boldsymbol{r}, t)/\partial t^2 \qquad (2.1)$$

where $\boldsymbol{E}$ is the electric field vector, $\boldsymbol{r}$ is the radius vector , $n(\boldsymbol{r})$ is the index of refraction and c is the speed of light in vacuum. For monochromatic waves, the solutions of (2.1) have the form:

$$\boldsymbol{E}(\boldsymbol{r}, t) = \boldsymbol{E}(\boldsymbol{r}) e^{i\omega t} \qquad (2.2)$$

where ω is the frequency. Substituting (2.2) into (2.1), the following equation can be obtained:

$$\nabla^2 \boldsymbol{E}(\boldsymbol{r}) + k^2 n^2(\boldsymbol{r}) \boldsymbol{E}(\boldsymbol{r}) = 0 \qquad (2.3)$$

where $k \equiv \omega/c$.

If in the three layer structure sketched in Fig. 2.1, the light waves are assumed to be uniform plane waves propagating in the z direction, i.e. $\boldsymbol{E}(\boldsymbol{r}) = \boldsymbol{E}(x, y) \exp(-i\beta z)$, where β is a propagation constant, the equation (2.3) becomes:

$$\frac{\partial^2 \boldsymbol{E}(x,y)}{\partial x^2} + \frac{\partial^2 \boldsymbol{E}(x,y)}{\partial y^2} + [k^2 n^2(\boldsymbol{r}) - \beta^2] \boldsymbol{E}(x, y) = 0 \qquad (2.4).$$

Since the waveguide is assumed infinite in the *y* direction, it is possible to write the equation (2.4) separately for the three regions along *x*:

$$\frac{\partial^2 \boldsymbol{E}(x,y)}{\partial x^2} + [k^2 n_i^2 - \beta^2]\boldsymbol{E}(x,y) = 0 \quad i = s, f, c. \qquad (2.5)$$

The solutions of (2.5) are either sinusoidal (if $[k^2 n_i^2 - \beta^2] > 0$) or exponential (if $[k^2 n_i^2 - \beta^2] < 0$) functions of x, moreover both $\boldsymbol{E}(x,y)$ and $\partial \boldsymbol{E}(x,y)/\partial x$ must be continuous, at the interfaces between the layers. By imposing these conditions the possible modes supported by the structure can be obtained. In a similar way it is possible to solve the Maxwell's equation for the magnetic field $\boldsymbol{H}(x,y)$.

In fig 2.2 the modes in a planar waveguide are represented as a function of β, for a constant frequency ω and assuming $n_f > n_s > n_c$. The last condition is necessary to obtain guided modes (i.e. modes which propagate in the waveguide) in the film region [83].

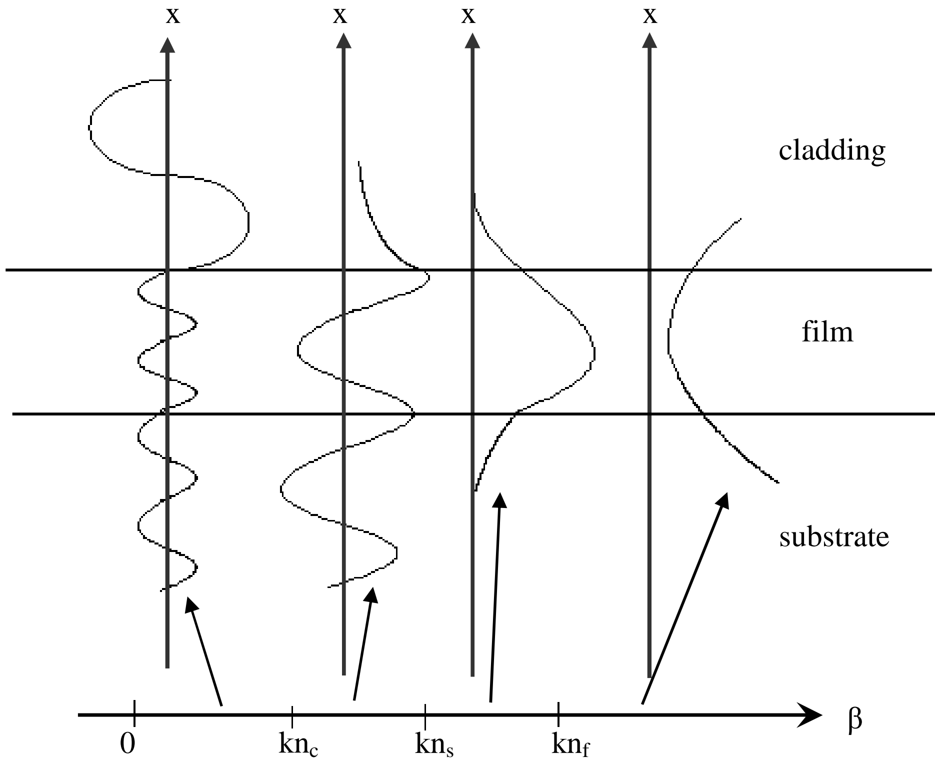

Fig 2.2: Diagram of the possible modes in a planar waveguide as a function of β.

As it can be seen in Fig. 2.2 well confined guided modes can be obtain only for $kn_s<\beta<kn_f$, these modes are generally referred as transverse electric modes, or TE modes, i.e. the electric field is directed parallel to the guide plane and perpendicular to the direction of propagation [84]. For β values greater than kn_f the mode is not physically acceptable since the field increases exponentially in both the substrate and cladding regions, implying an infinite energy. For $kn_c<\beta<kn_s$ the mode is confined at the cladding-film surface but it is sinusoidal in the substrate region, therefore it is supported by the waveguide structure but it loses energy across the substrate and it is not useful for the signal transmission. This kind of modes are defined as substrate radiation modes. Finally if $\beta<kn_c$ the field has a sinusoidal behavior in all the three layers of the waveguide, the modes are not guided modes since they can spread out of the film region, usually they are referred as air radiation modes.

Formally solving the Maxwell's equation and applying the boundary conditions [12], it can be proved that to obtain guided modes in the film region, β can have only discrete values between kn_s and kn_f. Of course the number of modes supported by the waveguide depend on the thickness of the guiding layer, on the index of refraction of the three layers and on the frequency ω. From a practical point of view it is very useful to calculate the cut-off condition, i.e. the values of the parameters below which propagation can not occur. Usually the frequency is fixed by the waveguide application, so it is very useful to calculated the cutoff condition for the index of refraction of the three layers.

In the most relevant cases for this thesis, i.e. the asymmetric planar waveguide in which $n_c<<n_s$ and $n_f\approx n_s$, the cutoff condition is given by [12]:

$$\Delta n = n_f - n_s > (2m+1)^2\lambda_0^2/(32 n_f t^2) \quad (2.6)$$

where m = 0,1,2,… represents the mode number, and λ_0 is the vacuum wavelength.

This relation has been derived for TE modes, but it can be proved [85] that the same condition is still applicable for transverse magnetic modes (TM modes).

2.2 Methods for Planar Waveguide fabrication

As evidenced in the previous chapter there are several methods to realize planar waveguides. In this section the most significant techniques will be briefly reviewed. A particular attention is devoted to thin film deposition methods, namely magnetron

sputtering, chemical vapor deposition, sol-gel processing and ion-exchange technique. The next section will be devoted to the Pulsed Laser Deposition technique, which was employed in this thesis for the deposition of the planar waveguides.

2.2.1 Magnetron Sputtering

In the basic sputtering process, a target (or cathode) plate is bombarded by energetic ions generated in a glow discharge plasma, situated in front of the target. The bombardment process causes the removal, i.e. ”sputtering', of target atoms, which may then condense on a substrate as a thin film, moreover during the process secondary electrons are also emitted [86]. To increase the deposition rate of the process, and the plasma ionization, magnetron sputtering was introduced. In magnetron sputtering a magnetic field is applied in order to force secondary electrons to be in motion in the vicinity of the target, in this way the probability to have an atom-electron collision is increased and consequently a dense plasma can be obtained. For the deposition of insulators, radio frequency (usually 13.56 MHz) sputtering is usually used, to reduce surface charge effects [87,88].

Sputtering was successfully used for the deposition of optical waveguides, both for silicate and tellurite glasses [72,77]. It is worth noting that high gain amplifiers can be obtained starting from thin films deposited by sputtering [72, 89]. In fact, the sputtering method allows to obtain a high index contrast with a consequent good confinement for both signal and pump modes [90], moreover the multi-component glassy thin films deposited present a high quality and homogeneity, which reduces the possibility of rare earth ions interactions and improves the spectroscopic properties of the material [90].

2.2.2 Chemical Vapor Deposition

In the chemical vapor deposition (CVD) method thin films are deposited by the decomposition of high pressure gases (precursors). The gaseous reactants are adsorbed onto the substrate surface and usually the reactions are activated heating the substrate. To reduce the substrate temperature, plasma enhanced CVD (PECVD) can be employed in which the film growth is activated by a glow discharge.

It should be noted that the range of material that can be deposited by PECVD is limited due to the difficulty to choice suitable precursors. In the case of SiO_2, thin films can be

deposited starting from e.g. (SiH_4/O_2) or (SiH_4/N_2 and N_2O) precursors. PECVD was successfully applied to realize low loss silica waveguides (propagation losses ~0.1 dB/cm) [91], and germanosilicate waveguides (propagation losses ~0.2 dB/cm) [92]. Moreover starting from SiH_4 and N_2O gases and P alkoxide and Er chelate, Er phosphosilicate glass waveguides were demonstrated with an optical gain of ~0.7 dB/cm [93].

The main advantage of PECVD is the compatibility with standard silicon-based technology and consequently the integration, onto silicon substrates, of both active and passive waveguides. Moreover low insertion loss waveguides can be realized by PECVD [94].

2.2.3 Sol-Gel Processing

Sol-gel technique can be used to achieve planar glass waveguides more rapidly and less expensively than by more conventional growth techniques, such as CVD. Thin films are usually formed by dipping the substrate into the sol (the sol can be defined as a colloidal suspension of solid particles in a liquid) and subsequently heating and spinning the substrate in order to improve the film uniformity and composition. The "gellation" of the sol creates a continuous suspension and form the thin film. Presently, the realization of silica guiding films with good propagation characteristics has been achieved by many groups working in the field and attention has shifted toward the preparation of more complex materials. Er-doped silica-germania and silica-titania planar waveguides have been widely investigated [95,96]. Er^{3+}-activated SiO_2-HfO_2-$AlO_{1.5}$ and SiO_2-HfO_2-TiO_2-$AlO_{1.5}$ waveguides, prepared by sol-gel processing, presenting a strong and stable PL signal have recently been demonstrated and high Er concentration, up to 1% mol, was achieved in this case [97].

2.2.4 Ion exchange technique

Planar waveguides can be realized not only by the deposition of a thin film onto a substrate with a lower refractive index (respect to the film), but it is possible to employ techniques that directly modify the refractive index of the glass (both bulk or in thin film form).

In ion exchange technique, the change in the refractive index can be achieved by immersion of the substrate into a molten salt bath, which provides a source of alkali ions which slowly exchange with the ions of the substrate material. A dated review about ion exchange glass waveguide fabrication can be found in [98]. Ion exchange planar waveguides were successfully obtained in phosphate and silicate glass with propagation losses below 1 dB/cm [68, 99], moreover both multimode and single-mode Er-doped tellurite planar waveguides were recently demonstrated [100].

2.3 Pulsed Laser Deposition Technique

The Pulsed laser deposition (PLD) technique is a very versatile technique for the deposition of thin films and it was applied to a range of materials and applications [101,102] such as superconductivity [103], diamond-like coatings [104], nitride thin films [105] to name few of the historical applications of PLD technique.
In this section PLD principle of operation and apparatus will be described, highlighting the advantages of PLD technique with respect to the other thin film deposition methods.

2.3.1 PLD: Operation principle

In standard pulsed laser deposition an UV laser, with nanosecond pulse duration, is directed onto a target in a vacuum chamber. UV light is strongly absorbed by many metals and other materials in contrast to IR light [102], for this reason the UV lasers are very attractive for materials processing and thin film production. Typical wavelengths for PLD are obtained from excimer lasers at 248 nm and 193 nm and by tripled Nd:YAG lasers at 355 nm.
The incident light is absorbed by electronic transitions in the solid (target). In a metal or semiconductor the light produces excited electrons which subsequently interact with the atoms. In an insulator (as the materials presented in this thesis) the light is absorbed by interband transitions or transitions from impurity levels, since insulating materials are transparent for photons of energy smaller than that of the band gap. The light is absorbed only for photon energies which exceed the energy of the bandgap or of the impurity

levels. With increasing the laser intensity other absorption processes, e.g. multiphoton and avalanche processes, play an increasing role [106]. A comprehensive review on the fundamental aspects of laser-solid interaction is given in [107]. The laser-target interaction causes an increase in the target temperature [102, 108] and the ejection of material from the target. This "explosive removal" of material expands perpendicularly to the target surface, forming a plume, and it is collected onto a substrate generally placed in front of the target. The accumulation of target material on the substrate from a large number of laser pulses leads to the gradual formation of the film.

Several parameters are a key role on the quality of pulsed laser deposited thin films, for example the laser fluence (the energy per unit area carried by a single laser pulse), the background gases and the substrate temperature. In particular the presence of a background pressure during the deposition is very critical.

In fact background gases (for example an inert gas as argon) change the dynamic expansion of the plume because of the collisions between plume particles and the background gas atoms . The gas actually acts as a moderator reducing the high impact energy of the ablated species [109,110]. The presence of a high gas pressure can be use, for example, to promote the growth of nanostructrured thin films [111].

Moreover a suitable gas can be inserted in the process chamber in order to induce gas chemical reactions between the plume atoms and the gas molecules during the transfer of the target material to the substrate.

In the case of oxide materials, to maintain the oxygen content in the growing film a background pressure of few Pa of O_2 is usually used during deposition.

A unique feature of the PLD is the high kinetic energy of the ablated particles, which strongly depends on the fluence. With time-of-flight spectra a kinetic energy which exceed 100 eV, even at relatively low fluences (~ 2 J/cm^2), has been demonstrated [112]. The collisions within the plasma and with the background gas reduce the energy of the ablated species, therefore to increase the mobility of the adatoms on the substrate surface the temperature of the substrate must be increased. Recently Sambri et al. demonstrated the influence of the substrate temperature also on the dynamic expansion of the plume: a reduction of the background gas resistance to plume propagation as the substrate temperature increases was observed [113].

2.3.2 Advantages of PLD technique

PLD technique presents several advantages with respect to other thin film deposition methods.

- ✓ The ablated species (ions and atoms in the plume) have very higher kinetic energy and internal excitation energy with respect to other techniques, such as sputtering, consequently thin films with a good adhesion to the substrate and good crystalline quality can be deposited at relatively low substrate temperature.
- ✓ Materials with complex stoichiometry can be deposited in a single step by PLD, since laser-target interaction causes the simultaneous evaporation of all the target constituents (congruent ablation). However deficiency of the lighter and most volatile elements (as oxygen) present in the plume can occur in the film composition, nevertheless, the use of a suitable background gas can compensate this deficiency.
- ✓ Reactive PLD is possible using suitable background gas (e.g. N_2 for nitride formation, O_2 for oxide compounds). Moreover since PLD is a non-equilibrium process, the formation of new compounds and metastable phases is possible [114].
- ✓ Multilayer thin films can be easily deposited in a single step by means of a multi-target system.

Two major drawbacks are related to the PLD process and should be considered.
Droplets and particulates can be deposited along with the film, however a careful choice of the deposition parameters (fluence, repetition rate, background pressure) can reduce this problem.
The thickness profile of the deposited films is inhomogeneous. In fact the angular distribution of the ablated materials has a strong peak in the forward direction (the film thickness profile follows a $\cos^n(\theta)$ law, where θ is the angle respect to the direction perpendicular to the target surface, n ranges from 2 to 20 (in vacuum) but even higher values have been reported [115]). It is possible to improve the film thickness profile by

changing the relative position between target and substrate or moving the substrate., In this last case it is possible to achieve uniform thin films on a large deposited area.

2.3.3 PLD of glass oxide planar waveguides

As underlined in the previous chapter glasses are very attractive for photonic applications and in particular for the development of low loss optical waveguides and high gain amplifiers. PLD, because of its unique properties, is very attractive for the synthesis of glass waveguides, however it has been rarely applied to the synthesis of glass oxide thin films.

In 1989 Vogel et al. demonstrated for the first time the possibility to apply PLD to obtain gallate, borosilicate and titanium-niobium silicate glass thin films, [116]. The first pulsed laser deposited Er-doped waveguide was demonstrated by the group of Afonso which exploited the possibility to deposited rare earth doped phosphate glass thin films. Unfortunately due to the poor quality of the substrate very high losses (11 dB/cm in the best case) were obtained [117].

The main reasons for the limited use of PLD for glass deposition is presumably due the difficulties in producing films with good surface quality, in fact surface roughness is a very critical aspect of oxide thin film deposition. As suggested by Mailis et al. the presence of particulate is strongly related to the laser parameters: the use of the 193 nm laser wavelength has been found to lead to smooth transparent phosphate glasses, while the same glass was hardly produced by using the 248 nm wavelength [118]. Moreover a great influence of laser wavelength, oxygen pressure, and thickness uniformity on the quality of lead germanate thin films was found [118]: under optimum conditions (laser wavelength = 248 nm, O_2 partial pressure = 1 Pa, and improved film thickness uniformity) propagation losses of 2.1 dB/cm were obtained.

More recently PLD was applied for the deposition of complex oxide glasses with very interesting and promising results. Gonzalo et al. investigated the properties of heavy metal oxide glass thin films and demonstrated the possibility to achieve by PLD transparent lead-niobium-germanate thin films in a range of composition much broader than in the case of bulk glasses [114]. This very interesting behavior was attributed to

the ability of PLD to produce metastable material phases. Further the influence of the fluence on these films was recently investigated [119]: the fluence was found to induce only weak effects on the film composition, but remarkable effects were found on the film surface morphology. In fact, high propagation losses were found with a minimum (6.5 dB/cm) at 2 J/cm^2 due to the presence of particulates at low fluence values and of large hemispherical droplets at high fluence values. At high energy densities, in fact, subsurface boiling induces the ejection of molten particulates that eventually reach the substrate. On the contrary at low energy densities, the increase of the ablation time required to deposit films leads to the degradation of the target surface and favors the ejection of solid particulates [120]. In a previous work Serra et al. showed that intermediate energy densities have to be used in order to achieve smooth films [121].
In this thesis tellurite and oxyfluoride silicate planar waveguides have been deposited. In fact, PLD, despite of its drawbacks, remains very attractive especially in the case of complex multicomponent oxide materials. Moreover, recently Caricato and co-workers at the University of Salento demonstrated the great advantages of using PLD technique for the fabrication of tellurite and oxyfluoride glass waveguides.
Tellurite thin films exhibiting the lowest propagation losses (0.8 dB/cm) for tellurite planar waveguides and more in general for pulsed laser deposited glass waveguides, have been demonstrated [76].
The role of oxygen background pressure to obtain transparent thin films with optical properties similar to the target ones was demonstrated for oxyfluoride silicate waveguides [122].

2.4 PLD: experimental apparatus

In fig 2.3 the experimental apparatus employed in this thesis for the deposition of the planar waveguides is sketched.

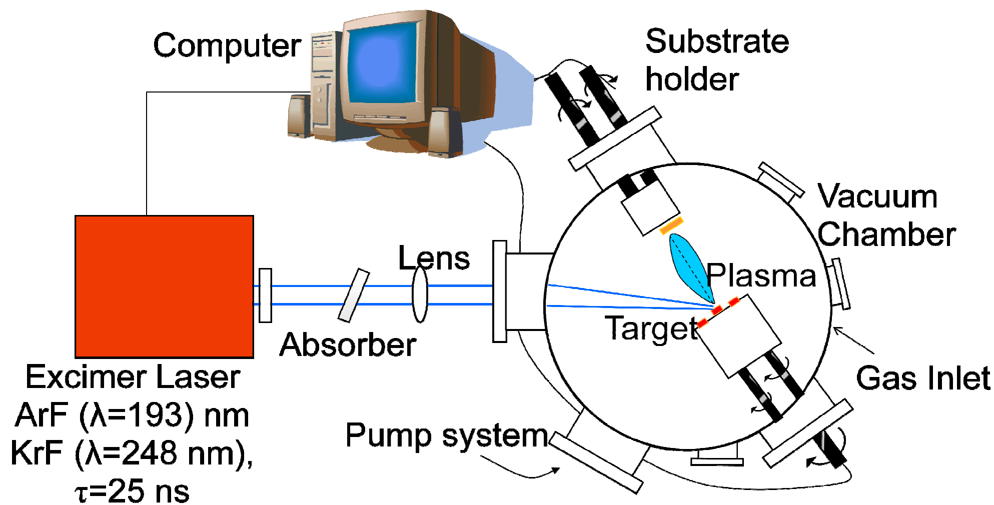

Fig. 2.3: PLD experimental apparatus

The main components of the PLD setup are:

- a multi-gas excimer laser (Lambda Physics LPX 305i) working at two different wavelengths:
  - ✓ 193 nm – ArF mixture;
  - ✓ 248 nm – KrF mixture.

  The laser can deliver a maximum output energy/pulse of about 800 mJ (at 248 nm), the pulse length is ~25 nm;
- a lens (focal length 30 cm), to focus the laser beam onto the target surface (the incident angle of the laser beam on the target is 45°);
- an UV variable attenuator, to select the laser energy and to control the fluence;
- a stainless steel high vacuum chamber equipped with an oil-free vacuum pump system. A dry scroll pump allows to evacuated the chamber from atmospheric pressure to ~ 5 Pa, then a turbomolecular pump is used to reach the high vacuum regime (~ 10^{-5} Pa) needed to perform the deposition;
- a vacuum gauge system formed by:
  - ✓ a capacitive vacuum gauge system (pressure range: atmospheric pressure - ~ 0.1 Pa);
  - ✓ a hot cathode ionization gauge (pressure range: ~ 1 Pa - 10^{-6} Pa);

- a quadrupole mass spectrometer to control the residual gases pressures and composition;
- inlet of reaction or background gases;
- a rotating target holder, which can hold up to three different targets. Two independent target motions allow a uniform ablation of the target and avoid drilling: the target rotates around its axis at a frequency of 3 Hz and it is vertically moved in order to span all the target area. Both the movements are controlled by a computer program;
- two substrate holders: the first can hold up to four substrates kept a room temperature and allows for multiple independent depositions without opening the system to air, the second can sustain a single substrate, and it is equipped with a heater in order to perform deposition at high temperatures (up to 700 °C). Both the substrate holders are mounted on a computer-controlled motion system, which allows two independent movements along the x and y directions in order to obtain uniform films on large area.

2.5 Pulsed laser deposition of tellurite planar waveguides

2.5.1 Experimental

Tellurite films have been produced starting from a tungsten tellurite glass of nominal composition 45%TeO_2–39%WO_3–15%Na_2O–1%ErO_3 (%mol).

An ArF excimer laser beam (λ=193 nm, τ=25 ns) was focused onto the target surface in order to obtain a laser spot of 1.7 mm^2. The laser beam energy was adjusted by means of a variable attenuator in order to achieve a laser fluence on the target surface of about 2 J/cm^2.

The films were deposited at three different substrate temperatures (RT, 100°C and 200°C) on pure silica (from Hereaus) in a background pressure of molecular oxygen (5 and 10 Pa).

The distance between the target and the substrate was 55 mm when operating at room temperature, and 45 mm for depositions performed at 100°C and 200°C.

Before starting the depositions the chamber was evacuated to a base pressure of 3×10^{-5} Pa, and the mass spectrum of the residual gases was acquired. Before the deposition 1000 laser pulses were used to remove a superficial layer from the target surface in order to avoid film contamination. A total number of 40000 laser pulses was used for each deposition. The substrate was mounted on a computer-controlled motion system and during the deposition was moved along a rectangular path in order to obtain a homogeneous thickness profile.
In table 2.1 the deposition parameters for the tellurite planar waveguides are summarized.

Tab 2.1: Parameter for the deposition of the tellurite planar waveguides

Sample	Substrate	$d_{Tar-Sub}$ (mm)	Fluence (J/cm^2)	Pulses number	$P(O_2)$ (Pa)	Substrate Temp (°C)
RT5P	Silica	55	2	40000	5	RT
100T5P	Silica	45	2	40000	5	100
200T5P	Silica	45	2	40000	5	200
200T10P	Silica	45	2	40000	10	200

The optical transmission spectra of the films were acquired by using a double beam spectrophotometer (Perkin-Elmer Lambda 900), in the NIR-Visible-UV regions (200-2500 nm).
Optical transmission spectra were analyzed by means of the Swanepoel method [123]: the thickness of the films and the dispersion curves of the refractive index (n) and of the extinction coefficient (k), were inferred from the spectra.
The thickness and the refractive index of the waveguides at 543.5, 632.8, 1319 and 1542 nm were also measured in TE and TM polarization by an m-line apparatus (Prism coupler 2010 – Metricon) based on the prism coupling technique [124], a rutile prism was used for coupling. The losses at 632.8 nm were measured by photometric detection of the light intensity scattered out of the waveguide plane, after the coupling of the light in the different mode.
The erbium luminescence of the samples was measured in waveguiding configuration (obtained through a rutile prism coupling) by exciting the sample with 514.5 nm Ar^+ ion laser. The luminescence was dispersed by a 320 mm single-grating monochromator (Jobin Yvon mod SPEX 320M) with a resolution of 2 nm. The signal was measured by

using InGaAs detector and a lock-in amplifier with the chopper frequency of 72 Hz. To measure the lifetime of the $^4I_{13/2}$ level, the luminescence signal was recorded by a digital oscilloscope (Tectronix mod. TDS 350).

Finally to check the stoichiometry of the films Rutherford backscattering spectroscopy (RBS) was performed, using a $^4He^+$ beam at 2.2 MeV. Films with a lower thickness respect that ones deposited on silica substrates were deposited on <100> silicon substrates to allow a non-ambiguous identification and quantitative determination of the different elements present in the films.

2.5.2 Results

Optical properties

Figure 2.4 shows the transmittance spectra of the films deposited at increasing substrate temperature (RT, 100°C and 200°C), at the same O_2 pressure (5 Pa). The films transmittance decreases as the substrate temperature increases. The oscillations observed in the spectra are typical fringes due to interference between the light reflected at the air-film and film-substrate interfaces.

Using the transmission spectra as input a computer code (Refractor), based on the Swanepoel method [125], calculated the dispersion curves of the refractive index n and of the extinction coefficient k for the different films (Figures 2.5 and 2.6). Higher values of refractive index and extinction coefficient were determined for the films deposited at 100 °C and 200 °C with respect to the ones deposited at RT.

10 Pa of O_2 ambient pressure was necessary to obtain a transparent film for deposition performed at the highest substrate temperature: the comparison between the transmission spectra of the films deposited at 200°C in different O_2 pressures is shown in figure 2.7.

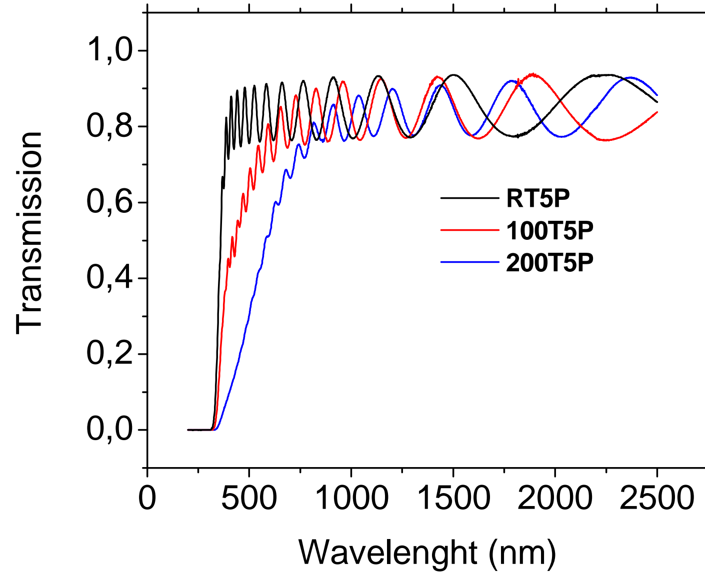

Fig. 2.4: Transmission spectra of the films deposited at different substrate temperatures in 5 Pa of O_2.

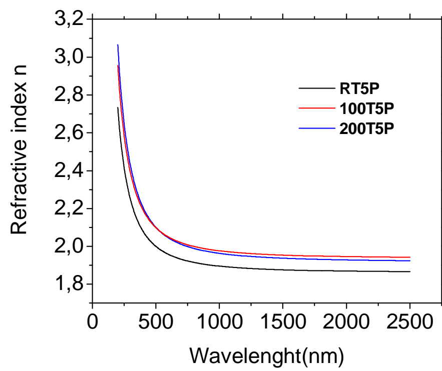

Fig. 2.5: Refractive index of the films deposited at different substrate temperatures in 5 Pa of O_2.

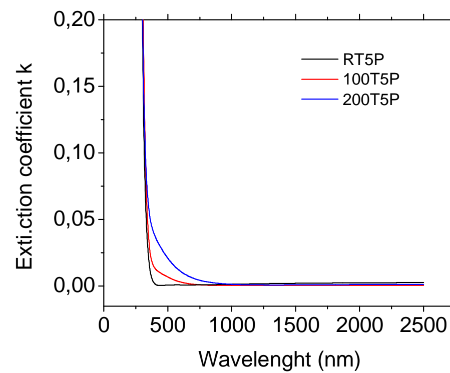

Fig. 2.6: Extinction coefficient of the films deposited at different substrate temperatures in 5 Pa of O_2.

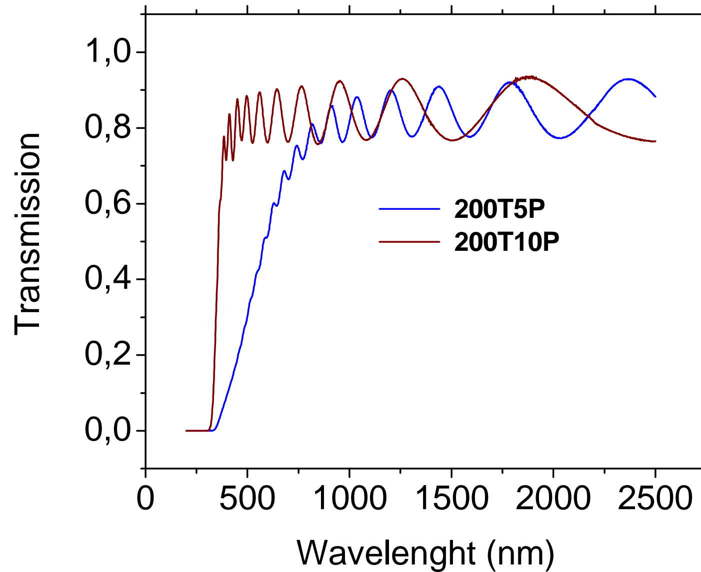

Fig 2.7: Films deposited at 200 °C at 10 Pa of O_2 (blue line) and at 5 Pa of O_2 (red line).

To control the guiding properties of the thin films, m-line spectroscopy was performed. The film deposited at 100 °C and 200 °C in 5 Pa of oxygen did not show good coupling of light at 543 nm, while the modes at 632.8 nm are very broad , this behaviour could be reasonably inferred to the high absorption in this region. A further evidence of this hypothesis is provided by the fact that these samples showed a better coupling (respect to the previous wavelengths) and sharp modes at 1319 and 1542 nm.

On the contrary the sample RT5P and 200T10P are transparent and colorless and exhibit good coupling of light. Fig 2.8 highlights this behavior, evidencing the quality of the coupling by prism method in the different waveguides at a wavelength of 632.8 nm for the TE modes.

A comparison between the refractive index and thickness values obtained by the transmission spectra analysis and the m-line technique is reported in table 2.2. The error in the refractive index measurements is about ± 0.002 and in the thickness is ± 50 nm for m-line and ± 40 nm for Refractor code. The thickness values are in good agreement within the experimental errors, while the refractive index values measured by the

Refractor code is lower then the m-line ones. The same behaviour was found in a previous work [122], and it could be explained by the non uniform thickness of the films.

Tab. 2.2: Comparison between the refractive index values and thickness obtained by the m-line measurements and the Refractor code for the RT5P waveguide. The value of the bulk refractive index is reported in last column for comparison.

Sample RT5P (T=RT, $P(O_2)$=5Pa)	M-line	Refractor	Bulk
n @ λ=543 nm	2.074 ± 0.002	1.978± 0.002	2.072± 0.002
n @ λ =632.8 nm	2.049± 0.002	1.947± 0.002	2.055± 0.002
n @ λ =1319 nm	1.994± 0.002	1.880± 0.002	-
n @ λ =1542 nm	1.987± 0.002	1.875± 0.002	-
Thickness (nm)	1137± 50	1193± 40	-

To evaluate the influence of the oxygen pressure and temperature on the film optical quality the refractive index of the RT5P and 200T10P samples, calculated by m-line technique, were compared (it is worth noting that both the films are transparent. The refractive index at four different wavelengths were fitted with a Cauchy dispersion law: $n=a + b/\lambda^2$ where n is the refractive index, λ the wavelength and a and b the fitting parameters. In fig 2.9 the fitting results were reported. As can be immediately seen, increasing the oxygen pressure and the temperature, an increase in the refractive index can be observed.

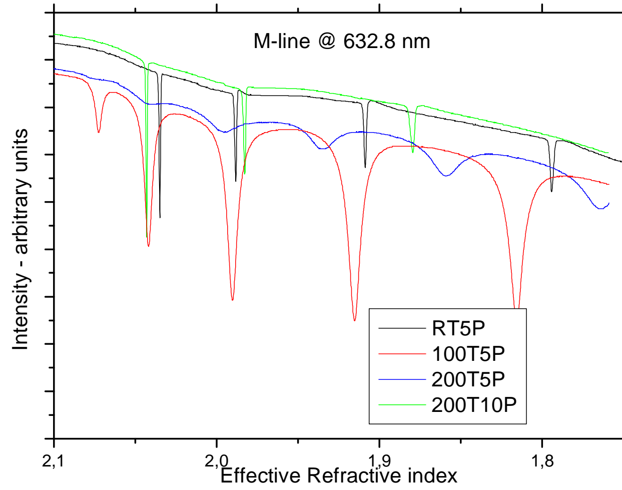

Fig 2.8: M-line spectra (at 632.8 nm) of the tellurite thin films deposited in different experimental conditions. Increasing the substrate temperature the quality of the light coupling decreases. At the highest used temperature (200°C) 10 Pa of oxygen were necessary to improve the light coupling.

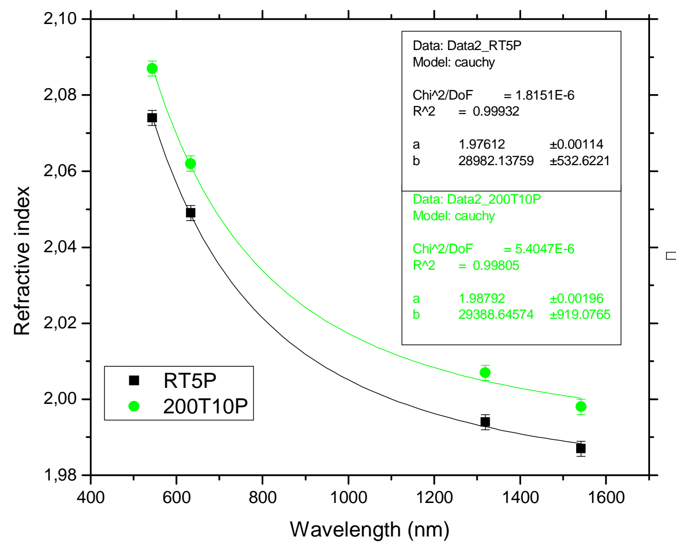

Fig 2.9: Refractive index of the transparent films deposited in different temperature and background oxygen pressure (RT-5 Pa (black), 200 °C -10 Pa (green)), as measured by m-line technique (scatter). The dispersion curve, as obtained by fitting the experimental data with a Cauchy law, are reported along with the relative fitting values.

Loss measurements

It was not possible to perform loss measurements on the samples 100T5Pa and 200T5Pa since they didn't show propagation. Unfortunately the sample 200T10P ruined very soon consequently loss measurements were performed only on the sample RT5P.

The results of the losses at 632.8 nm for this waveguide are very high and are reported in table 2.3

The unit is dB/cm and the error (due to short propagation length and high scattering), has to be considered very high (5dB/cm).

Tab 2.3: Losses for RT5P waveguide

n° mode	TM	TE
1	9	18
2	15	18
3	18	15

IR luminescence

Though the sample 200T10P did not show good propagation at 514 nm as compared to the RT deposited one, the luminescence intensity of Er (at 1530 nm) in the former looked higher than the Er luminescence in sample RT5P in similar experimental conditions.

The shape of luminescence appears different with respect to the bulk one (the emission cross section was calculated from absorption spectrum), especially in RT5P sample as evidenced in figure 2.10. It witnesses a change of environment of rare earth ions.

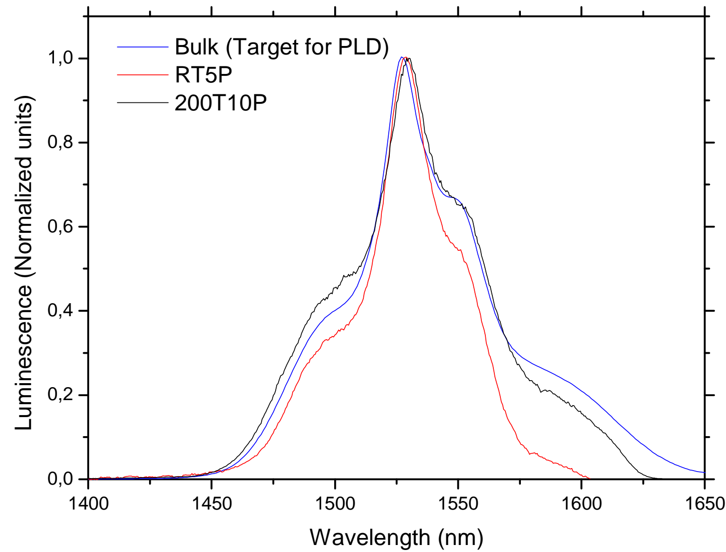

Fig 2.10: Er photoluminescence spectra of RT5P and 200T10P samples. The PL of the bulk is reported for comparison.

The lifetime of the 200T10P sample was measured at two different laser powers (360 mw and 200 mw on the prism) (Fig 2.11). The experimental values were fitted with a single exponential decay. The lifetime measured at the higher power was 0.67 ± 0.1ms lower than the one measured at the lower power (0.75± 0.1ms), due to the presence of an increased depopulating rate of $^4I_{13/2}$ level due to upconversion (or other cooperative process).

The luminescence signal was very low so the lifetime was measured using an amplified signal.

The lifetime of sample RT5P was found to be much lower (<0.2 ms) and not determinable while using the amplifier.

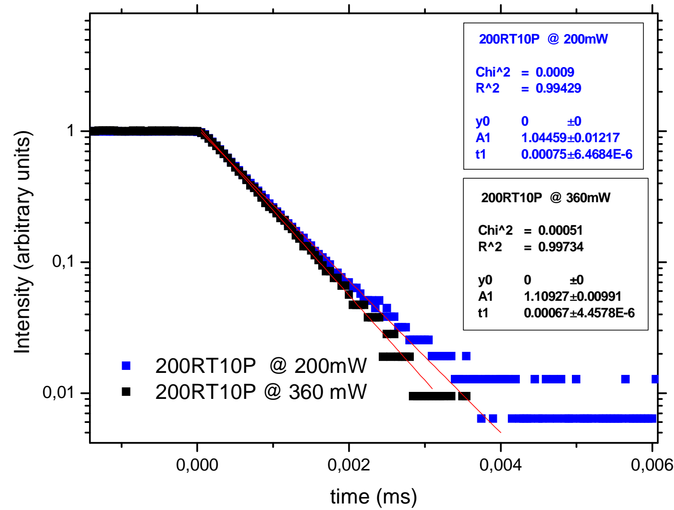

Fig. 2.11: Lifetime of the $^4I_{13/2}$ level for the sample 200RT10P at two different pump power: 200 mW (blue) and 360 mW (black), @ 514 nm

Compositional analysis

To correlate the optical properties with the stoichiometry of the films, RBS analysis was performed and the experimental spectra were simulated with the RUMP computer program [126] . In table 2.4 the results of RBS analysis are reported. Films deposited at RT and at 100 °C presented almost the same composition of the target. At the substrate temperature of 200 °C two aspects become evident: on one hand the oxygen content of the film decreases, on the other the relative concentration of tungsten atoms appears to increase. At highest temperature (200°C) the lack of oxygen is partially restored using a higher O_2 pressure (10 Pa) during the deposition.

Tab. 2.4: Composition of target and films as determined by RBS, the error is 5%.

Sample	%O	Te%	W%	Na%	Er%
Target	66.2	13.2	11.5	8.8	0.3
RT5P	66.4	14.3	12.4	6.3	0.6
100T5P	66.4	14.3	12.4	6.3	0.6
200T5P	60.4	15.9	15.9	7.1	0.7
200T10P	62.4	14.9	14.9	6.6	0.7

2.5.3 Discussion

A fundamental issue, for optical application, is the transparency of the films in the wavelength range of interest (the IR range for waveguide amplifier). In literature the role of oxygen background pressure in the deposition of transparent glassy oxide thin films is extensively discussed [127], while the role of the substrate temperature is often ignored. Usually in PLD process, the substrate temperature has the role to promote the crystalline growth, increasing the mobility of the adatoms, consequently no much attention is devoted to the temperature in the case of amorphous materials. The results presented in this thesis clearly show that the temperature can have a critical function in the growth mechanisms.

RBS analysis demonstrated that even if the ablation process lead to a congruent transfer of the target stoichiometry to the layer, the films grown at different temperatures can have very different physical and optical properties. It is worth noting in fact the RT5P and 100T5P films present the same composition and have the same stoichiometry of the target within the experimental errors, nevertheless they are very different in terms of transparency. The complex physical phenomena (dynamic expansion of the plasma plume and the plume-sample interaction) involved in the growth of the PLD films could contribute to different rearrangements (respect to the target) of the ablated material on the substrate surface. From the results it is evident that the substrate temperature induces

additional effects on the film bonding formation and configuration. These effects could be related to the network rearrangement originated by the heating as a consequence of changes in the surface mobility of the ablated products during the growth process.

The fact the film deposited at 200 °C shows a lower content of oxygen respect to RT and 100 °C deposited films suggests that surface oxidation processes are relevant in the case of tellurite thin film deposition, and that temperature can affect the oxidation state of the deposited materials. Oxygen is the main constituent of glasses and can enter in the glass network either as a bridging or non-bridging ion [128]. Oxygen deficiency modifies the glass structure and can even prevent its formation, moreover a high oxygen deficiency generally leads to absorbing films [127]. Obviously the high absorption prevents the propagation in the waveguide, as evidenced by m-line technique, and consequently the use of such films as waveguides.

A very interesting behavior is represented by the dramatic change in the properties of the films increasing the oxygen background pressure: a high transmission is achieved and the guiding properties of the layer are improved. This fact is not surprising, since increasing the oxygen pressure, oxidation of the ablated species can occur during the plasma expansion, consequently the formation of monoxides in the gas phase contributes to the increase of the overall oxygen content in the films, moreover monoxides have a lower angular scattering than atomic oxygen and as a consequence a narrow deposition distribution, due to their higher mass with respect to atomic oxygen.

Nevertheless it is interesting to note that the films still remain sub-stechiometric in oxygen, therefore the increase in the oxygen content can not fully explain the remarkable change in the film properties. Gonzalo and co-workers demonstrated in the case of lead-niobium-germanate glass, the possibility to obtain transparent films presenting a lower oxygen content than the bulk one [114]. In the case of tellurite thin films the same behavior can be observed and it can be ascribed to the unique capabilities of PLD to form metastable phases.

Concerning the luminescence and waveguide properties, the results are not satisfactory. Even for the RT5P sample which presents optical properties (transparency and refractive index) very close to the bulk ones, the Er IR luminescence is quite different from the target one, and the lifetime is very short, as a consequence a modification in the glass

network formation and in the rare earth ion environment can be supposed. The sample 200T10P showed better luminescence properties respect to the previous one, unfortunately it ruined very soon and a complete characterization of its properties was not possible. Probably the structural weakness of this sample can be ascribed to the substrate temperature used during the deposition and in particular to the stress induced during the growth by the different expansion coefficient of film and substrate.

2.6 Pulsed laser deposition of oxyfluoride silicate planar waveguides

2.6.1 Experimental

The experimental setup for the deposition and characterization of the silicate planar waveguides was similar to the one presented in the previous section, for this reason in this section only the remarkable differences between the two apparatus will be underlined. Er-doped silicate thin films were deposited by the PLD technique using a target glass of nominal composition $65SiO_2$ – $3Al_2O_3$ – $11Na_2O$ – $10PbF_3$ – $10LaF_3$ – $1ErF_3$ (% mol). During preliminary tests we found that ablation with a KrF laser resulted in poor quality films with microcrystalline structure. The deterioration in the film transmission characteristics was attributed to the reduced absorption of the 248 nm radiation by the target. Consequently the silicate glass target was ablated using an ArF excimer laser (λ=193 nm, pulse length ~ 25 ns). The laser fluence at the target surface was set at 2 J/cm^2, just above the ablation threshold, to obtain a smooth ablation process. The ablated material was collected on a 7 cm^2 substrate made of pure silica. Due to the quite large area of the substrate a particular attention was devoted to the substrate motion to ensure a high uniform thickness of the film.

The influence of substrate temperature was investigated and the depositions were performed from RT to 350 °C.

For each deposition up to 1x10^5 consecutive laser pulses were used. A dynamic flow of oxygen at the pressure of 5 Pa was maintained in the chamber. Preliminary tests showed that this was the lowest optimal pressure which ensured a good transparency of the films. Pressures higher than this value yielded clustered films with whitish appearance,

whereas at lower pressures than 5 Pa, the deposited films had color centers in visible and near-IR and consequently enhanced attenuation in these spectral regions.

Table 2.5 summarizes the used parameters for the oxyfluoride silicate thin films depositions.

Tab. 2.5: Parameter for the deposition of the oxyfluoride silicate planar waveguides

Sample	Substrate	$d_{Tar-Sub}$ (mm)	Fluence (J/cm^2)	Pulses number	$P(O_2)$ (Pa)	Substrate Temp (°C)
SRT	Silica	55	2	100000	5	RT
S200	Silica	55	2	100000	5	200
S300	Silica	55	2	100000	5	300
S350	Silica	55	2	80000	5	350

Since silicate thin films have lower refractive index than tellurite ones, m-line measurements were performed using a different prism (Metricon 200-P-1 prism), with the same m-line apparatus (Metricon 2010).

The waveguide losses were measured by the optical fiber method: in a first step the light was inserted into the waveguide by the prism coupling method then the loss measurement was performed by scanning a fiber optic probe down the length of the propagating streak to measure (by InGaAs photodetector) the light intensity scattered from the surface of the guide. The assumption is that at each point on the propagating streak the light scattered from the surface and picked up by the fiber is proportional to the light which remains within the guide. The best exponential fit to the resulting intensity vs distance curve yields the loss in dB/cm.

The PL spectra and lifetime measurements were not acquired in waveguide configuration, since a different experimental setup was used, namely an Edinburgh Instrument Ltd spectrometer (mod. FLS920P) using an InGaAs detector. For PL measurements the samples were excited with an Ar+ ion laser while for lifetime measurements a Xe arc lamp was employed.

The morphology of the films was studied by using optical microscopy, and a Field-Emission Scanning Electron Microscopy (SEM-FEG), LEO Gemini 1530, for high

resolution, up to 1-2 nm, working at 3 kV. The samples before to be submitted to SEM analysis, were coated with 3 nm of gold in order to avoid effects of electronic charge.

2.6.2 Results

Optical properties

The deposited films were observed to be transparent to the naked eye. In Fig. 2.12 the transmission spectra of the films deposited at different temperatures are shown. The waveguides showed a transmission higher than 90% in the wavelength range of interest, very close to the substrate transmission value which is 92%. The less pronounced ripples, respect to the case of tellurite thin films, are due to the small difference between the substrate and thin film refraction indexes. The transmission spectra were analyzed by the Refractor code to obtain the spectral dependence of the refractive index and extinction coefficient.

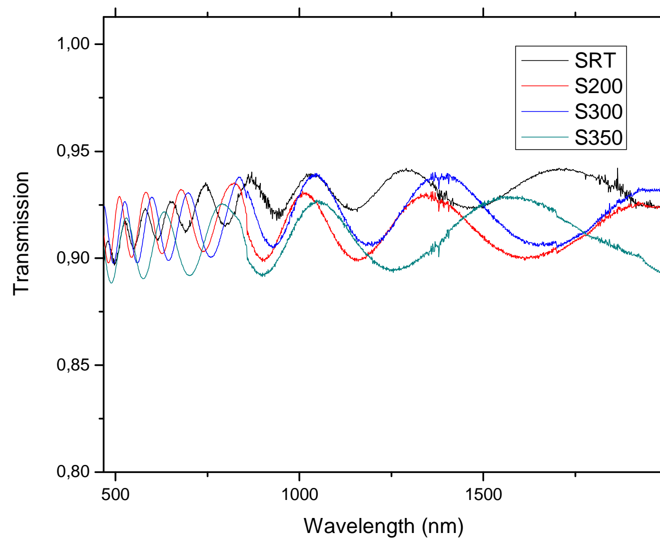

Fig. 2.12: Transmission spectra of the oxyfuoride silicate thin films deposited at different temperature

M-line analysis performed on the samples at two wavelengths, 632.8 nm and 1321 nm, showed that all the thin films supported guiding modes, moreover all the waveguides

exhibited very good coupling of the light. The refractive index and the thickness of the waveguide as obtained by m-line analysis are summarized in table 2.6. The error in the refractive index measurements is about ± 0.002 and in the thickness is ± 50 nm.

Tab. 2.6: Refractive index, thickness and number of optical modes measured using m-line spectroscopy at 632.8 nm and 1321 nm.

Sample	SRT (RT)		S200 (200°C)		S300 (300 °C)		S350 (350 °C)	
Source (nm)	633	1321	633	1321	633	1321	633	1321
Ref. index (± 0.002)	1.524	1.507	1.568	1.552	1.590	1.574	1.591	1.575
Thickness (nm) (± 50)	1755		1342		1333		1000	
Number of modes	3	1	3	1	3	1	2	1

It is immediately evident that increasing the temperature the refractive index of the films increases. This trend is further evidenced in the figure 2.11, where the refractive index of the films as a function of the substrate temperature is reported. In the insets, the dispersion curve of the refractive index and of extinction coefficient, as obtained by Refractor, at two representative temperatures (RT and 200°C) are reported.

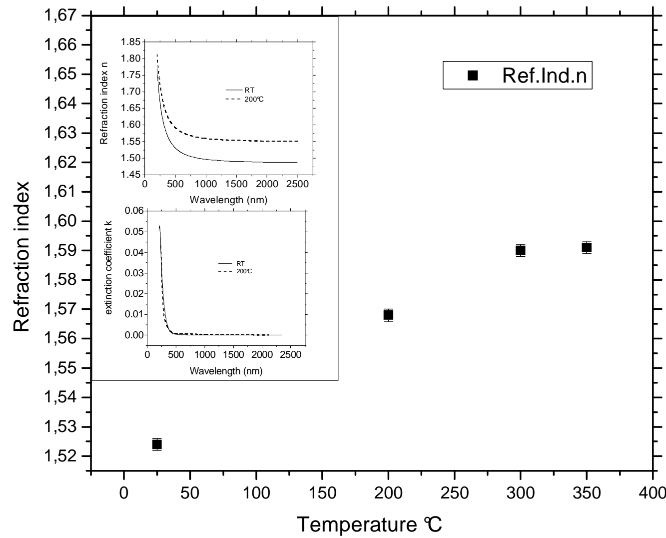

Fig. 2.11: Thin films refractive index as a function of substrate temperature. In the insets the dispersion curve of n and k are reported for two representative temperature (RT and 200 °C)

Loss measurements

The surface of the films deteriorated as a result of the different analyses performed on the samples, consequently the prism coupling of the light became very difficult. Propagation losses could be measured only on the samples SRT and S200. In tab 2.7 the results, at the wavelength of 632.8 nm, are reported. Very low values were obtained in the range of 1dB/cm.

Losses for the S300 sample were roughly estimated for the TE_0 mode and a value of ~3.5 dB/cm was obtained.

Tab. 2.7: Propagation losses (dB/cm) for each of the optical modes of SRT and S200 waveguide as measured by prism coupling and detecting the scattered light (at a wavelength of 633 nm).

Sample	Mode 1	Mode 2	Mode 3
SRT	1.02	0.83	0.74
S200	1.20	2.00	2.44

IR Luminescence

IR analysis was not performed in waveguide configuration, but lighting directly the sample surface. No Er photoluminescence signal was detected for the SRT sample even at high pump power (above 1 W). Fig 2.12 shows the PL spectra of the silicate thin films deposited at different temperatures, acquired in the same experimental condition. The PL intensity of the films appears to improve increasing the temperature.

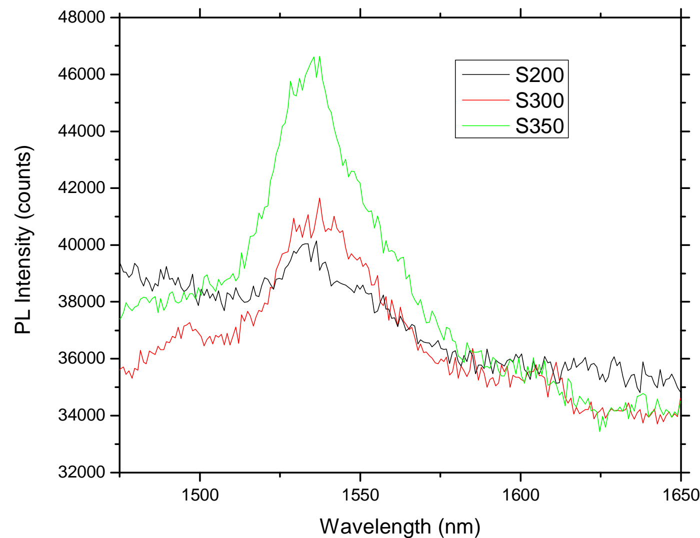

Fig. 2.12: Er photoluminescence spectra of the S200, S300, S350 sample, acquired in the same experimental condition.

The lifetime was measured for all the samples using a setup similar to the PL one, but by means of a Xe arc lamp. The intensity decays were fitted by a single exponential law, but very poor results were obtained: the resulting lifetimes were much lower than the target one (10 ms), and the fitting function did not agree well with the experimental data. The intensity decay were fitted with a double exponential curve, two contributes can be distinguish, a fast decay (with lifetime τ1), and a second slower decay with a characteristic lifetime, τ2, similar to the bulk one. In order to fix the attention to the first decay process, which is assumed to be caused by cooperative processes between Er

ions, the fitting procedure was repeated assuming a value equal to the bulk one for τ2. In Fig 2.13 the experimental values along with two different fit results, namely single exponential and double exponential decay (with fixed τ2), are reported. The values of τ1 obtained by the fitting procedure are reported in table 2.8. τ1 appear to be longer with higher deposition temperatures.

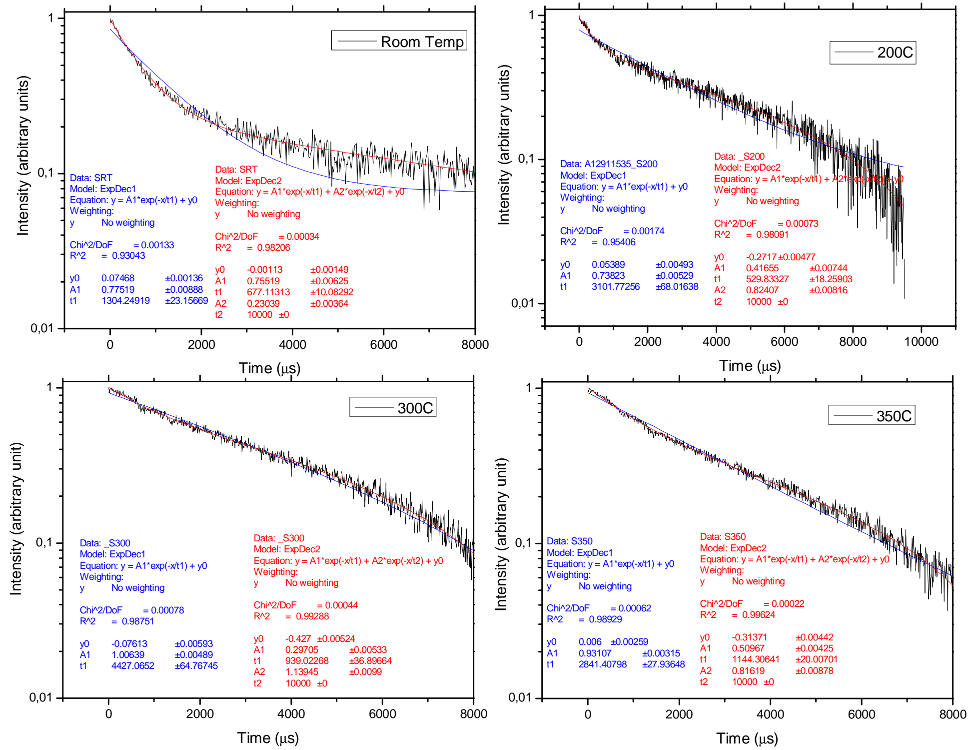

Fig. 2.13: Lifetime of the $^4I_{13/2}$ level for the samples deposited at different temperatures. The experimental values were fitted by a single exponential (blue) and a double exponential (red) decay.

Tab. 2.8: τ1 values obtained by fitting the intensity decay with a double exponential curve and fixing τ2 at 10 ms.

	SRT	S200	S300	S350
τ1 (µs)	677 ±10	530±20	940 ±40	1144 ±20
τ2 (ms)	10	10	10	10

Film morphology

The silicate thin films were subjected to SEM inspection in order to examine the film morphology. In Fig 2.14 the SEM images of the different films are shown. The temperature strongly influenced the structure of the films. The films presented a micro-grain structure and increasing the temperature the grain dimensions decreased and the films appeared more dense. This aspect was in agreement with the increase of the refractive index at high temperatures.

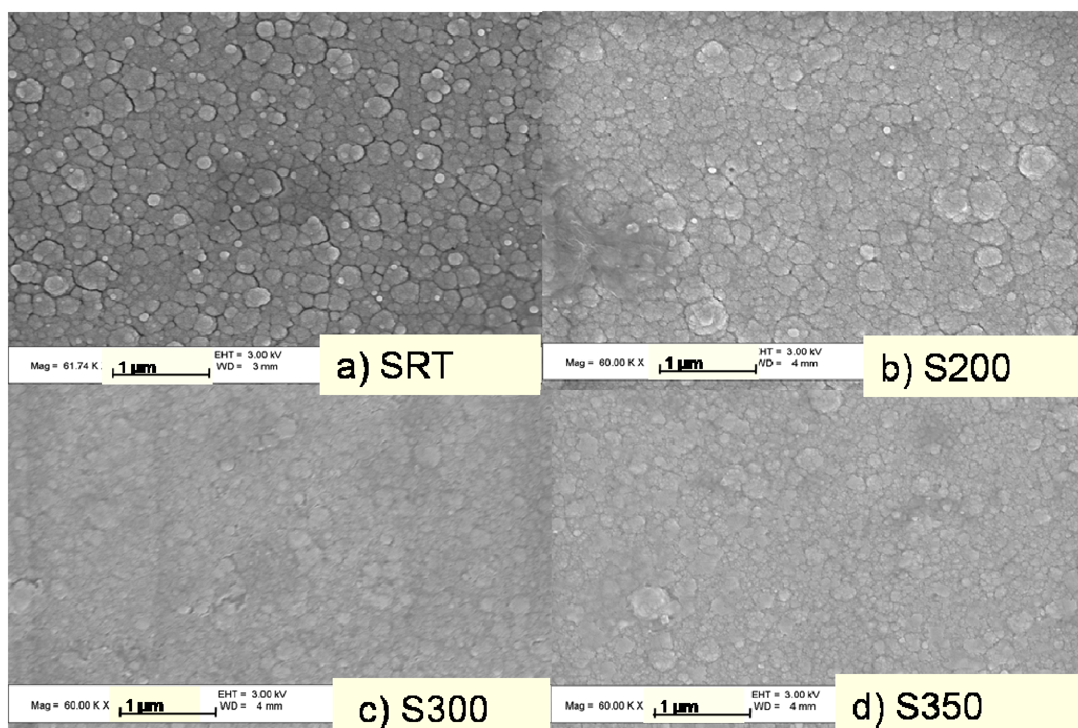

Fig 2.14: SEM pictures of the silicate thin films deposited at different temperatures

2.6.3 Discussion

For the deposition of oxyfluoride silicate waveguides the temperature is found to have a fundamental role as in the case of tellurite thin films. Two important effects can be distinguished: from one hand the temperature influences the glass network formation, from the other hand it strongly affects the morphology and the structure of the films.

The effects of substrate temperature on silica-based thin films were studied by Serra and co-workers, which found a shift of the Si−O−Si stretching frequency with the substrate temperature [121].

In the case of the silicate thin films studied in this thesis the increase in the substrate temperature has two main consequence: an increase in the refractive index of the deposited thin films and an increase in the erbium luminescence.

Concerning the last aspect, it is possible to suppose that substrate temperature promote the right glass network formation and above all, the arrangement of the erbium ions in the correct network sites. The temperature is responsible of an increase in the mobility of the deposited species, and consequently the film bonding configuration can be affected, as demonstrated by Serra et al.. In particular the high temperature seems to inhibit erbium-erbium interaction. This assumption is justified by the increase in the erbium photoluminescence at high temperatures, due probably to a reduced quenching effect.

A further validation of this hypothesis is supplied by the lifetime behavior: an initial fast decay component can be observed, which evolves into a slower decay. This trend can be attribute to cooperative processes between rare-earth ions which depopulate the $^4I_{13/2}$ level.

If the lifetime of the slower component ($\tau 2$), is assumed equal to the bulk one, as presented in the result section, the lifetime of the fast decay ($\tau 1$) can be assumed as a direct measurements of the quenching effect. From the data of table 2.8 it is evident that the S350 sample has the highest $\tau 1$value, consequently the lowest quenching effects.

Substrate temperature appears to influence also the microstructure of the films. The films are formed by a grain structure and in particular increasing the temperature the films appear to be formed by smaller grains. Moreover films deposited at 300°C and 350°C do not show a valuable contrast amongst the particles, possibly indicating a higher cohesion and a higher film packing density. This aspect is evidenced by the SEM images and confirms the behavior of the increase of the refractive index with the temperature. This aspect is very interesting for technological reasons since it could allow to tailor the characteristic of the films simply changing the substrate temperature during deposition.

It is worth noting, in fact, that all the films are very transparent and above all the waveguides exhibit good propagation properties. In particular very low losses (in the range of 1 dB/cm) have been found.

Another interesting properties of the films deposited at high substrate temperatures is their robustness. In fact, a different behavior was observed between the samples deposited at room temperature and the ones deposited at higher temperatures when submitted to SEM inspection.

Due to the nature of the SEM apparatus, structural changes can be viewed in real time during the inspection. The film deposited at RT was crack free at the beginning of SEM analysis, but cracks were seen to appear in real time as a result of the interaction with the electron beam. The film deposited at higher temperatures, remained crack-free after inspection. In figure 2.15 the SEM images of the SRT and S200 samples are reported: the films fabricated on moderately heated (200 °C) substrates were found to withstand the SEM inspection. This aspect even if not surprising is very interesting from a technological point of view, in fact robust and stable films are well suited for the development of integrated circuits since they could be submitted to all the standard processes employed in integrated optics, such as lithography and etching.

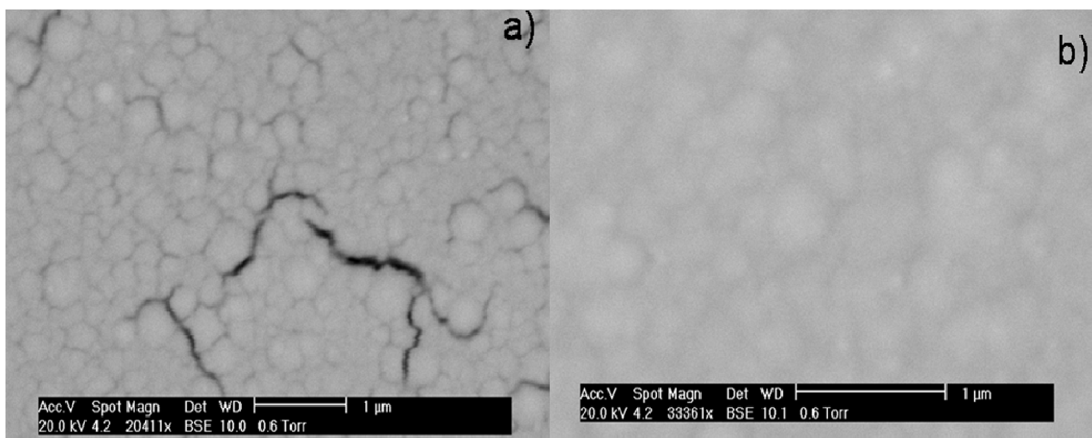

Fig. 2.15: SEM images of films deposited at RT (a) and at 200 (b).

Chapter 3

2D Oxyfluoride Silicate Waveguide

Contents

3.1 Rectangular Waveguides ... 65
3.2 2D waveguide fabrication ... 66
3.2.2 Reactive Ion Etching: operation principle and apparatus ... 67
3.2.2 Reactive Ion Etching of glasses ... 69
3.3 2D waveguide fabrication by "Standard Method" ... 70
3.3.1 Experimental ... 70
3.3.2 Results ... 71
3.3.3 Discussion ... 75
3.4 2D waveguide fabrication by "Inverse Method" ... 76
3.4.1 Experimental ... 76
3.4.2 Results ... 79
3.4.3 Discussion ... 82

Several applications require optical confinement in two dimensions therefore planar waveguides present in many cases some limitations and can not be used. For example two dimensional confinement is useful to guide light from two point of an optical integrated circuit or to interconnect two circuit elements. In this chapter, after a brief introduction to rectangular waveguides, two different technological approaches to obtain 2D waveguides will be presented, the "standard method", in which the 2D waveguides were etched in the PLD films, and the "inverse method", in which the channels were defined in the bulk substrate and then the waveguide were deposited inside the channels by PLD. The results obtained for 2D oxyfluoride silicate waveguide fabrication and characterization will be presented and discussed.

3.1 Rectangular Waveguides

Figure 3.1 schematically shows the cross sections of different waveguide structures which can be used to obtain 2D confinement.

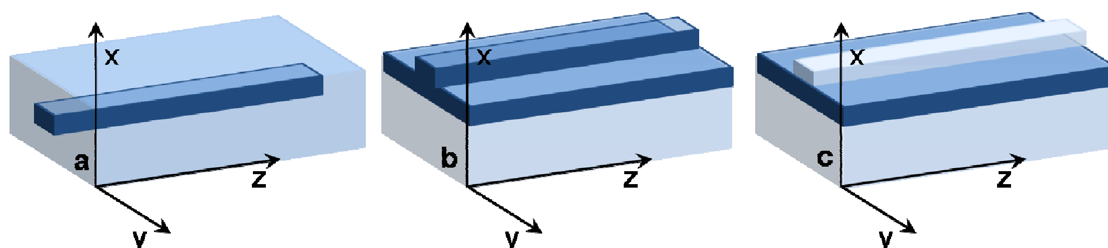

Fig. 3.1: Different structures to realize rectangular waveguides.

The channel waveguide (Fig. 3.1.(a)) is the basic rectangular waveguide and consists of a waveguide region surrounded by a medium which presents a lower index of refraction respect to the guiding core. A variation on the channel waveguide structure is the ridge waveguide (Fig. 3.1(b)), in which the lateral confinement is achieved removing laterally a portion of the planar waveguide in order to create a refractive index contrast between the high refractive index core layer and the air. Optical mode confinement can also be obtained by putting a strip of cladding material on a planar core layer, resulting in a strip loaded waveguide (Fig. 3.1 (c)).

The exact solution of the wave equation for a general rectangular waveguide, i.e. a core layer surrounded by one or more different materials, with lower refractive index, is extremely complicated and it has not been obtained yet. However it is possible to obtain approximate solutions assuming that the guiding modes supported by the waveguide, are "well guided", i.e. well above the cutoff condition. Under this assumption it is possible to consider that the electromagnetic fields decay exponentially out of the guiding region. Imposing this condition it is possible to solve the Maxwell's equations in the core region and to found the modes supported by the waveguide [129]. As in the case of planar waveguide, rectangular waveguides support a discrete number of guided modes. The mode are usually distinguished by two mode numbers, which correspond to the number of peaks of the field distribution in the x and y directions.

As evidenced exact analytical methods are heavily restricted to the analysis of only very simple slab devices, consequently, for the analysis of more complex structures, in the last years much attention has been focused on Numerical and approximate Semi-Analytical methods [130]. Such methods can obviously be applied to rectangular waveguides and they allow not only to calculate the number of modes but also to simulate the light propagation in the guiding region. In chapter 4 a discussion about numerical methods will be provided

3.2 2D waveguide fabrication

The state of art in glass-based EDWA was presented in chapter 1 and contextually a brief review of the methods employed to realized 2D waveguides was drawn. In this section the methods employed in this thesis to realize 2D waveguides will be briefly presented.

Since oxyfluoride silicate thin films showed superior characteristics with respect to the tellurite ones, only silicate 2D waveguides were realized.

Two main methods were employed.

The first method employed to realized 2D waveguide, was performed at the University of Edinburgh and it is a standard technological method, i.e. the 2D structures were realized directly on the deposited thin films, by means of Reactive Ion Etching (RIE) (see Fig 3.2a).

In the second method ("inverse method"), developed to overcome some limitations presented by the first one, a different approach was employed. In fact, in a first step the channel structures were etched directly onto the substrate by dry etching, and in a second step the oxyfluoride silicate glass was deposited inside the channels by means of PLD (see Fig 3.2b).This method was developed and performed by the L3 Group at the University of Salento.

It must be mentioned that in both methods the etching process was preceded by photolithography in order to define on the film or substrate a mask with the desired pattern. The successive etching processes allowed the selective removal of unmasked material areas respective to the masked ones. Since photolithography is a well defined technique in microfabrication processes, it doesn't require a complete description and

only the experimental details will be provided in the experimetal sections. On the contrary some useful comments on RIE and in particular on glass etching will be provided in the next section.

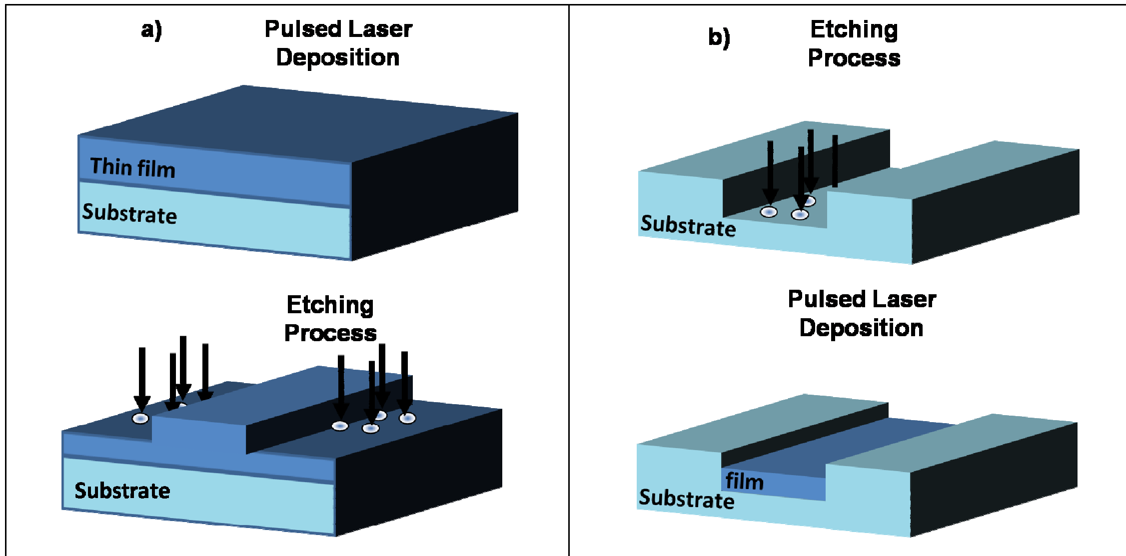

Fig. 3.2: Methods for the fabrication of 2D waveguides. a) Standard method: after the thin film deposition the 2D wg. is defined by etching. b) Inverse method: the substrate is etched and then the film is deposited inside the channel, realizing a 2D wg

3.2.2 Reactive Ion Etching: operation principle and apparatus

Microelectronics industry has developed many plasma based techniques for material etching, the most common is the Reactive Ion Etching (RIE).

In RIE, the sample is placed inside a reactor in which several gases are introduced. The standard RIE apparatus (Fig. 3.3) is constituted by a vacuum chamber housing a parallel plate electrodes. The samples are placed on the bottom electrode. Plasma is initiated in the system by applying a strong radio frequency (rf) electromagnetic field to the wafer platter. The field is typically set to a frequency of 13.56 MHz. The ions in the plasma are accelerated towards, and reacts at, the surface of the material being etched, forming another gaseous material. This is known as the chemical part of reactive ion etching. There is also a physical part which is similar in nature to the sputtering process. If the ions have high enough energy, they can remove atoms out of the material to be etched without a chemical reaction. It is a very complex task to develop dry etch processes that

balance chemical and physical etching, since there are many parameters to control. In fact, it is worth noting that by changing the balance it is possible to influence the anisotropy of the etching being the chemical part of the etching isotropic and the physical part highly anisotropic [131]. This a very important issue in all the applications since anisotropic etching is required to obtained a vertical shape of the sidewalls and to reproduce the mask pattern along all the depth of the etched zone.

To achieve higher plasma density with respect of conventional RIE, the Inductively Coupled Plasma (ICP) etching was developed.

While in a conventional RIE system the plasma is generated by a rf electric-field, in an ICP tool two RF power supplies are employed. One is capacitively coupled to one electrode, as in RIE, whilst the other is inductively coupled through the walls of the chamber by wrapping the electrode in the form of a coil around it. This inductive component is the high power supply and is used to generate the plasma. This current induces an electric field in the plasma region which is primarily tangential to the plasma boundary. The tangential component of the rf induction electric field may then penetrate the plasma region 1-2 cm and generate an intense plasma. Most significantly, the plasma is sustained without creating a high voltage sheath at the plasma-wall boundary. This improves the purity of the process and greatly increases the ion generation efficiency.

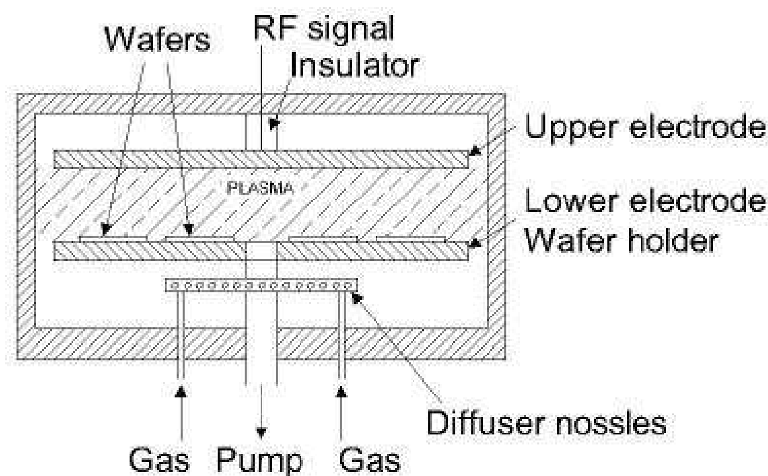

Fig. 3.3: Standard parallel plate RIE apparatus.

3.2.2 Reactive Ion Etching of glasses

With the development of glass-based devices, the micro-structuring of glass surfaces for the fabrication of optical waveguides, gratings and diffractive optical elements, became very relevant [132,133]. RIE was intensively applied for processing both SiO_2/Si substrates and silica substrates by semiconductor industries, nevertheless there has been limited studies of RIE of multicomponent glasses.

In the case of silicon dioxide (silica), CF_4 and/or CHF_3 are commonly used dry etching gases because they generate highly volatile SiF_4, CO/CO_2 and H_2O reaction products; the net reaction using CF_4, for example, is:

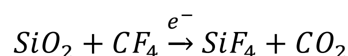

$$SiO_2 + CF_4 \xrightarrow{e^-} SiF_4 + CO_2$$

The reaction mechanism, however, is quite complex. It is mediated by the presence of electrons in the plasma which create reactive atoms, radicals and ions which drive the chemical reaction.

Steinbruchel [134] described the RIE of pure silica in a fluorocarbon plasma to be a process of ion enhanced chemical reaction. He showed that the etch rate was directly dependent on the density of the highly reactive ions in the rf diode reactor. Similarly, RIE of pure silica in a CF_4/CHF_3 plasma using an electron cyclotron resonance reactor (ECR) led Oerlein et al. [135] to a similar conclusion. In the case of borosilicate [136] and soda lime glasses [137,138] low etch rates compared to pure silica using fluorocarbon RIE were found.

Leech [139] showed that small concentrations of bulk impurities (> 25 ppm) such as Al, Ca, Na in silica glass decreased the etch rate by ~25% (in CHF_3/CF_4 plasmas) compared to higher purity silica substrates (impurities < 0.2 ppm). The author attributed this to the formation of less-volatile compounds of AlF_3, CaF_2 and NaF. However, no work has been reported to directly characterize the etched surfaces of multicomponent glasses nor to define the rate controlling mechanism.

More recently Metwally and Pantano, made a study on the etching rate of multicomponent silicate and phosphate glasses as a function of the plasma power,

plasma composition and glass composition, by means of a magnetically enhanced reactive ion etching apparatus (MERIE) [140]. They found that in fluorocarbon plasmas, the etch rate of glasses decreased as the concentration of less-volatile oxides in the glass increased. These etching rates were interpreted in terms of ion enhanced chemical reaction and physical sputtering. In general, the rate controlling mechanisms of etching by the RIE process may be due to physical effects (as in sputtering with inert ions), or chemical phenomena in the sense that the ion bombardment enhances surface chemical reactions with the reactants yielding highly-volatile reaction products.
In the case of multicomponent glasses a high chemical reaction rate between the reactive (ion) species in the plasma and the glass surface was observed during the early stages of etching while at longer times the etching was dominated by physical sputtering.

3.3 2D waveguide fabrication by "Standard Method"

3.3.1 Experimental

Ridge waveguides were fabricated starting from oxyfluoride silicate thin films, deposited by pulsed laser deposition technique. Only the films deposited at room temperature and at 200 °C were submitted to the etching procedure. The film were deposited in the same experimental conditions of SRT and S200 samples as presented in the previous chapter (see table 2.5).
To fabricate rib waveguides, a UV sensitive photoresist (Shipley 1813) was spun onto the film surface. The sample was then baked for 30 minutes at 90 °C. The rib structures (widths 2 → 15 μm) were defined onto the resist by UV illumination for 15 seconds through a chrome-on-silica mask. The resist was then developed using the resist developer and the resultant resist mask baked for 2 hours at 95 °C. Finally, the sample surface was etched for 105 minutes in an Oxford Plasma Technology RIE80 reactive ion etcher using CHF_3 gas.
The final etch depth was measured by Atomic Force Microscope (AFM) analysis while the rib morphology was investigated by optical microscope and SEM.

Waveguide facets for coupling light were prepared in order to allow fiber-waveguide coupling. The guiding properties of the waveguides were investigated by coupling light into the waveguide using fiber-waveguide butt-coupling and imaging the waveguide output facet onto an IR Vidicon camera. By pumping the waveguides at 980 nm through a 980 / 1550 nm fused fiber wavelength division multiplexer, fluorescence emission around 1550 nm was collected and analyzed using an optical spectrum analyzer.
The $^4I_{15/2} \rightarrow {^4I_{13/2}}$ transition absorption in the waveguide was determined by measuring the insertion losses of one of the smaller width waveguides (closer to single mode) across the erbium absorption band using a broadband Amplified Spontaneous Emission (ASE) source (Thorlabs ASE-FL 7002-C4).
The $^4I_{13/2} \rightarrow {^4I_{15/2}}$ transition fluorescence lifetime was measured by electronically modulating the 980 nm pump lasers and detecting the fluorescence emission perpendicular to the waveguide surface using a room temperature germanium detector with pump blocking filters.

3.3.2 Results

Structural analysis

The film deposited at room temperature cracked during the etching process, on the contrary the film deposited at 200 °C was successfully processed. In Fig 3.4 optical images of the ridge waveguides realized starting from films deposited at RT and 200°C are reported.

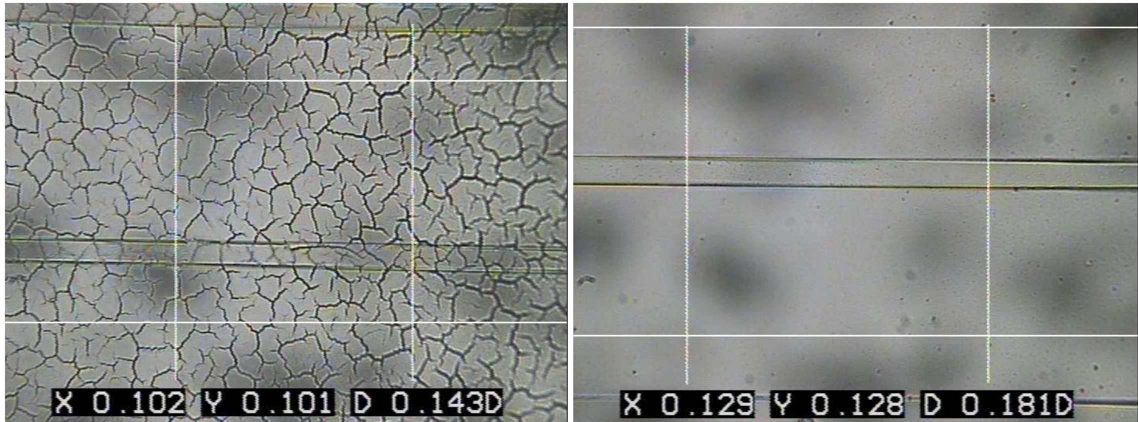

Fig 3.4: Optical images of the film deposited at RT (left), and 200°C (right) after the etching process. RT deposited film is clearly cracked.

Using AFM the final etch depth was measured to be 0.9µm. In fig 3.5 both SEM and AFM images of a 12 µm width waveguide are reported.

a) b)

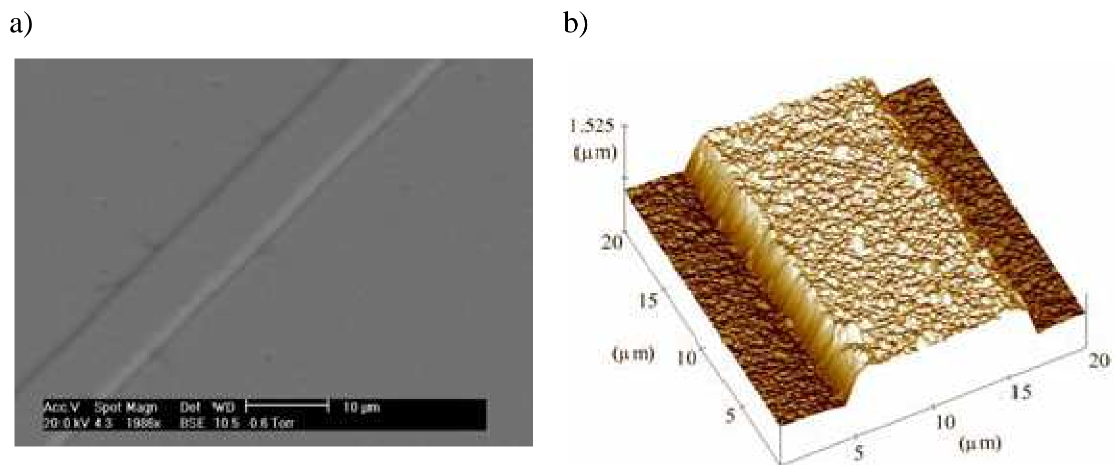

Fig 3.5: (a) SEM and (b) AFM images of a rib waveguide fabricated on an Er-doped thin film realizeed using PLD.

The sample was coated with a stress free polymer in order to produce a good facet for coupling light into and out of the waveguide and then it was diced perpendicular to the direction of the waveguide axis. Although in some cases it was possible to achieve a

good facet, despite extensive attempts, the process was not found to be repeatable. For this reason an alternative method was then employed: the sample was covered with the resist and photolithography was used to define a straight edge along the facet. The waveguide was then etched to produce a straight perpendicular facet. Fig. 3.6 shows the results of the two facet preparation methods. As can be seen, the results of the etching method produced a good facet quality which was easily repeatable.

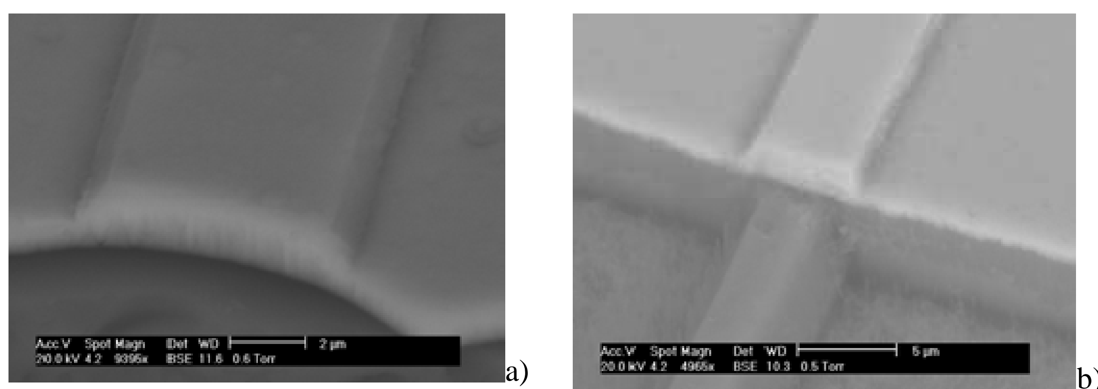

Fig 3.6: SEM pictures of a waveguide facet produced using dicing (a) and etching (b)

Waveguide characterization

By imaging the output facet of the fabricated waveguides onto an IR Vidicon camera, and coupling a signal at the desired wavelength into the waveguide at the other end, the guiding properties at various wavelengths of each waveguide could be examined. All the waveguides were found to support guiding at both 980 nm (the usual pump wavelength for Er-doped amplifiers) and 1550 nm (the signal wavelength).

All waveguides tested produced characteristic fluorescence in the 1550 nm region. The Fig. 3.7 shows a comparison of the normalized erbium emission cross section measured from one of the fabricated waveguides with the normalized emission cross section measured from the bulk glass.

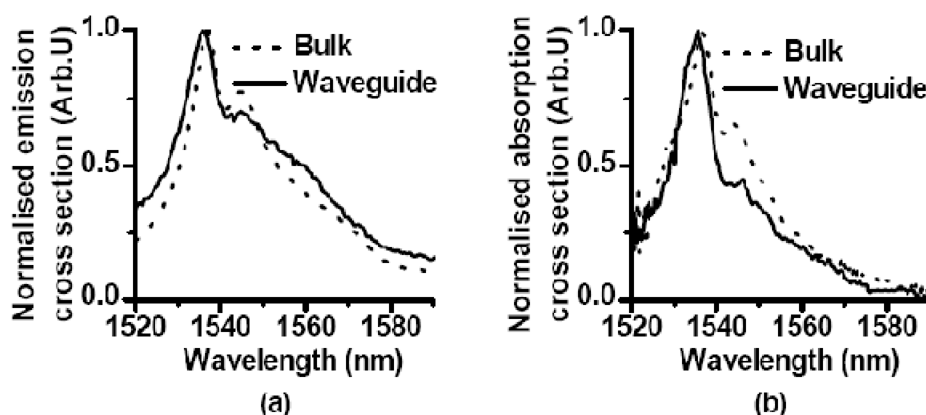

Fig3.7: (a) Comparison of the normalized emission cross section from the bulk and from the film. (b) Comparison of the normalized absorption cross section for the $^4I_{15/2} \rightarrow {}_4I_{13/2}$ transition as measured in the bulk target and one of the fabricated rib waveguides.

By measuring the insertion losses of the waveguide realized with the smallest width (closer to single mode) across the erbium absorption band using a broadband ASE source, the amount of absorption present in the waveguide could be measured quantitatively. Using this technique, the peak erbium absorption was measured to be 4.6 $dBcm^{-1}$. This value is slightly higher than that of the bulk which was measured to be 3.4 $dBcm^{-1}$.

Fig. 3.7 (b) shows a comparison of the normalized erbium absorption cross section measured in one of the fabricated waveguides with the normalized absorption cross section measured in the bulk glass.

The minimum measured background insertion loss (outside the $^4I_{15/2} \rightarrow {}^4I_{13/2}$ transition absorption band) was approximately 20 dB for a 0.76 cm long, 4 μm wide rib waveguide. The majority of this value is thought to be due to poor mode matching between the 1550 / 980nm WDM coupler fiber and waveguide.

The fluorescence lifetime of the optically active erbium was measured to be 0.1ms. This is far from that measured in the bulk sample (≈10ms).

3.3.3 Discussion

The optical images of the thin films after the etching process, clearly confirmed the importance of the substrate temperature to obtain good quality and mechanical stable waveguides. The same behavior reported during SEM inspections and presented in the previous chapter was observed under RIE. The film deposited at room temperature cracked during the RIE process under the action of the plasma. On the contrary, it was possible to realize rib waveguides from films deposited at 200°C films.

Rib quality was quite good even if the waveguides sidewalls were not vertical, therefore it was necessary to further optimize the etching process to achieve vertical sidewalls.

The waveguides supported a well confined mode at both 980 nm and 1550 nm. The guiding at 1550 nm was of a high enough quality to allow direct measurement of the erbium absorption lineshape by direct fiber-waveguide-fiber coupling of a broadband ASE source. A peak erbium absorption coefficient of 4.6 $dBcm^{-1}$ indicated that a large concentration of erbium was incorporated into the film and it was indicative of a stoichiometric transfer of material from the bulk to the film. Unfortunately fluorescence lifetime was very low: as in the case of the measure on thin films it was indicative of the presence of a significant quenching mechanism in the material. Two possible sources of luminescence quenching can be suggested: the presence of hydroxyl (O-H) impurities [141] or the strong energy transfer/cooperative upconversion mechanisms [22]. Probably both the mechanisms are responsible of the lifetime behavior.

Concerning the presence of O-H impurities it should be considered that the film was found to be granular in structure which may result in a significantly low packing density, leaving the film susceptible of water absorption, moreover it should be considered that etching in CHF_3 plasma can add a further source of O-H impurities. Insertion loss measurements revealed an unexpected increase in the insertion loss at 1426 nm, close to the first vibrational overtone of the O-H hydroxyl group. It must be mentioned, in fact, that out of the erbium absorption band the insertion losses usually decrease. This is a strong indication that water absorption is a significant problem resulting in the reduction of the $^4I_{13/2} \rightarrow {}^4I_{15/2}$ transition fluorescence lifetime.

Moreover cooperative mechanisms should be not ruled out since pumping at 980 nm showed a large amount of green up conversion which could point towards ion-ion clustering as a significant problem. Moreover, as underlined in the previous chapter, even though ion-ion interaction appears to decrease as the substrate temperature increases, at 200°C (the used temperature for the film submitted to RIE) Er-Er interaction is still dominant and can not be neglected.

3.4 2D waveguide fabrication by "Inverse Method"

The standard method provides very good results in the fabrication of silicate ridge waveguides but two important aspects are evident: from one hand mechanically stable films are required to obtain good quality waveguides, and from the other smooth waveguide facets can be obtain only by a further etching procedure (as evidenced in the previous section) due to the delicate nature of the thin films.

To overcome these two drawbacks, the inverse method was developed.

In this methods the etching process involves only the substrate, in which the channels of the suitable dimensions are defined, while the guiding layer is simply deposited inside the channel by means of the PLD technique.

Obviously, in this method a very important role is attributed to the etching of the substrate, since the performance of the final waveguide strongly depends from the quality of the bottom and of the sidewalls of the channel.

In this section the experimental details of the etching process will be presented while concerning the film deposition the same experimental parameters, which have been described in the previous chapter, should be considered.

3.4.1 Experimental

The channel were fabricated in pure silica substrates (Heraeus), moreover a preliminary test was also performed on a SiO_2/Si (SOS) wafer.

Two different masks were used to defined the channel pattern on the substrate: a polymer mask and a chromium mask.

Before the photolithography process the substrates were baked for 5 minutes in acetone and successively 5 minutes in isopropyl alcohol in order to remove contaminants from the surface.

To fabricate the polymer mask, a positive photoresist (Shipley AZ 5214 E), was spun onto the silica plate, after that the sample was baked for 1 minute at 120°C. Then the channel pattern (width ranging from 5 to 100 μm) was defined onto the resist by UV illumination (λ = 365 nm) for 15 seconds through a chrome-on-silica mask, afterward the photoresist was developed by using the resist developer.

To produce the chromium mask, a thin film of chromium (thickness ~70 nm) was evaporated onto the pure silica substrate. Then the sample was subject to optical lithography. A UV sensitive photoresist (AR-P 5350 from Allresist GmbH) was spun onto the film surface and baked for 4 minutes at 110°C. A series of channels with a length of 2 cm and with a width ranging from 5 to 100 μm was then defined onto the resist by UV illumination (λ = 320 nm) for 12 seconds through a chrome-on-silica mask, afterward the photoresist was developed by using the resist developer. Finally the chromium was wet etched and the photoresist removed, leaving a chromium mask with the desired pattern. The same procedure was employed for the SiO_2/Si wafer.

The samples were then subjected to etching procedure by ICP-RIE. The ICP etch source, (STS Advanced Oxide Etch (AOE^{TM})) uses a planar inductively coupled radio frequency (13.56MHz) plasma coil with multipolar magnetic confinement at the chamber sidewalls and high-rate vacuum pumping

The etching was performed by using a mixture of CF_4, C_4F_8 and O_2 gas. The total etching process time was 4 minutes. The etching parameters were summarized in table 3.1.

Table 3.1: Parameters for the silica and SOS substrate etching.

Sample	Mask	Substrate	Gas (total pressure 4 mTorr)	Coil/Platen power	Process time
P-S	Polymer	Silica	CF_4 (flow 20 sccm) C_4F_8 (flow 20 sccm)	1250W/200W	4’
C-S	Chromium	Silica	CF_4 (flow 20 sccm) C_4F_8 (flow 20 sccm)	1250W/200W	4’
C-S-O	Chromium	Silica	CF_4 (flow 20 sccm) C_4F_8 (flow 20 sccm) O_2 (flow 4 sccm)	1250W/200W	4’
C-SOS-O	Chromium	SiO_2/Si	CF_4 (flow 20 sccm) C_4F_8 (flow 20 sccm) O_2 (flow rate 4 sccm))	1250W/200W	4’

After the etching the residuals of the masks were removed.

The channel morphology was analyzed by atomic force microscopy (AFM), and high resolution scanning electron microscopy, a JEM JEOL 6500F instrument equipped with a Field Emission Gun (SEM-FEG) was used in the secondary electron detection mode. The nominal image resolution of the instrument is 1.5 nm at 15 kV and 5 nm at 1 kV.

In the second phase oxyfluoride silicate glasses were deposited onto the patterned channels using the same experimental conditions of the silicate thin films described in the previous chapter (see table 2.5). The morphology of the channel waveguides were investigate by SEM analysis (SEM-FEG, LEO Gemini 1530).

3.4.2 Results

Channel characterization

The total etch depth was measure by AFM and a value of ~1.3 µm was found.

The channel morphology was investigated by means of SEM analysis.

The sample etched using the photoresist mask presented two important drawbacks: first of all after the etching process the photoresist film was firmly adherent on the glass substrate, and it can not be removed using acetone or the commercial stripping solution, moreover some residual due to re-deposition of the etching products or to polymerization were found on the bottom and on the sidewalls of the channels. In figure 3.8 the SEM micrographs of the samples exhibiting residual polymer after the etching are shown.

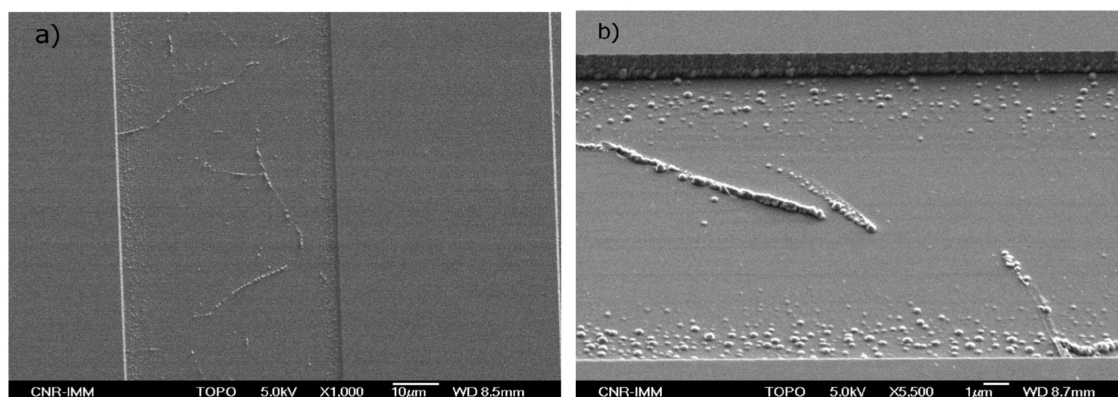

Fig 3.8: SEM micrographs of the channel obtained by using a polymer mask during the etching process a). A higher magnification view of the same channel b).

A similar behavior was found using the chromium mask, but in this case the residual mask was removed by baking the sample in the chromium removal solution at 50 °C. Moreover to reduce polymerization during the etching procedure, O_2 was added during the process. Very good results were obtained, as demonstrated by the SEM images reported in figure 3.9.

AFM analysis performed on the silica sample showed that a very low roughness (average roughness ~1.5 nm) was achieved on the channel bottom.

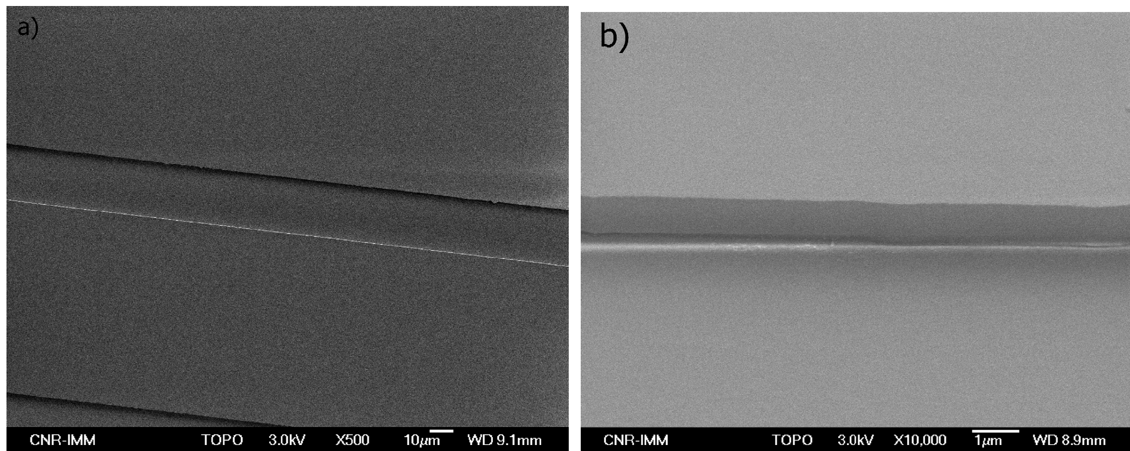

Fig 3.9: SEM micrographs of the channel obtained in the sample C-S-O. In b) a closer view of the channel sidewalls is shown.

Morphology characterization of the waveguide

Silicate glass waveguides were deposited inside the channel by PLD. The most important aspect of the inverse method is the possibility to deposit by PLD good quality films directly onto non-planar substrates. In fact the SEM images demonstrate that the deposited thin films follow exactly the geometries of the silica channels and in particular the vertical profile of the sidewalls, as evidenced in Fig 3.10.

The structure of the deposited layer is granular as in the case of the thin films deposited on flat substrates. As example in Fig 3.11a top view of a waveguide deposited in the same condition of the S200 (substrate temperature 200°C, background oxygen pressure 5 Pa) sample is reported. The vertical profile of the sidewalls is evident.

Depositions were performed also on SiO_2/Si substrates, and good results were obtained in this case too. Fig 3.12 shows a sample deposited on a SOS substrate.

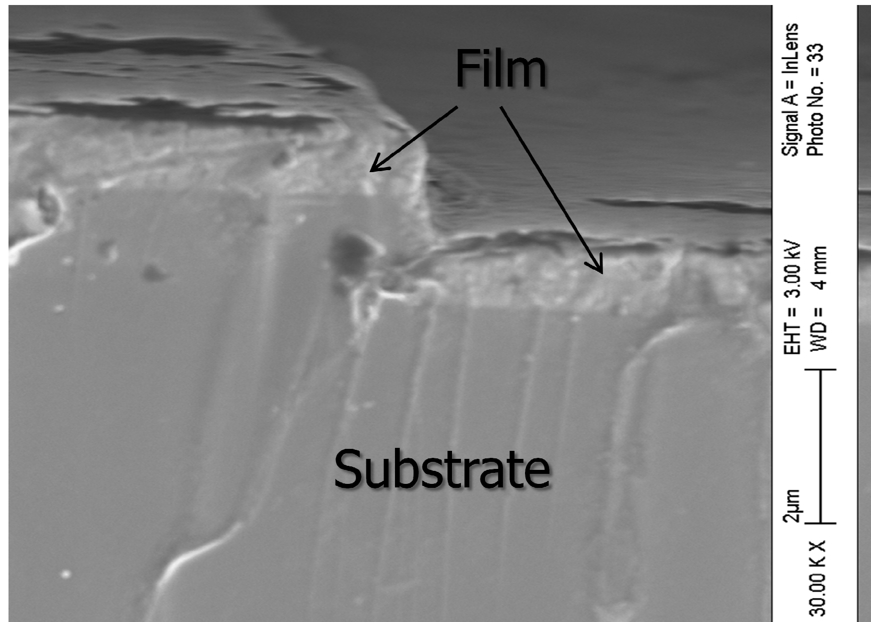

Fig 3.10: SEM micrograph of the waveguide deposited on the C-S-O sample. The defects on the film surface are due to the sample preparation for the SEM analysis.

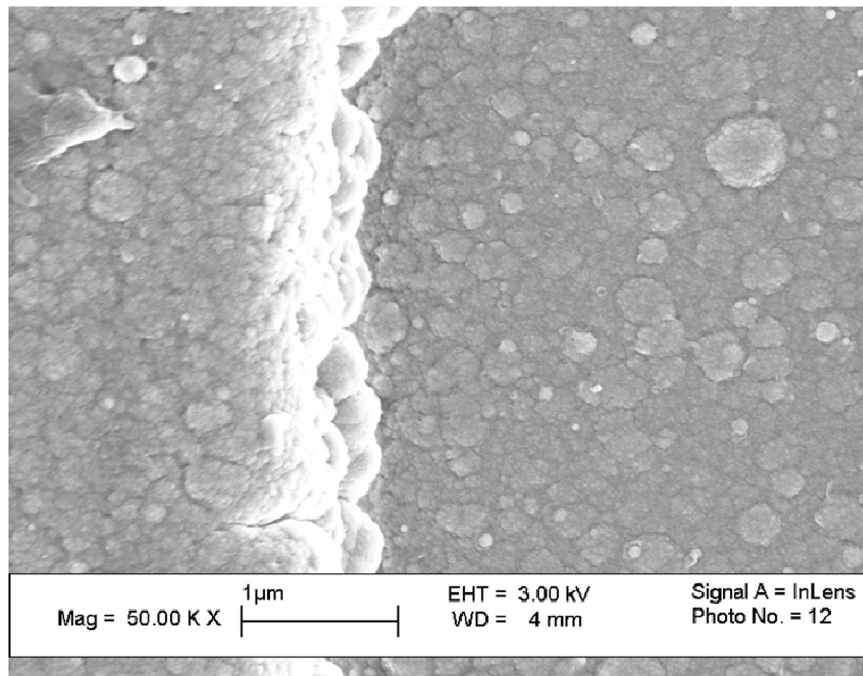

Fig 3.11: Top view of a waveguide deposited at a substrate temperature of 200°C. On the right side of the image it is possible to see the bottom of the channel waveguide.

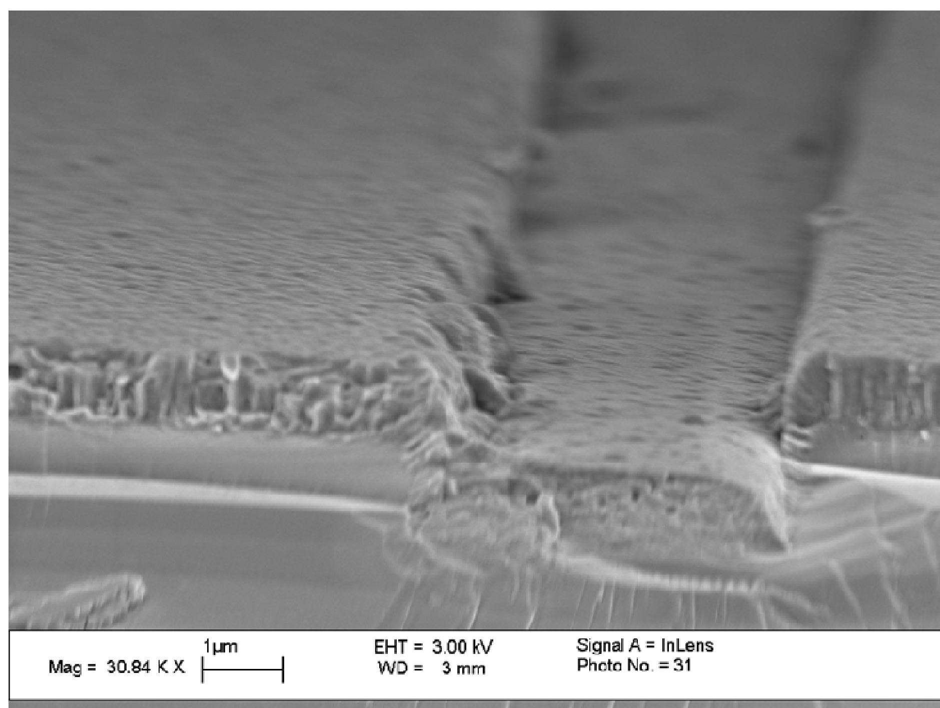

Fig 3.12: Top view of a waveguide deposited on a SOS substrate.

3.4.3 Discussion

The inverse method is quite promising for the realization of 2D waveguide. The main advantage of the inverse method is that the optimization of the etching procedure and of the thin film deposition can be made independently.

Concerning the realization of the channels in silica substrates, the etching procedure gave very good results. A chromium mask was used to define the pattern on the substrate. The polymer mask in fact after the etching was hardly removed: this behavior was found also by Metwalli et al. [140], and can be presumably ascribed to interface reactions caused by the ion bombardment or by the applied electric-field. It is worth noting that while Metwalli succeeded to remove the hardened photoresist by means of a low pressure (50 mTorr) and low rf power (200 W) O_2 plasma after the etching process, in the case presented in this thesis, the photoresist could not be removed using the O_2 plasma. This was probably due to the nature of the etching apparatus, which was

specifically designed for the etching of oxide materials, and provided a very dense plasma.

In the experiment performed using a pure fluorocarbon plasma, residual polymer were found on the bottom and on the sidewalls of the channel. The presence of the residual polymer was essentially due to redeposition of the etching products.

The redeposition effect was significantly affected by the amounts of particles sputtered from the bottom, which can be mainly related to the bottom etch rate [142], which was very high in the experiment performed in this thesis (~300nm/min). Moreover the amount of particles sputtered from the bottom is determined by various factors such as the energy and flux of ions incident on the bottom, the thickness of the polymer film formed on the bottom surface, and the thickness of the SiO_xF_y layer present at the interface between the fluorocarbon-polymer film and the SiO_2 layer [143].

Min et al. demonstrated that the redeposition is higher for CF_4 with respect to C_4F_8 plasma [144] since in the case of CF_4 plasma, F radicals contribute to the etching of the bottom while CF_2 radicals contribute to the deposition of a fluorocarbon polymer film on the bottom surface, eventually retarding the reaction between F and the bottom.

Moreover the redeposition of bottom-emitted particles on the sidewall surface directly affected the formation of a sidewall polymer film.

As result the sidewalls became very rough after etching as can be observed by SEM images in figure 3.8. This result was demonstrated for CF_4 plasma and it was attributed to the particles redeposited from the bottom that initiated surface polymerization, leading to the formation of a rough fluorocarbon film on the sidewall surface [145].

The addition of O_2 at the fluorocarbon plasma improved the quality of the etching, and very good results were obtained. In fact when using O_2 in the plasma, the amount of sputtered particles decreases. Moreover as the O_2 concentration increased, the concentration of CF_2 radicals, a polymer precursor, decreased and O radicals simultaneously consumed the fluorocarbon polymer formed on the bottom and, as a result, the redeposition effect by the polymer fragments decreased [145].

Concerning the second step of the proposed “inverse method”, the deposition of the waveguides inside the channel provided very interesting results especially when compared with the results obtained by the “standard method”. In fact by using the

standard method a 200°C substrate temperature was strictly necessary to make mechanically stable films and to obtain good quality rib waveguides, on the contrary in this new approach no invasive process interested the thin films and good results were obtained keeping the substrate at room temperature too (see figure 3.12). The most important aspect of our experiment was the possibility to deposit by PLD good quality films directly onto non-planar substrates. In fact we demonstrated that the deposited thin films followed exactly the geometries of the silica channels and maintained the vertical profile of the channel sidewalls. This is a key aspect to realize laterally confinement in guiding structures since it allows to reduce the losses due to the spreading of the radiation out of the guiding channel.

Another key feature of this new method was due to the consideration that only the substrate undergoes the etching process and the preparation of the waveguide facets became less problematic since it can be performed before the deposition of the thin films. This aspect probably can reduce the insertion losses when testing the guiding properties of the structures.

Unfortunately the guiding properties of the waveguide were not characterized as the maximum film thickness was ~1.3 µm, and fibers with a core dimension comparable to this value (in order to have good mode matching between the fiber and the waveguide and to obtain low insertion losses) were not available. Nevertheless since the guiding layer was simply deposited on the patterned substrate it is reasonable to consider the properties of the rectangular waveguide as good as the guiding properties of the planar thin films.

Finally, the preliminary results obtained on the SiO_2/Si wafer make this approach to realize 2D waveguides very attractive since it allows to easily achieve the integration of the waveguide in a optical circuit.

Chapter 4

Design of a Y-junction: towards an integrated optical amplifier

Contents

4.1 Methods for Optical Waveguide Analysis 86
4.1.1 Finite-Difference Time-Domain method (FDTD) 87
4.1.2 Beam Propagation method (BPM) 88
4.2 Design of a Y-junction 89
4.2.1 Y-junction geometry 89
4.2.2 Results 91
4.2.3 Discussion 94

After the realization of 2D active waveguides, it is straightforward to study and realize more complex guiding structures (with respect to the simple channel waveguide) in order to develop new devices or to fully integrated the erbium doped waveguide in an integrated circuit.

To actually realize an integrated EDWA, in fact, it is necessary to launch inside the waveguide both the signal to be amplified (at 1550 nm) and the pump (at 980 nm or 1480 nm depending of the used pumping scheme). The signal-pump coupling in the amplifier, can be successfully realized by a Y-junction coupler, in which the pump and signal power propagating in two input arms of the Y are multiplexed in the output arm of the junction.

A careful design of the junction geometry is required, in order to optimize both the signal and pump propagation as a function of the waveguide parameters.

In this thesis a Y coupler was designed starting from the results of the previous chapters.

In this chapter, the numerical method, based on the Finite-Difference Beam Propagation Method, employed to simulate the wave propagation in the guiding structure will be described and the results of the simulation will be presented.

4.1 Methods for Optical Waveguide Analysis

Many types of methods for the analysis of optical components exist, which can be classified into Analytical, Numerical and Semi-Analytical methods. Unfortunately analytical methods can be employed only in a limited number of problems concerning simple slab planar devices. When the analysis concerns complex 3D structures, analytical methods are inapplicable. Consequently, a lot of effort has been focused on Numerical and approximate Semi-Analytical methods.

Rigorous numerical methods, such as the Finite Difference (FD)[146,147] or Finite Element (FE)[148] methods can be successfully employed for optical components analysis. However numerical methods often require memory size and long computational time. Consequently, in certain situations, it is extremely difficult to apply numerical methods, especially when large and/or complex waveguide structure is considered. In these cases, a Semi-Analytical method, such as the Effective Index (EI) method [149], Spectral Index (SI) method [150], or Free Space Radiation Mode (FSRM) method [151] may be chosen, depending on the geometry, to solve the electromagnetic problem. Semi-analytical methods are useful to reduce the computational complexity of the numerical code, in fact semi-analytical methods use appropriate approximations, which can result in fast applications suitable for design purposes, with the additional advantages of much lower requirements in CPU time and memory size. These methods sometimes provide results comparable with those of numerical methods, and can be useful tools along with other methods. However, since semi-analytical methods involve some approximations, in complex waveguide structures the accuracy of the results can be reduced: in these cases numerical methods must be employed.

Two main numerical methods should be considered for the analysis of optical waveguides, the Finite-Difference Time-Domain method (FDTD) and the Beam Propagation Method (BPM) .

This section has not the aim to represent a full comprehensive description neither of the two methods nor of their implementation since several texts can be found on this topic. For an exhaustive description about the methods for the analysis of optical waveguides see for example [130]. In the following a brief description of the two methods will be provided pointing out their main advantages and drawbacks.

4.1.1 Finite-Difference Time-Domain method (FDTD)

The FDTD method was developed by Yee [152] and directly solves the time-dependent Maxwell's equations for the electric (**E**) and magnetic (**H**) fields:

$$\nabla x \boldsymbol{E} = -\frac{\partial \boldsymbol{B}}{\partial t}$$

$$\nabla x \boldsymbol{H} = -\frac{\partial \boldsymbol{D}}{\partial t} + \mathbf{J}$$

$$\boldsymbol{D} = \varepsilon \boldsymbol{E}$$

$$\mathbf{B} = \mu \mathbf{H}$$

where **D** is the displacement field, **J** is the current density, **B** is the magnetic flux density (often called the magnetic field). The quantities $\varepsilon = \varepsilon_0 \varepsilon_r$ and $\mu = \mu_0 \mu_r$ define the electromagnetic properties of the medium, and are the dielectric constant and the magnetic permeability of the medium respectively: $\varepsilon_0 = 8.854x10^{-12}$ *F/m* is the dielectric constant of vacuum and $\mu_0 = 4\pi x10^{-7}$ *H/m* the magnetic permeability of vacuum. ε_r and μ_r are the relative permittivity and permeability of the material. μ_r=1 when non-magnetic materials are considered.

FDTD methods divide space and time into a finite rectangular grid. As the FDTD is an explicit scheme, the time step in the calculation is defined by the spatial discretization width: if the grid resolution doubles, the number of time steps doubles as well.

The main disadvantage of the FDTD method is that the amount of required computational memory is enormous especially for 3D structures. In fact it requires that the entire computational domain be gridded, and the grid spatial discretization must be sufficiently fine to resolve all the features of the waveguide structure.

A strength of the time-domain method is the ability to obtain the entire frequency spectrum of responses (or eigenfrequencies) in a single simulation, by Fourier-transforming the response to a short input pulse.
A comprehensive and complete description of the FDTD method is illustrated in [153].

4.1.2 Beam Propagation method (BPM)

BPM was developed for the analysis of non-uniform structures slowly varying in one direction. Various kinds of BPMs were exploited such as the Fast Fourier Transform BPM [154], the Finite Element BPM [155] and the Finite Difference BPM [156].
In particular in this thesis the FD-BPM was employed, since it is very powerful and has been widely applied to design and to optimizes optical waveguides.
FD-BPMs sample both the structure and the electromagnetic field: sampling procedure is commonly performed at regular spatial intervals. In FD-BPM the calculation is performed as follows: starting from the know values of the electromagnetic field in a set of points (initial condition), the field at the following step is calculated. Obviously the knowledge of the waveguide structure at all sampled points is required. This process is repeated for each new set of calculated field points, and so the simulation “propagates” along the waveguide structure.
Among the developed FD-BPMs, the scheme implemented by Chung and Dagli [155] represent the state of art from the viewpoints of accuracy, numerical efficiency and stability. The last aspect is very useful since it allows to use the method in actual design, moreover it allows propagation steps relatively large respect to other numerical methods, reducing the computational time.
A relevant problem in numerical simulation is represented by the boundary condition. In fact in actual design a limited analysis window has to be considered, therefore the effects of the reflection at the boundaries should be taken in consideration. The radiated waves, after the reflection, return to the guiding area, where they interact with the propagating fields. This interaction perturbs the propagating fields and greatly affects the calculation accuracy. Hadley developed the Transparent Boundary Conditions (TBC) which efficiently suppress the reflection [157]. TBC were based on the assumption that the radiation fields have a complex exponential behaviour near the boundary. The fields

outside the sample area were predicted using this assumption, making the boundary transparent and allowing the energy to leave the computational domain.
It must be mentioned that the FD-BPM can be easily integrated with computer-aided design (CAD) software, which can allow the use of the numerical methods with minimal mathematical knowledge. A good commercial example of this is the BeamProp by RSoft Design Group, Inc. [158].

4.2 Design of a Y-junction

The analysis of the propagation of a Y-junction was performed by a FD-BPM numerical code, implemented in C++ language by the Electromagnetic Field Group of the Dipartimento di Elettronica ed Elettrotecnica of the Politecnico di Bari.

4.2.1 Y-junction geometry

The basic Y-junction structure employed for the simulation is represented in figure 4.1. Some aspects must be highlighted before to present the results of the simulation:

- since the proposed "inverse method" to realize guiding structures, appeared very promising from a technological point of view and gave attractive results as evidenced in the previous chapter, the structure of the waveguide was chosen in order to reproduce the typical geometry obtained by the inverse method, i.e. the waveguide core deposited inside the silica channel (Fig. 4.1b);
- since oxyfluoride silicate waveguides exhibited better structural and optical properties with respect to tellurite waveguides, the simulation was performed using, for the guiding region, the refractive index of the oxyfluoride silicate glasses. In particular, the refractive index of the film deposited at room temperature as presented in Chapter 2 was employed;
- in order to satisfy the need for integration, the simulation was performed using a SiO_2/Si substrate, with a silica thickness of 9 μm.

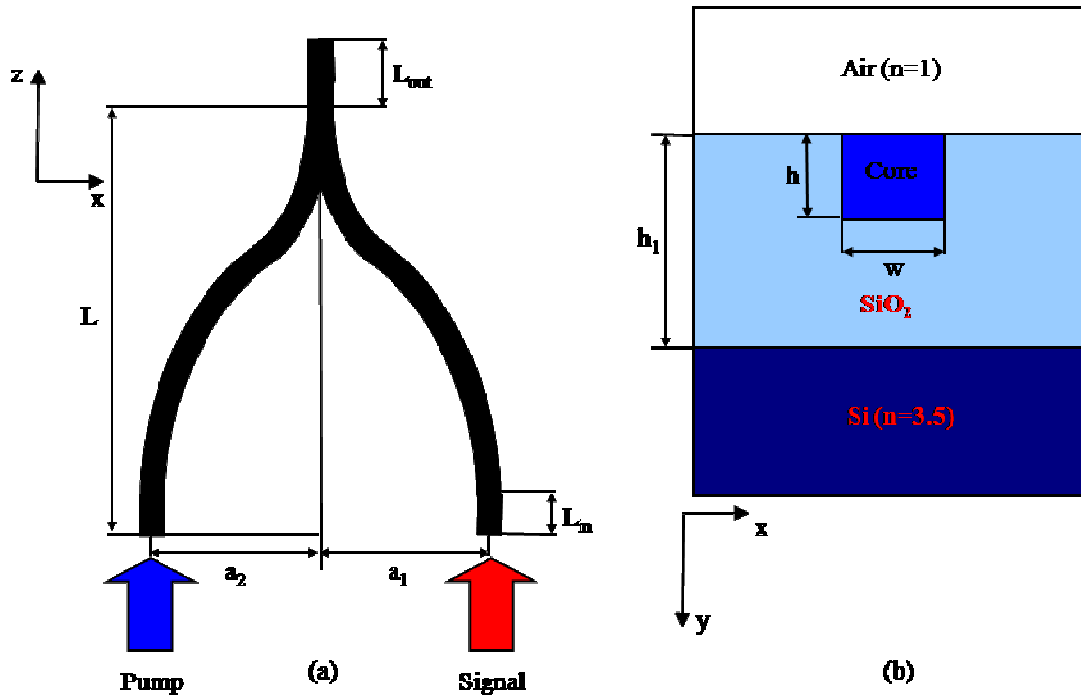

Fig. 4.1: Y-junction structure: a) x-z section (top view)of the Y geometry, b) cross section of the waveguide.

Table 4.1 summarizes the main parameters which were employed in the simulation. The geometric dimensions of the waveguide cross section, namely w and h (see Fig. 4.1 b)), were evaluated from a first rapid calculation in order to obtain a single mode waveguide at the signal wavelength.

To perform the simulation a Gaussian beam centered with the signal/pump branch was launched, and TBC were imposed at thee boundary of the computational domain. In BPM method only one wavelength at the time can be launched, therefore the simulation was perform for each branch separately.

In the BPM scheme one fundamental parameter is represented by the step size along the propagation direction (z axis), since the numerical code calculates the propagating fields at one point from the values of the fields at the previous step. Therefore the step size must be small enough to assure an adequate accuracy in the calculation and to allow a satisfactory sampling of the waveguide geometry. Obviously decreasing the step size the computational time increases. In the simulation the step size was set to $\lambda/10$ (where λ is

the wavelength of the propagating signal), since it represents a reasonable compromise between the two requirements.

Table 4.1: Main parameters employed in the simulation of the Y-junction. In last column is specified if the parameter was maintained fix during the simulation or was employed as a simulating variable.

Parameter	Value	Variable
Signal wavelength	1550 nm	no
Pump wavelength	980 nm	no
Waveguide refractive index	1,588@ 980 nm 1,582@1550 nm	no
Waveguide width (w)	3 μm	no
Waveguide depth (h)	3 μm	no
SiO_2 refractive index	1,439@ 980 nm 1,430@1550 nm	no
SiO_2 thickness (h_1)	9 μm	no
Input waveguide Length (L_{in})	400 μm	no
Output waveguide Length (L_{out})	600 μm	no
Coupling length (L)	/	yes
Distance of the signal branch from the Y axis (a_1)	/	yes
Distance of the pump branch from the Y axis (a_2)	/	yes

4.2.2 Numerical Results

To estimate the properties of the Y-junction, the transmittance $\eta = \frac{P_{out}}{P_{in}}$ along the waveguide branches was evaluated, where P_{in} and P_{out} represent respectively the power launched at the input waveguide and the power at the waveguide output.

In Fig 4.2 η is reported as function of the distance of the branch from the Y-junction axis for different coupling length values, L. In particular fig. 4.2a reports the numerical results obtained by varying a_1 (the distance between the signal branch and the Y-junction axis) and fig. 4.2b depicts the results pertaining to a_2 (the distance between the pump branch and the z axis). In order to study the dependence of the transmittance from the transversal dimensions of the waveguide, further simulations were performed fixing the

coupling length (L) at 9 mm and considering two different waveguide widths: w=3 μm and w=4 μm. The results obtained are shown in Fig 4.3, where η as function of a_1 (signal branch) (Fig. 4.3a) and a_2 (pump branch) (Fig. 4.3b) is reported.

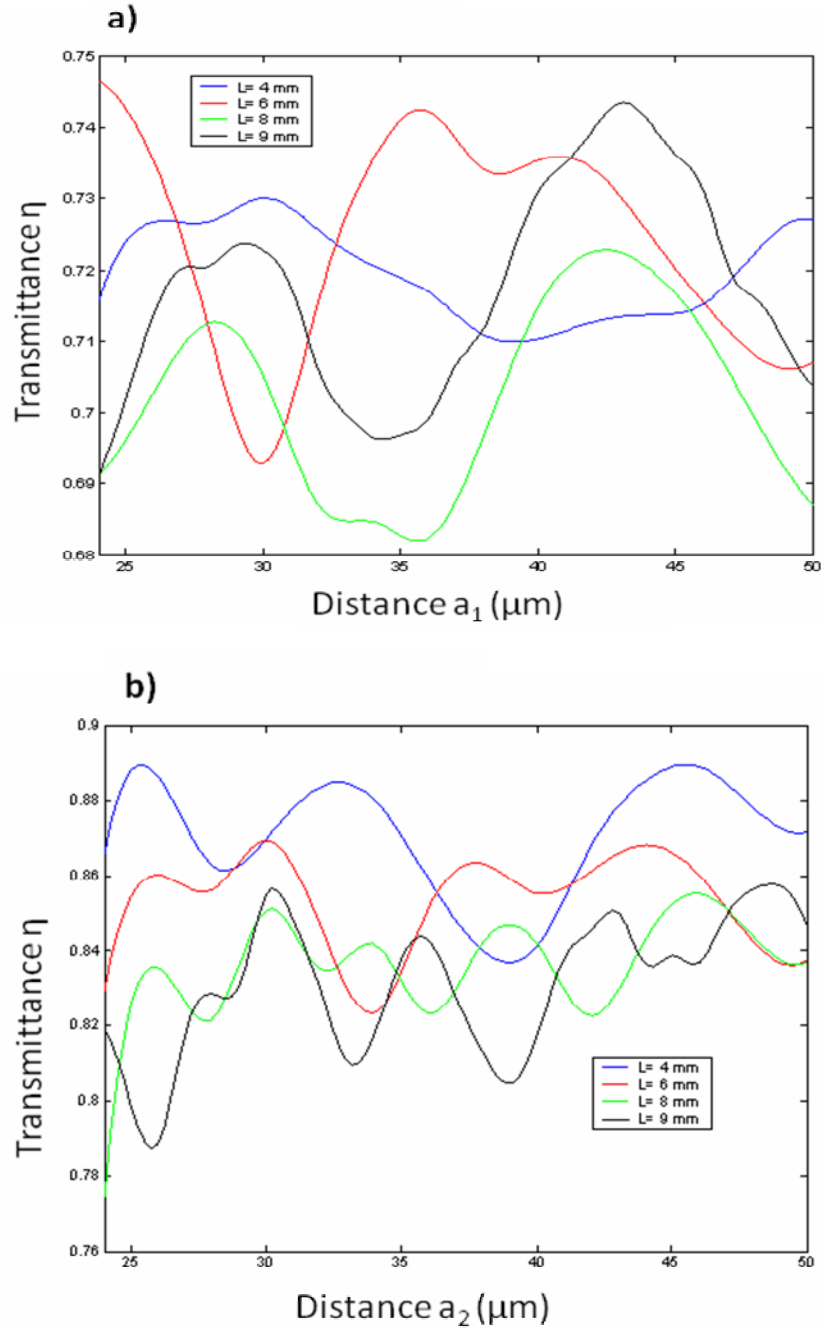

Fig 4.2: Transmittance values η, as function of the distance a_1 between the coupler axis and the signal branch (a) and the distance a_2 between the coupler axis and the pump branch (b). The simulations were performed for different coupling lengths, L.

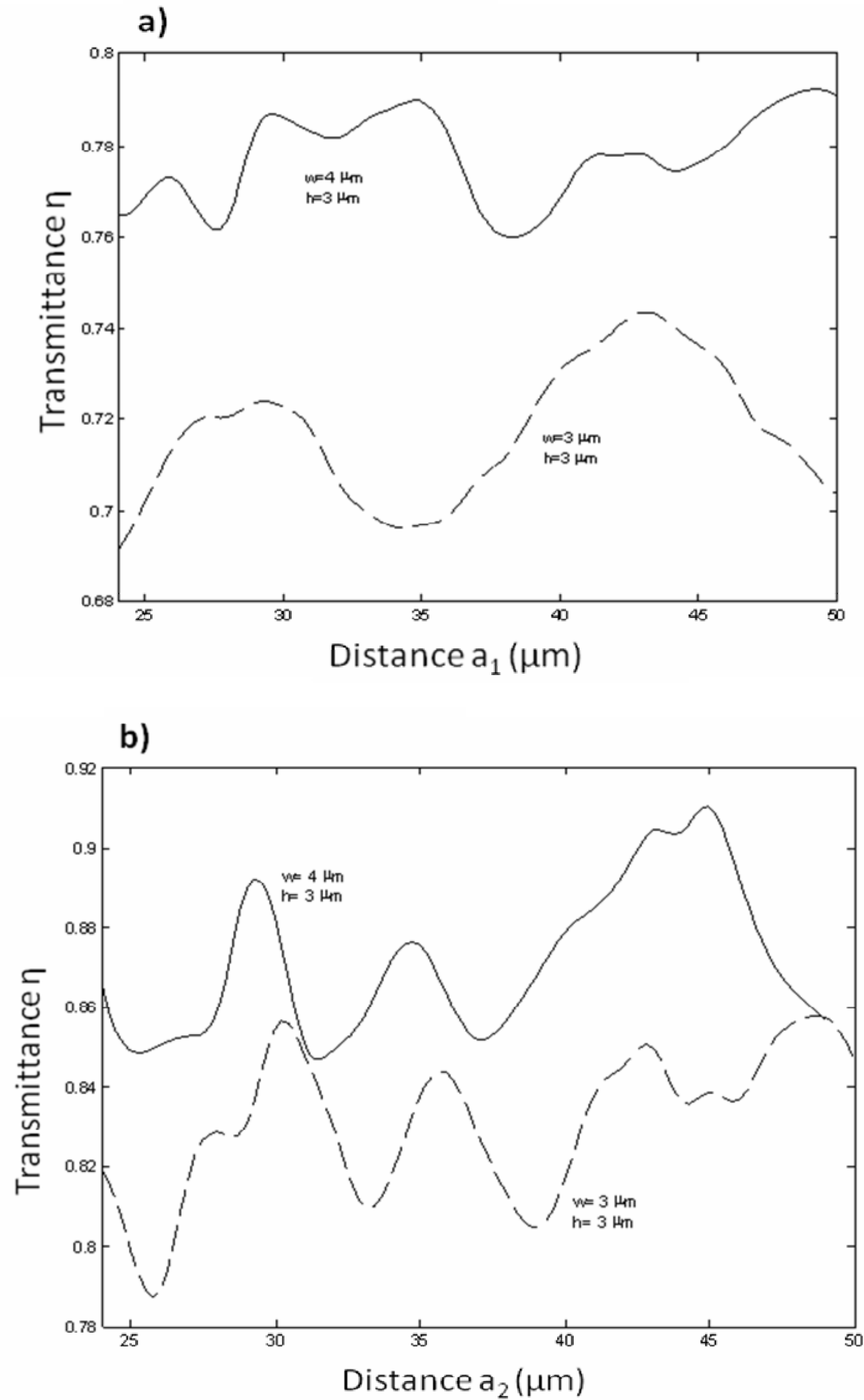

Fig 4.3: Transmittance values η, as function of the distance a_1 between the coupler axis and the signal branch (a) and the distance a_2 between the coupler axis and the pump branch (b).The simulations were performed for two different waveguide widths (3 μm and 4 μm) while the coupling length, L was fixed at 9 mm.

4.2.3 Discussion

The analysis of the propagation by the FD-BPM allows to simulate the behaviour of the Y coupler at two different wavelengths, the signal at 1550 nm and the pump at 980 nm. In order to design a suitable coupler the simulation was performed fixing the transversal waveguide dimension in order to obtain a single mode waveguide and varying the geometry of the junction in terms of the coupling length, L, and of the distance between the two Y branches and the coupler axis (a_1 and a_2 for signal and pump branch respectively).

From figure 4.2a it is possible to observe that the maximum signal transmittance η=75%, was obtained for a coupling length L= 9 mm and a branch distance a_1=43µm. For the same values the transmittance for the pump was ~85%.

This condition appears to be a good compromise for the fabrication of the coupler. It is worthwhile to note, in fact, that in this condition the Y-junction is symmetric. This aspect is very relevant from a technological point of view since it simplifies both fabrication and fiber-waveguide coupling.

A further simulation was performed to analyze the dependence of the coupler performances from the waveguide width. The comparison between the numerical results obtained for w=3 µm and w=4 µm shows that the transmittance increases as the width increases, nevertheless the waveguide is found to support more than one mode at the pump wavelength.

In figure 4.4 the intensity pattern of the electromagnetic field along both the signal (fig 4.4b) and the pump (fig. 4.4a) branch, presenting w=4 µm, is reported.

This aspect can cause some drawbacks since a good spatial overlap between the pump and signal is required to improve the pumping efficiency. In addition, the multimode operation produces a spreading of the input pump power between the guided modes.

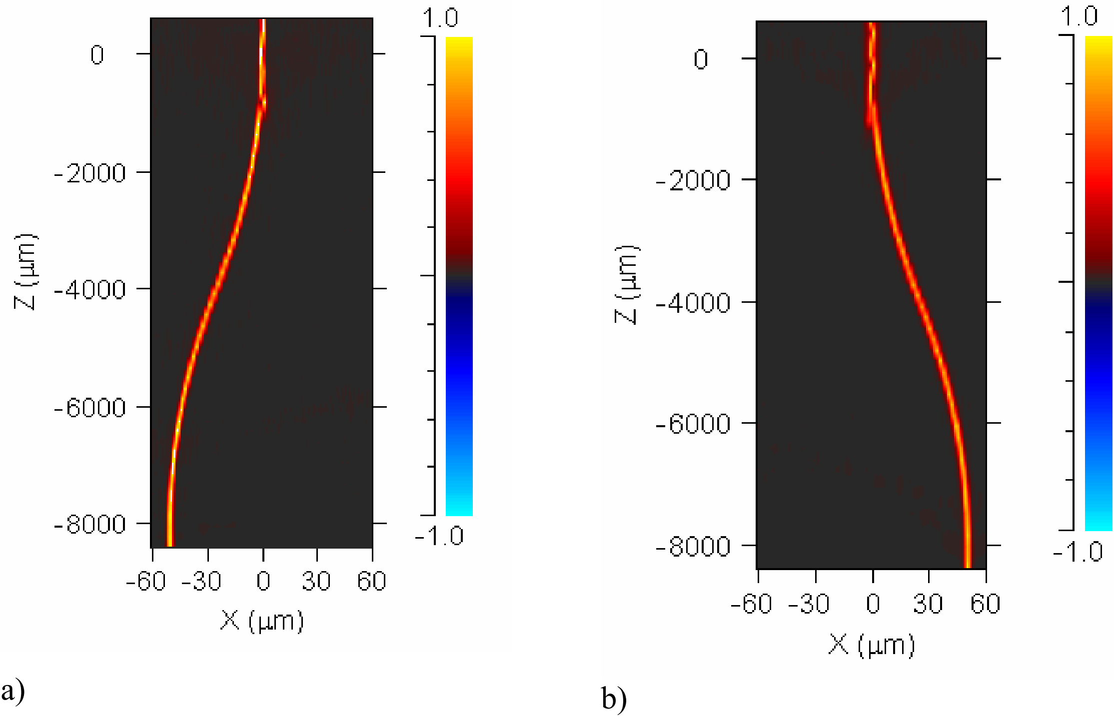

Fig 4.4: Intensity e.m. field pattern along the a) pump (λ_p=980 nm) and b) the signal branch (λ_s=1550 nm). Coupling length, L= 9 mm, waveguide width, w=4 μm, waveguide depth h= 3 μm, distance between the coupler axis and the signal and pump branches a_1= a_1 = 50μm

Future Works and Conclusion

The results presented in this thesis and in particular the attractive characteristic of the waveguides described in the previous chapters have as immediate consequence the possibility to realize with few efforts an Erbium-Doped Waveguide Amplifier integrated in an optical circuit. The realization and test of the final device was not carried out in this thesis work but the remaining steps for the fabrication of such device can be easily covered.

Following an inverse order with respect to the one presented in this thesis, the first step will be to realize a suitable photolithographic mask for the Y-junction realization with the designed geometry, presented in the last chapter.

The "inverse method", proposed in this thesis is extremely appropriate for the technological development of the final device, therefore it can be applied without (or with minor) further optimization work. The etching procedure is in fact completely optimized. Excellent results were obtained both on silica and SiO_2/Si substrate: channels with vertical shape sidewalls and very smooth bottom were realized.

Oxyfluoride silicate glass waveguide with very low propagation losses were deposited onto planar and patterned substrate nevertheless the deposition of the silicate glass could require some efforts in order to reduce the quenching effects on the erbium luminescence and to further discuss the role of the deposition temperature on the final performances of the amplifier.

Concerning the tellurite glasses, it is worth noting that interesting results were achieved by mean of the PLD technique, very transparent films were obtained with optical properties similar to the bulk ones.

Moreover the application of the "inverse method", can allow the fabrication of 2D tellurite waveguides and amplifiers, since the possibility to realize lateral confinement, in this method, is independent from the structural properties and stability of the starting

material, therefore also fragile materials, such as tellurite glasses, can be successfully employed for the realization of rectangular waveguides.

This thesis is entirely founded on the unique properties of the PLD technique. Very attractive results were obtained on multicomponent glasses, both in planar and in rectangular waveguides, moreover the strength of the “inverse method” itself is based on the ability of PLD in depositing films onto non-planar substrates, without affecting the film properties.

It is worth noting that of the different techniques employed to fabricate planar devices and in particular EDWAs, no one emerged up to now as the definitive technique in this field. This aspect is very stimulating, and in this context this thesis can represent the strong point in behalf of the Pulsed Laser Deposition as the new method for integrated optics application.

References

[1] R.J. Mears, L. Reekie, I.M. Jauncey and D.N. Payne, *Electron. Lett*., 23, 1026 (1987)

[2] E. Desurvire, J. Simpson, and P.C. Becker, *Optics Letters*, 12, 888 (1987)

[3]H. Onaka, H. Miyata, G. Ishikawa, K. Otsuka, H. Ooi, Y. Kai, S. Kinoshita, M. Seino, H. Nishimoto, and T. Chikamaet, *Optical Fiber Communication Conference 1996 (OFC'96)* PD-19

[4]A. H. Gnauck, A. R. Chraplyvy, R. W. Tkach, J. L. Zyskind, J. W. Sulhoff, A. J. Lucero, Y. Sun, R. M, *Optical Fiber Communication Conference 1996 (OFC'96)* PD-20

[5]Y. Yano, T. Ono, K. Fukuchi, T. Ito, H. Yamazaki, M. Yamaguchi, and K. Emura, *Optical Communication (ECOC'96)*, **5**, 3 (1996)

[6] K. Fukuchi, T. Kasamatsu, M. Morie, R. Ohhira, T. Ito, K. Sekiya, D. Ogasawara, and T. Ono, *Optical Fiber Communication Conference 2001 (OFC 2001)*, PD-24

[7] T.B. Astle, A.R. Gilbert, A. Ahmad, S. Fox, *"Optical components – the planar revolution?* ", Merril Lynch & Con., Global Telecom Equipment, Wireline (2000)

[8] A. J. Kenyon, *Progress in quantum electronic*, **26**, 225 (2002)

[9] D. R. Zimmermann, L. H. Spiekman, *IEEE J. Lightwave Tech.*, Vol. **22**, 63, (2004).

[10] P. Urquhart, *IEE Proceedings*, **135**, 385, (1988).

[11] H. Nishihara, M. Haruna, T. Suhara, "*Optical Integrated Circuits"*, McGraw-Hill, (1989).

[12] T. Tamir, "*Integrated Optics*", Springer-Verlag Berlin Heidelberg New York (1979)

[13] http://www.photeon.com/

[14] W.J. Miniscalco, "*Optical and electronic properties of rare earth ions in glass*", in *Rare-Earth-Doped fiber laser and amplifiers*, Second edition, edited by M. J. F. Digonnet, Marcel Dekker Inc., New York (2001)

[15] W.J. Miniscalco, *J. Ligthwave Tech.*, **9**, 234 (1991)

[16] M.P. Hehlen, N.J. Cockroft and T.R. Gosnell, Phys. Rev. B **56,** 9302 (1997)

[17] P. C. Becker, N. A. Olsson, and J. R. Simpson, *Erbium-Doped Fiber Amplifier Fundamentals and Technology,* Academic Press (1999)

[18] D.E. McCumber, *Phys. Rev*., **134**, A229 (1964)

[19] W.J. Miniscalco, R.S. Quimby, *Optics Letters,* **16**, 258 (1991)

[20] S.A. Payne, L.L. Chase, L.K.Smith, W.L. Kway, W.F. Krupke, *IEEE J. Quantum Electr*., **28** 2619 (1992)

[21] R.S. Quinby, *J. Appl. Phys,* **92**, 180 (2002)

[22]E. Desurvire, *Erbium-Doped Fiber Amplifier: Principles and Applications,* John Wiley & Sons, Inc. (1995)

[23] A. Lidgard, A. Polman, D. C. Jacobson, G. E. Blonder, R. Kistler, J. M. Poate and P. C. Becker, *Elet. Lett*., **27**, 993 (1991)

[24] S. Todorikki, H. Hirao, and N. Soga, *J. Appl. Phys*., **72**, 5853, (1992)

[25] M. R. X. de Barros, G. Nykolak, R, Ghosh, C. F. Kane, J. Shmulovich, D. J. Di Giovanni, A. Bruce, *Proceeding TELEMO*, **145**, (Curitiba, Brazil, 1996).

[26] J.A. Làzaro, J.A. Vallès, M.A. Rebolledo, *IEEE J. Quantum Electr.*. **35**, 827 (1998)

[27] J. Amin, B. Duassardier, T. Schweizer, M. Hempsted, *J. Lumin*., **69**, 17 (1996)

[28] F. Caccavale, C. Sada, F. Segato, B. Allieri, L.E. Depero, L. Sangaletti, V.A. Fedorov, Yu.N. Korkishko, T.V. Morozova*, J. Non-Cryst. Sol.,* **280**, 156 (2001)

[29] B. Herreros, G. Lifante, F. Cusso, J.A. Sanz, A. Kling, J.C. Soares, M.F. da Silva, P.D. Townsend, P.J. Chandler, *J. Phys.- Cond Matt*. **10**, 3275 (1998)

[30] C. Becker, T. Oesselke, J. Pandavenes, R. Ricken, K. Rochhausen, G. Schreiberg, W. Sohler, H. Suche, R. Wessel, S. Balsamo, I. Montrosset, and D. Sciancalepore, *IEEE J. Sel. Top. Quantum Electron*. **6**, 101 (2000)

[31] M. Mattarelli, S. Sebastiani, J. Spirkova, S. Berneschi, M. Brenci, R. Calzolai,A. Chiasera, M. Ferrari, M. Montagna, G. Nunzi Conti, S. Pelli, G.C. Righini, *Opt Mat*., **28**, 1292 (2006)

[32] A. Polman, *J. Appl. Phys*., **82**,1 (1997)

[33] C. E. Chryssou, A. J. Kenyon,T. M. Smeeton and C. J. Humphreys and D. E. Hole, *Appl. Phys. Lett*., **85**, 5200 (2004)

[34] G.N. Van den Hoven, E. Snoeks, A. Polman, C. van Dam, J.W.M. van Uffelen, M.K. Smit, *J. Appl. Phys*. **79**, 1258 (1996)

[35] C.E. Chryssou, C.W. Pitt, *IEEE J. Quant. Elect*. **34**, 28 (1998)

[36] A. Polman, *Proceedings of the Tenth European Conference on Integrated Optics (ECIO),* 75 (2001)

[37] H. Liang, Z. Zheng, B. Chen, Q. Zhang, and H. Ming, *Mater. Chem. Phys*. **86**, 430 (2004)

[38] L.Eldada, L.W. Shackelette, *IEEE J. Sel Top Quantum Electr*., **6**, 54 (2000)

[39]F. W. Billmeyer, Jr., *Textbook of Polymer Science*, 2nd ed., Wiley, New York (1970)

[40] L. H. Slooff, A. van Blaaderen, A. Polman, G. A. Hebbink, S. I. Klink, F. C. J. M. Van Veggel, D. N. Reinhoudt, and J. W. Hofstraat, *J. Appl. Phys*. **91**, 3956 (2002)

[41] A. Q. Le Quang et al., *Proc. SPIE* **6123**, 612302 (2006)

[42] J. N. Sandoe, P. H. Sarkies, and S. Parke, *J. Phys. D* **5**, 1788 (1972).

[43] D.J. DiMaria, J.R. Kirtley, E.J. Pakulis, D.W. Dong, T.S. Kuan, F.L. Pesavento, T.N. Theis, J.A. Cutro, S.D. Brorson, *J. Appl. Phys.*, **56**, 401 (1984)

[44] T. Shimizu-Iwayama, K. Fujita, S. Nakao, K. Saitoh, T. Fujita, N. Itoh, *J. Appl. Phys*, **75** 7779 (1994).

[45] A.J. Kenyon, P.F. Trwoga, C.W. Pitt, G. Rehm, *Appl. Phys. Lett*., **73**, 523 (1998)

[46] A.J. Kenyon, C.E. Chryssou, C.W. Pitt, T. Shimizu-Iwayama, D.E. Hole, N. Sharma, C.J. Humphreys, *J. Appl. Phys,* **91**, 367 (2002)

[47] J. Lee, J. H. Shin and N. Park, *J. Lightwave Tech*., **23**, 19 (2005)

[48] M. Semenkoff, M. Guibert, D. Ronarch, Y. Sorel, and J. F. Kerdiles, *J. Non-Cryst. Sol.*, **184**, 240 (1995).

[49] T. Whitley, C. A. Miller, R. Wyatt, M. C. Brierly, and D. Szeberta, *Elect. Lett.*, **27**, 1785 (1991)

[50] R. Reisfeld and Y. Eckstein, *J. Non-Cryst. Sol*. **15**, 125 (1974)

[51] V. P. Gapontsev, S. M. Matitsin, A. A. Isineev and V. B. Kravchenko, *Opt. Laser Tech.*, **14**, 189 (1982)

[52] S. Jiang, M. Myers and N. Peyghambarian, *J. Non-Cryst. Sol*., **239**,143 (1998)

[53] Y.H. Wang, Ohwaki, *Appl. Phys. Lett*. **63**, 3268 (1999)

[54] Y. Kawamoto, R. Kanno, J. Qiu, *J. Mater. Sci*., **33**, 63 (1998)

[55] Y. Morishita, K. Muta, N. Sugiyama, *Mater. Res. Soc. Symp. Proc*., **244**, 163 (1992)

[56] C. Strohhofer, J. Fick, H.C. Vasconcelos, R.M. Almeida, *J. Non-Cryst. Sol*., **226**, 182 (1998)

[57] V. K. Tikhomirov, D. Furniss, A. B. Seddon, I. M. Reaney, M. Beggiora, M. Ferrari, M. Montagna, and R. Rolli, *Appl. Phys. Lett.*, **81**, 1937 (2002)

[58] S.X. Shen, and A. Jha, *Opt. Mater*., **25**, 321 (2004)

[59] R. Reisfeld and Y. Eckstein, *J. Non-Cryst. Sol.,* **15**, 125 (1974)

[60] A. Mori, Y. Ohishi and S. Sudo, *Elect. Lett.*, **33**, 863-864 (1997)

[61] M. Yamada, A. Mori, K. Kolayashi, H. Ono, T. Kanamosi, K. Oikavia, Y. Nishida, and Y. Ohishi, *IEEE Phot. Tech.. Lett*. **10**, 1244 (1998).

[62] Z. Pan, S. H. Morgan, K. Dyer, A. Ueda, and H. Liu, *J. Appl. Phys*., **79**, 8906 (1996)

[63] L. Le Neindre, S. Jiang, B. Hwang, T. Luo, J. Watson, and N. Peyghambarian, *J. Non-Cryst. Sol*., **255**, 97 (1999)

[64] S. Shen, M. Naftaly, A. Jha, *Opt.Comm*. **205**, 101 (2002)

[65] L. Petit, T. Cardinal, J. J. Videau, G. Le Flem, Y. Guyot, G. Boulon, M. Couzi and T. Buffeteau, *J. Non-Cryst. Sol.*, **298**, 76 (2002)

[66] M. Mattarelli, M. Bouazaoui, B. Capoen, S. Turrell, A. Chiasera, M. Ferrari, L. Zampedri, M. Montagna, H. Portales, G. Nunzi-Conti and G.C. Righini, *SPIE Proc.* **5451**, 337 (2004)

[67] Y. C. Yan, A. J. Faber, H. de Waal, P. G. Kik, A.Polman, *Appl. Phys lett.*, **71**, 2922 (1997).

[68] S. F. Wong, Y. B. Pun, P. S. Chung, *IEEE Pho. Tech. Lett.*, **14**, 80 (2002).

[69] F. D. Patel, S. DiCarolis, P. Lum, S. Venkatesh, J. N. Miller, *IEEE Pho. Tech. Lett*, **16**, 2607 (2004)

[70] K. Liu, E. Y. B. Pun, T. C. Sum, A. A. Bettiol, J.A. van Kann, F. Watt, *Appl. Phys. Lett*., **84**, 684 (2004)

[71] G. Della Valle, R. Osellame, N. Chiodo, S. Taccheo, G. Cerullo, P. La Porta, A. Killi, U. Morgner, M.Lederer, D. Kopf, *Opt. Exp*., **13**, 5976 (2005).

[72] C. C. Li, H. K. Kim, M. Migliuolo, *IEEE Pho. Tech. Lett*, **9**,1223 (1997).

[73] W. Huang, R. R. Syms, *J. Lightwave Tech.*, **21**, 1339 (2003).

[74] S. Pelli, M. Bettinelli, M. Brenci, R. Calzolai, A. Chiasera, M. Ferrari, G. Nunzi Conti, A. Speghini, L. Zampedri, J. Zheng, G. C. Righini, *J. Non-Cryst. Sol.*, **345&346**, 372 (2004).

[75] N. D. Psaila, R. R. Thomson, H. T. Bookey, A. K. Kar, N. Chiodo, R. Osellame, G. Cerullo, A. Jha, S. Shen, , *Appl. Phys. Lett.*, **90**, 131102 (2007).

[76] A.P. Caricato, M, Fernández, M. Ferrari, G. Leggieri, M. Martino, M. Mattarelli, M. Montagna, V. Resta, L. Zampedri, R.M Almeida, M.C. Conçalves, L. Fortes, L.F. Santos, *Mat. Sci. Eng. B***, 105,** 65 (2003)

[77] E.B. Intyushin and Y.I, Chigirinskii, *Glass Phys.Chem.,* **31,** 162 (2005)

[78] S. Sakida,T. Nanba and Y. Miura, *Mat. Lett.*, **60**, 3413(2006)

[79] G.C Righini, I Bányász, S. Berneschi, M. Brenci, A. Chiasera, M. Cremona, D. Erht, M. Ferrari, R.M. Montereali, G. Nunzi Conti, S. Pelli, S. Sebastiani, C. Tosello, *SPIE Proc*., **5840**, 649 (2005)

[80] S. Berneschi, G. Nunzi Conti, I. Bányász, A. Watterich, N. Q. Khanh, M. Fried, F. Pászti, M. Brenci, S. Pelli, G. C. Righini, *Appl. Phys. Lett*., **90**,121136, (2007)

[81] P.K. Tien, *Appl. Opt*., **10**, 2395 (1971)

[82] H.F. Taylor and A. Yariv, *Proc. IEEE*., **62**, 1044 (1974)

[83] R.G. Hunsperger, "*Integrated Optics Theory and Technology"*, 5th Edition, Springer-Verlag, Berlin, (2002)

[84] A. Yariv in *Introduction to optical electronics,* 2nd Edition, Holt Rinehart and Winston, New York (1976)

[85] M. Barnoski, *"Introduction to integrated optics"*, Plenum , New York (1974)

[86] S. M. Rossnagel *"Sputter Deposition",*in W.D Sproul, K.O. Legg*, Opportunities for Innovation: Advanced Surface Engineering.* Switzerland: Technomic Publishing Co. (1995)

[87] M. Scherer, J. Schmitt, R. Latz, M. Schanz, *J Vac Sci Technol A,* **10**, 1772 (1992)

[88] W. D. Sproul, M. E. Graham, M.S. Wong, S. Lopez, D.Li, R.A. Scholl, *J Vac Sci Technol A*, **13**, 1188 (1995)

[89] Y. C. Yan, A. J. Faber, H. de Waal, P. G. Kik, A. Polman, *Appl. Phys. Lett*., **71**, 2922 (1997).

[90] P. G. Kik, A. Polman, *MRS Bulletin* **23**, 48 (1998)

[91] G. Grand, J.P. Jadot, H. Denis, S. Valette, A. Fournier, A.M. Grouillet, *Elect. Lett*. **26**, 2135 (1990)

[92] F. Ay, A. Aydinii, and S. Agan,, *Appl. Phys. Lett*. **83**, 4743 (2003)

[93] K. Shuto, K. Hattori, T. Kitagawa, Y. Ohmori, M. Horiguchi, *Electr. Lett*., **29**, 139 (1993).

[94] K.Worhoff, P.V. Lambeck,, A. Driessen, *J. Lightwave Tech*., **17,** 1401 (1999)

[95] M. Benatsou and M. Bouazaoui, *Opt. Comm*., **137**, 143 (1997)

[96] R.M. Almeida, X.M. Du, D. Barbier, and X. Orignac, *J. Sol-Gel Sci. Technol*. **14**, 209 (1999)

[97] R.M. Almeida, A. C. Marques and R. Cabeça, L. Zampedri, A. Chiasera, M. Ferrari, *J. Sol-Gel Sci. Technol,* **31**, 317 (2004)

[98] R. V. Ramaswamy and R. Srivastava, *J. Lightwave Technol*., **6**, 984 (1988)

[99] S. Berneschi, M. Bettinelli, M. Brenci, R. Calzolai, A. Chiasera, M. Ferrari, G. Nunzi Conti, S. Pelli, S. Sebastiani, A. Speghini, J. Zheng, G. C. Righini, *SPIE Proc.*, **5350**, 140(2004).

[100] V.A.G. Rivera, E.F. Chillcce, E. Rodriguez, C.L. Cesar and L.C. Barbosa, *J. of Non-Cryst. Solids***, 352**, 363 (2006)

[101] D.B. Chrisey and G.K. Hubler *"Pulsed Laser Deposition of Thin Films"*, Wiley, New York (1994)

[102] D. Bäuerle, *Laser Processing and Chemistry*, 3rd ed. ,Springer, Berlin (2000)

[103] P.H. Hor, L. Gao, R.L. Meng, Z.J. Huang, Y.Q. Wang, K. Forster, J. Vassilious, C.W. Chu, M.K. Wu, J. R. Ashburn and C.J. Torng, *Phys. Rev. Lett.,* **58**, 911, 1987

[104] A. A. Voevodin, M.S. Donley, *Surf. Coat. Tech*., **82**, 199 (1996)

[105] A. Perrone, *J. Appl. Phys*., **41**,2163 (2002)

[106] M. Reichling, in: *Laser Ablation and Desorption*, Eds. J. C. Miller and R. F. Haglund, *Experimental Methods in the Physical Sciences vol. 30*, Academic Press, New York (1998)

[107] J. Schou, *Laser Beam-Solid Interactions*: "*Fundamental Aspects*" in *Materials Surface Processing by Directed Energy Techniques* ,edited by Y. Pauleau, Elsevier (2005).

[108] S. Amoruso, *Appl. Phys. A*, **69**, 323 (1999)

[109] J.C.S. Kools, *J. Appl. Phys*. **74**, 6401 (1993)

[110] J. Gonzalo, C.N. Afonso, I. Madariaga, *J. Appl. Phys*. **81**, 951 (1997)

[111] M. Kawakami, A.B. Hartanto, Y. Nakata, T. Okada, *Jpn. J. Appl. Phys*. **42** L33 (2003)

[112] T. N. Hansen, J.Schou and J. G. Lunney, *Appl.Phys. Lett*. **72**, 1829 (1998)

[113] S. Sambri, S. Amoruso, X. Wang, M. Radovic', F. Miletto Granozio, R. Bruzzese, *Appl. Phys. Lett*, **91** 151501 (2007)

[114] J. Gonzalo, A., Perea, J.M. Femandez-Navarro, C.N Afonso, J. Garcia Lopez, *Appl. Phys. A* **76**, 943 (2003)

[115] K. L. Saenger, in: *Pulsed Laser Deposition of Thin Films*, Eds. D.B. Chrisey and G.K. Hubler, Wiley, New York (1994)

[116] E.M.Vogel,E.W. Chase,J.L. Jackel, B.J. Wilkens 1989, *Appl. Opt.* **28**, 649 (1989)

[117] C. N. Afonso,J.M. Ballesteros, J. Gonzalo, G.C. Righini, S. Pelli, *Appl. Surf. Sci.* **96-98:** 760 (1996)

[118] S. Mailis,C. Riziotis, J. Wang, E. Taylor, A. Anderson ,S.J. Berrington, H.N.Rutt, R.W. Eason, N.A.Vainos, C. Grivas, *Opt. Mat.* **12**, 27 (1999)

[119] D. Munoz-Martin, J. Gonzalo, J.M. Fernandez-Navarro, J. Siegel, C.N. Afonso, *Appl. Surf. Sci*. **254**, 1111 (2007)

[120] L.Chen in *Pulsed Laser Deposition of Thin-films,* Eds D. B. Chrisey and G. K. Hubler, Wiley, New York (1994)

[121] J. Serra,S. Liste, P. Gonzalez , C. Serra, J.P. Borrajo, S. Chiussi, B. Leon, M. Perez-Amor, *Appl. Phys. A* **79**, 983 (2004)

[122] M. Martino, A. P. Caricato, A. Fazzi, F. Romano, V.K. Tikhomirov, A.B. Seddon, M. Matterelli, A. Chiappini, K.C. Visnhubhatla, *J.Non Cryst. Solids* **351**, 1810 (2005)

[123] R. Swanepoel, *J. Phys. E: Sci. Instrum*. **16**, 1214 (1983)

[124] P.K. Tien and R. Ulrich, *J. Opt. Soc. Am*. **60**, 1325 (1970)

[125] A.P. Caricato, A. Fazzi, G. Leggieri, *Appl. Surf. Sci.* **248,** 440 (2005)

[126] L. Doolittle*, RUMP RBS Simulation Program*, Computer Graphics Service, Ltd. 1993

[127] O.Sanz, J. Gonzalo,A. Perea, J.M. Femandez-Navarro, C.N Afonso, J. Garcia Lopez, *Appl. Phys. A* **79,** 1907 (2004).

[128] M.K.Th.Clement, J.S. Hayden, Y.T. Hayden, H.J. Hoffmann, F.T. Lentes, N. Neuroth,, "*Optical properties*" in: *The Properties of Optical Glass,* H. Bach and N. Neuroth, eds., Springer-Verlag, Berlin (1995).

[129] A.A.J. Marcatilli, *Bell Syst. Tech. J*, **48**, 2071 (1969)

[130] K. Kawano, T. Kitoh, *"Introduction to optical waveguide Analysis"*, Wiley & Sons, NewYork (2001)

[131] M. Kohler, "*Etching in microsystem technology"*, Wiley-VCH, Weinheim, New York (1999)

[132] M. Esashi, *Microsyst. Technol*. **1**, 2 (1994)

[133] C. Pierrat, T. Siegrist, J. de Marco, L. Harriott, S. Vaidya, *J. Vac. Sci. Technol. B* **14**, 63 (1996)

[134] C. Steinbruchel, *J. Electrochem. Soc*. **130** , 648 (1983)

[135] G.S. Oehrlein, Y. Zhang, D. Vender, O. Joubert, *J. Vac. Sci. Technol. A* **12**, 333 (1994)

[136] C. Constantine, *Micromach. Dev*. **2**, 12 (1997)

[137] S. Ronggui, G.C. Righini, *J. Vac. Sci. Technol. A* **9,** 2709 (1991)

[138] D.A. Darbyshire, A.P. Overbury, C.W. Pitt, *Vacuum* **36**, 55(1986)

[139] P.W. Leech, *Vacuum* **55**,191 (1999)

[140] E. Metwalli, C.G. Pantano , *Nucl. Instr. and Meth. in Phys. Res. B* **207**, 21 (2003)

[141] L.H. Slooff, M.J.A. de Dood, A. Van Blaaderen, A. Polman, *J. Non-Cryst. Solids*, **296**, 158 (2001)

[142] J.-H. Min, S.-W. Hwang, G.-R. Lee, and S. H. Moon, *J. Vac. Sci. Technol. A* **20**, 1574 (2002).

[143] D. Zhang and M. J. Kushner, *J. Vac. Sci. Technol. A* **19**, 524 (2000)

[144] J.-H. Min, , G.-R. Lee,J. K. Lee and S. H. Moon *J. Vac. Sci. Technol. B* **22**, 2580 (2004),

[145] J.-H. Min, S.-W. Hwang, G.-R. Lee, and S. H. Moon, *J. Vac. Sci. Technol. B* **21**, 1210 (2003).

[146] Pao-Lo Liu, S L Yang and D M Yuan, *IEEE J. Quantum Electron.*, **29**, 1205 (1993)

[147] M. S. Stern, *Inst. Elec. Eng. Proc. J.*, **135**, 56 (1998)

[148] F. Fernandez and Y Lu, *"Microwave and Optical Waveguide Analysis by the Finite Element Method"*, Research Studies Press Ltd. Great Britain (1996)

[149] R. M. Knox and P. P. Toulios, *Proc. M. R. I. Symp. Sub-millimeter waves*, Ed J. Fox, Brooklyn, N. Y.: Polytechnic Press, 497 (1970)

[150] P. W. A. McIlroy, *"Spectral Index method: Single Rib Waveguide",* in *Rib Waveguide Theory by the Spectral Index Method,* ed. P. N. Robson, P. C. Kendall, Wiley (1990)

[151] C. J. Smartt, T. M. Benson and P. C. Kendall, *IEE Proc. J.,***140**, 56 (1993)

[152] *K. Yee , IEEE Trans Antennas and Propagat. ,**14,** 302 (1966).*

[153] A. Taflove and S. C . Hagness, *"Computational Electrodynamics—The Finite Difference Time Domain Method"*, 2nd Ed., Artech House (2000).

[154] L. Thylen, *Opt. Quantum Electron.*,**15**, 433 (1978)

[155] M.Koshiba, Y. Tsuji, IEEE Photon. Technol. Lett., **8**, 1208 (1996)

[156] Y. Chung and N. Dagli, , *IEEE J. Quantum Electron.*, **26**, 1335(1990)

[157] G. R. Hadley, *Opt. Lett.*,**17**, 1426 (1992)

[158] Rsoft inc., http://www.rsoftdesign.com/

Publications

D. Valerini, A. P. Caricato, M. Lomascolo, F. Romano, A. Taurino, T. Tunno, M. Martino, "Zinc oxide nanostructures grown by pulsed laser deposition" accepted for publication in Applied Physics A

A.P. Caricato, S. Capone, G. Ciccarella, R. Rella, F. Romano, J. Spadavecchia, A. Taurino, T. Tunno, D. Valerini, M. Martino,"TiO_2 nanoparticle thin film deposition by matrix assisted pulsed laser evaporation for sensing applications " Applied Surface Science, **253**, 7937 (2007)

A.P. Caricato, M.G. Manera, R. Rella, F. Romano, J. Spadavecchia, T. Tunno, D. Valerini, M. Martino, "Uniform thin films of TIO_2 nanoparticles deposited by Matrix-assisted Pulsed Laser Evaporation" Applied Surface Science, **253**, 6471 (2007)

T. Tunno, A.P. Caricato, M. E. Caruso, A. Luches, M. Martino, F. Romano, D. Valerini, M. Anni, "Matrix-assisted pulsed laser evaporation of polyfluorene thin film" Applied Surface Science, **253**, 6461 (2007)

A.P. Caricato, M. Fernàndez, G. Leggieri, M. Martino, F. Romano, T. Tunno, D.Valerini, A. Luches, "Reactive pulsed laser deposition of gold nitride thin films" Applied Surface Science, **253**, 8037 (2007)

A. Luches, S.A. Mulenko, V.P. Veiko, A.P. Caricato, V.A Chuiko, Y.V. Kudryavtsev, A.V. Lopato, A.A. Petrov, F. Romano, D. Valerini, "Laser-assisted synthesis of semiconductor chromium disilicide films" Applied Surface Science, **253**, 6512 (2007)

A.P. Caricato, A. Fazzi, A. Jha, A. Kar, G. Leggieri, A. Luches, M. Martino, F. Romano, S. Shen, M. Taghizadeh, R. Thomson, T. Tunno, **"**Er-doped oxyfluoride silicate thin films prepared by pulsed laser deposition" Optical Materials **29**, 1166, (2007).

M Bouazaoui, B Capoen, A P Caricato, A Chiasera, A Fazzi, M Ferrari, G. Leggieri, M Martino, M Mattarelli, M Montagna, F Romano, T Tunno, S Turrel and K Vishnubhatla "Pulsed Laser Deposition of Er doped tellurite films on large area" Journal of Physics: Conference Series **59,** 475 (2007) [Eighth International Conference on Laser Ablation]

R. Brunetto, F. Romano, A. Blanco, S. Fonti, M. Martino, V. Orofino, C. Verrienti "Space weathering of silicates simulated by nanosecond pulse UV excimer Laser" , Icarus **180**, 546 (2006)

S. Lattante, F. Romano, A.P. Caricato, M. Martino, M. Anni "Low electrode induced optical losses in organic active single layer polyfluorene waveguides with two indium tin oxide electrodes deposited by pulsed laser deposition", Applied Physics Letters **89,** 031108 (2006)

A.P. Caricato, M. Catalano, G. Ciccarella, M. Martino, R. Rella, F. Romano, J. Spadavecchia, A.Taurino, T. Tunno, D.Valerini, "Matrix Assisted Pulsed Laser Evaporation for TiO_2 nanoparticle thin film depositio*n*", Digest Journal Nanomaterials and Biostructures **1,** 43 (2006)

R.R. Thomson, H.T. Bookey, A.K. Kar, M.R. Taghizadeh, A. Klini, C. Fotakis, F. Romano, A.P. Caricato, M. Martino, S. Shen, A. Jha "Erbium doped waveguide fabrication via reactive pulsed laser deposition of multicomponent erbium doped oxyfluoride-silicate glasses" Electronic Letters **41**, 1376 (2005)

M. Martino, A.P. Caricato, A. Fazzi, F. Romano, V.K. Tikhomirov, A.B. Seddon, M.Mattarelli, A. Chiappini, K.C. Vishnubhatla "Pulsed laser deposition of Er3+-doped oxyfluoride thin films" Journal of Non-Crystalline Solids **351** , 1810 (2005)

Acknowledgements

This thesis work required the help and the collaboration of various groups; I had the opportunity to work with expert and competent scientists. I would like to thank all the people I met during these years, since they contribute not only to achieve the results presenting in this thesis but also to my personal growth.

First of all I am grateful to Prof. Maurizio Martino for the great opportunities he gave me during the PhD course, and for the autonomy he provided me in the scientific activity.

A particular thank is dedicated to Dr. Anna Paola Caricato: without her help this thesis work would not be possible, she supported me during these years (not merely) scientifically, her friendship represented the engine of my daily work.

The results on the tellurite planar waveguide are due to the collaboration with the CSMFO group of the University of Trento and in particular to Dr. Maurizio Ferrari and Dr. Maurizio Mattarelli.

I thank Prof. Animesh Jha and Dr. Shaoxiong Shen and the IMR group of the University of Leeds: the excellent results on silicate waveguide are obtained thanks to their fruitful collaboration.

The expertise of Dr. Robert Thomson made possible to perform the “standard method” and to characterize the silicate ridge waveguides at the University of Edinburgh.

Many thanks to Gianmichele Epifani and Prof. Massimo de Vittorio, I benefited of their skills and their facilities to realize the silica channels at National Nanotechnology Laboratory.

I’m very grateful to Dr. Luciano Mescia and Prof. Francesco Prudenzano for their irreplaceable help in the Y-junction coupler design.

Numerous analyses were necessary to completely characterized the thin films and the waveguides, I desire to thanks all the people that help me in the different analyses: Prof. Gilberto Leggieri and Prof. Giuseppe Majni for the RBS analysis, Dr. Antonietta Taurino for the SEM-FEG examination on the silica channels, Prof. Sergio Fonti and Dr. Marcella D’Elia for the UV-Vis transmission spectra and Dr. Andrea Fazzi for the analyses with the Refractor code.

And now…

E ora passiamo ai ringraziamenti meno formali.

Il primo e più importante ringraziamento va alla mia famiglia. Senza l'appoggio dei miei genitori non sarei qui oggi e non avrei potuto portare a termine questa esperienza (ormai sono abituati ai ringraziamenti dei figli, speriamo che questo ringraziamento non vada sprecato!!!) Un ringraziamento va al mio "fratellino" Simone, perché è con lui che ho condiviso giorno per giorno i dubbi e la stanchezza, nelle quotidiane "passeggiate" in auto verso Lecce.

Desidero ringraziare i veri compagni di avventura in questi anni: Anna Paola, Daniele e Tiziana. Molti (troppi???) sono stati i momenti divertenti, e tante le occasioni per confrontarsi scientificamente e non solo… E che dire di Daniele poi? Ho imparato davvero tanto da lui (dai dottò non dire di no!!!) ed è con lui che ho condiviso la quotidianità in laboratorio (anche se l'esperienza non sempre è stata facile e chi lo conosce sa di cosa parlo!!!).

Ringrazio tutti quelli che hanno condiviso con me la "stanza dottorandi", in particolare Monica, Elisabetta (i pomeriggi con lei e Daniele restano imbattuti) e Mariangela l'ultima arrivata (peccato solo che viaggi un po' troppo!).

Un ringraziamento va al Prof. Armando Luches, modello scientifico ed umano, per la sua costante disponibilità e per le opportunità che mi ha concesso.

Tutti coloro che non sono compresi in questa pagina non me ne vogliano, ho preferito evitare di compilare una lunga lista con la sola preoccupazione di non dimenticare nessuno. Chi c'è, c'è! e chi non c'è, l'importante è che ci sia stato!!!